

**THE EVALUATION OF ANTIPROLIFERATIVE  
AND STRUCTURAL EFFECTS OF STATINS ON  
NON-SMALL-CELL LUNG CANCER CELL LINE  
A549**

**A Thesis Submitted to  
the Graduate School of Engineering and Sciences of  
İzmir Institute of Technology  
in Partial Fulfillment of the Requirements for the Degree of**

**MASTER OF SCIENCE**

**in Biotechnology**

**by  
Hatice Nurdan AKSOY**

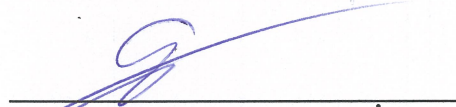
**July 2019  
İZMİR**

We approve the thesis of **Hatice Nurdan AKSOY**

**Examining Committee Members:**



**Assoc. Prof. Dr. Çağatay CEYLAN**  
Department of Food Engineering, İzmir Institute of Technology



**Assoc. Prof. Dr. Efe SEZGİN**  
Department of Food Engineering, İzmir Institute of Technology



**Asst. Prof. Dr. İpek ŞAHİN**  
Department of Physics, Ege University

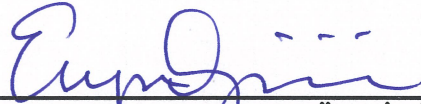
18 July 2019



**Assoc. Prof. Dr. Çağatay CEYLAN**  
Supervisor, Department of Food  
Engineering, İzmir Institute of Technology



**Prof. Dr. Ali ÇAĞIR**  
Co-Supervisor, Department of Chemistry,  
İzmir Institute of Technology



**Assoc. Prof. Dr. Engin ÖZÇİVİCİ**  
Head of the Department of Biotechnology  
and Bioengineering

**Prof. Dr. Aysun SOFUOĞLU**  
Dean of the Graduate School of  
Engineering and Sciences

## **ACKNOWLEDGMENTS**

Foremost, I would like to offer my sincere gratitude to my supervisor Assoc. Prof. Dr. Çağatay Ceylan for his guidance, contributions, support, advices throughout my thesis studies.

Also I would like to thank Biotechnology and Bioengineering Research Center specialist Yekta Günay for her kind help during my research studies.

I also wish to thank my dear close friends, Merve Özer, Menşure Elvan, Mehmet Kılınç, Nazlı Merve Demir, Altuğ Ali Arkalı and Mehmet Salih Yıldız for their motivation, moral and consistent support.

Lastly, I would like to express my grateful thanks to my whole family; especially my father Ali İhsan Aksoy, mother Feride Aksoy and brother Nuri Aksoy for their endless love, support, understanding and encouragement throughout my life.

## ABSTRACT

### THE EVALUATION OF ANTIPROLIFERATIVE AND STRUCTURAL EFFECTS OF STATINS ON NON-SMALL-CELL LUNG CANCER CELL LINE A549

Statins are commonly prescribed anti-lipidemic and anti-cholesterol class of drugs. In addition to their major role, they have been found to have anti-cancer effects on *in vitro*, animal and clinical studies. The aim of this study was to investigate the structural effects of 6 different statins (rosuvastatin, pravastatin, simvastatin, lovastatin, fluvastatin and atorvastatin) on A549 cells by a spectroscopic method. MTT viability tests were carried out to detect the half maximal inhibitory concentrations ( $IC_{50}$ ) of each statin on A549 cells. The  $IC_{50}$  values were 50  $\mu$ M for simvastatin, 150  $\mu$ M for atorvastatin and pravastatin, and 170  $\mu$ M for fluvastatin, 200  $\mu$ M for rosuvastatin and lovastatin on A549 cells. The cells were treated with  $IC_5$ ,  $IC_{10}$  and  $IC_{50}$  values of each statins concentration and their whole cell extracts and lipid extracts were compared using FTIR spectroscopy which is one of the most useful techniques to evaluate the structural changes at the macromolecular functional group level. The results indicated that different statins have different prominent effects on A549 cells. All the statins studied caused observable conformational changes on DNA and proteome of A549 cells. Whereas atorvastatin led to lipidation, lovastatin and pravastatin indicated enormous lipid-lowering properties. Based on the cell lipid extracts it was found that hydrocarbon chain length, unsaturation index, phospholipid containing lipids and carbonyl index showed increasing except for rosuvastatin-treated A549 cells. This study indicated that statins caused significant structural and compositional changes on A549 cells based on a spectroscopic evaluation.

## ÖZET

### STATİNLERİN A549 KÜÇÜK HÜCRELİ DIŞI AKCİĞER KANSERİ HÜCRE HATTI ÜZERİNDEKİ ANTİPROLİFERATİF VE YAPISAL ETKİLERİNİN DEĞERLENDİRİLMESİ

Statinler yaygın olarak kullanılmakta olan anti-lipidemik ve anti-kolesterol sınıfında yer alan ilaçlardır. Bu ana fonksiyonlarının yanı sıra anti-kanser etkileri *in vitro*, hayvan ve klinik çalışmalarda ortaya çıkarılmıştır. Bu çalışmanın amacı yapısal olarak birbirinden farklı olan 6 adet statinin (rosuvastatin, pravastatin, simvastatin, lovastatin, fluvastatin ve atorvastatin) A549 hücreleri üzerindeki yapısal etkilerinin bir spektroskopi yöntemiyle incelenmesidir. Yarı maksimum inhibitör konsantrasyonunu ( $IC_{50}$ ) belirlemek amacıyla MTT canlılık testi A549 hücrelerine uygulandı.  $IC_{50}$  değerleri simvastatin için 50  $\mu M$ , atorvastatin ve pravastatin için 150  $\mu M$ , fluvastatin için 170  $\mu M$  rosuvastatin ve lovastatin için 200  $\mu M$  olarak bulunmuştur. Hücreler statinlerin  $IC_5$ ,  $IC_{10}$  ve  $IC_{50}$  değerlerine tabi tutularak tüm hücre ve lipit ekstraktları, makromoleküler fonksiyonel grup seviyesinde değişimlerinin incelenmesinde çok kullanışlı bir yöntem olan FTIR spektroskopisi ile karşılaştırılmıştır. Sonuçlar farklı statinlerin A549 hücreleri üzerinde farklı önemli etkilere sahip olduğunu göstermiştir. Tüm statinler A549 hücreleri DNA'sında ve proteomunda gözlenebilir konformasyonel değişiklikler meydana getirmiştir. Atorvastatin lipidasyona sebep olurken, lovastatin ve pravastatin önemli derecede lipit düşürücü özellik göstermiştir. Hücre lipit ekstraktı sonuçlarına göre, hidrokarbon zincir uzunluğu, doymamışlık indeksi, fosfolipit içeren lipitler ve karbonil indeksi rosuvastatin muamele edilmiş A549 hücreleri hariç artış göstermiştir. Bu çalışmada statinlerin A549 hücreleri üzerinde önemli yapısal ve kompozisyonel değişikliklere sebep olduğu bir spektroskopik değerlendirme ile tespit edilmiştir.

# TABLE OF CONTENTS

ABSTRACT.....	iv
ÖZET .....	v
LIST OF TABLES.....	ix
LIST OF FIGURES .....	x
CHAPTER 1 INTRODUCTION .....	1
1.1. Cancer .....	1
1.1.1. Metabolic Reprogramming in Cancer Development.....	2
1.1.2. Alteration of Lipid Metabolism in Cancer .....	3
1.2. The Lungs and Lung Cancer .....	4
1.2.1. The Lungs .....	4
1.2.2. Lung Cancer.....	5
1.2.3. Lung cancer and lipid metabolism .....	6
1.3. The Mevalonate Pathway and Cholesterol Synthesis .....	7
1.4. Statins.....	7
1.5. Fourier Transform Infrared (FTIR) Spectroscopy .....	10
CHAPTER 2 MATERIALS AND METHODS .....	15
2.1. Chemicals.....	15
2.2. Cell Culture .....	15
2.2.1. Cell Passaging .....	15
2.2.2. Cell counting .....	16

2.2.3. Freezing Cells .....	16
2.2.4. Thawing Cells.....	16
2.2.5. Measurement of Cell Viability by MTT Assay .....	17
2.3. Preparation of Statins .....	17
2.4. Sample Preparation for FTIR Spectroscopy .....	18
2.4.1. Samples Preparation for Freeze Drying .....	18
2.4.2. Lipid Extraction.....	18
2.5. FTIR Spectrum Data Analyses.....	19
CHAPTER 3 RESULTS .....	20
3.1. Antiproliferative Effects of Statins on A549 Cells .....	20
3.2. The Effects of Statins on A549 Cells Studied by FTIR Spectroscopy .....	21
3.2.1. The Effect of Rosuvastatin on A549 Cells Studied by FTIR Spectroscopy: 24	
3.2.2. The Effect of Fluvastatin on A549 Cells Studied by FTIR Spectroscopy: ... 27	
3.2.3. The Effect of Simvastatin on A549 Cells Studied by FTIR Spectroscopy: .. 29	
3.2.4. The Effect of Atorvastatin on A549 Cells Studied by FTIR Spectroscopy: . 32	
3.2.5. The Effect of Pravastatin on A549 Cells Studied by FTIR Spectroscopy: ... 34	
3.2.6. The Effect of Lovastatin on A549 Cells Studied by FTIR Spectroscopy: .... 37	
3.3. The FTIR Band Ratios of The Non-Treated A549 Cells And Three Different Doses of Statin Treated A549 Cells .....	39
3.3.1. The Ratio of Amide I/II.....	39
3.3.2. The Ratio of 1740/Amide I.....	40
3.3.3. Ratio of 1740/1080.....	40
3.3.4. Ratio of Amide I/1080.....	40
3.4. The FTIR Spectra of Lipid Extracts of Statin Treated A549 Cells.....	41
3.4.1. The comparison of the FTIR spectra of the different statin groups for same concentration.....	49

3.4.2. The band ratios of the lipid extracts of non-treated A549 cells and three different doses of statins treated A549 cells .....	52
3.4.2.1. Unsaturation index.....	52
3.4.2.2. Hydrocarbon chain length .....	53
3.4.2.3. PO <sub>2</sub> /CH <sub>2</sub> .....	53
3.4.2.5. Number of acyl chains.....	53
CHAPTER 4 DISCUSSION.....	54
CHAPTER 5 CONCLUSION.....	57
REFERENCES .....	59



## LIST OF TABLES

<b><u>Table</u></b>	<b><u>Page</u></b>
Table 3. 1. The general FTIR band assignments of A549 cells.....	22
Table 3. 2. FTIR band ratios of the non-treated A549 cells and the doses of IC <sub>5</sub> , IC <sub>10</sub> and IC <sub>50</sub> of statins treated A549 cells .....	41
Table 3. 3. The FTIR band assignments of lipid extracts of A549 cells. ....	43
Table 3. 4. FTIR band ratios of the non-treated A549 cells and three different doses of the six different statins treated A549 cells. ....	52

# LIST OF FIGURES

<u>Figure</u>	<u>Page</u>
Figure 1. 1. Rearrangement of hallmarks of cancer .....	2
Figure 1. 2. The histology of the lungs .....	4
Figure 1. 3. The types of lung cancer . .....	6
Figure 1. 4. Overview of the mevalonate pathway and its blockage by statins .....	9
Figure 1.5. Molecular structures of the statins .....	10
Figure 1.6. A representation of the electromagnetic spectrum .....	11
Figure 1.7. Virtual energy levels for IR spectroscopy.....	12
Figure 1. 8. The types of molecular vibrations.....	13
Figure 3. 1. The cytotoxicity profiles of statins on A549 cells.....	20
Figure 3. 2. The general FTIR spectrum of A549 cells.....	21
Figure 3. 3. The FTIR spectra of the three different doses of rosuvastatin-treated and control A549 cells between 3768 and 2608 $\text{cm}^{-1}$ .....	25
Figure 3. 4. The FTIR spectra of the three different doses of rosuvastatin-treated and control A549 cells between 1777 and 1481 $\text{cm}^{-1}$ .....	25
Figure 3. 5. The FTIR spectra of the three different doses of rosuvastatin-treated and control A549 cells between 1276 and 783 $\text{cm}^{-1}$ .....	26
Figure 3. 6. The FTIR spectra of the three different doses of fluvastatin-treated and control A549 cells between 3710 and 2682 $\text{cm}^{-1}$ .....	27
Figure 3. 7. The FTIR spectra of the three different doses of fluvastatin-treated and control A549 cells between 1767 and 1493 $\text{cm}^{-1}$ .....	28
Figure 3. 8. The FTIR spectra of the three different doses of fluvastatin-treated and control A549 cells between 1273 and 786 $\text{cm}^{-1}$ .....	29
Figure 3. 9. The FTIR spectra of the three different doses of simvastatin-treated and control A549 cells between 3704 and 2784 $\text{cm}^{-1}$ .....	30
Figure 3. 10. The FTIR spectra of the three different doses of simvastatin-treated and control A549 cells between 1769 and 1479 $\text{cm}^{-1}$ .....	31
Figure 3. 11. The FTIR spectra of the three different doses of simvastatin-treated and control A549 cells between 1274 and 785 $\text{cm}^{-1}$ .....	31

<u>Figure</u>	<u>Page</u>
Figure 3. 12. The FTIR spectra of the three different doses of atorvastatin-treated and control A549 cells between 3688-2727 $\text{cm}^{-1}$ . .....	32
Figure 3. 13. The FTIR spectra of the three different doses of atorvastatin-treated and control A549 cells between 1768-1481 $\text{cm}^{-1}$ . .....	33
Figure 3. 14. The FTIR spectra of the three different doses of atorvastatin-treated and control A549 cells between 1270-781 $\text{cm}^{-1}$ . .....	33
Figure 3. 15. The FTIR spectra of the three different doses of pravastatin-treated and control A549 cells between 3685-2672 $\text{cm}^{-1}$ . .....	35
Figure 3. 16. The FTIR spectra of the three different doses of pravastatin-treated and control A549 cells between 1773-1479 $\text{cm}^{-1}$ . .....	35
Figure 3. 17. The FTIR spectra of the three different doses of pravastatin-treated and control A549 cells between 1275-764 $\text{cm}^{-1}$ . .....	36
Figure 3. 18. The FTIR spectra -of the three different doses of lovastatin-treated and control A549 cells between 3734-2837 $\text{cm}^{-1}$ . .....	38
Figure 3. 19. The FTIR spectra -of the three different doses of lovastatin-treated and control A549 cells between 1774-1476 $\text{cm}^{-1}$ . .....	38
Figure 3. 20. The FTIR spectra -of the three different doses of lovastatin-treated and control A549 cells between 1281-786 $\text{cm}^{-1}$ . .....	39
Figure 3. 21. The general FTIR spectrum of the lipid extract of A549 cells.....	42
Figure 3. 22. The FTIR spectra of the three different doses of lovastatin treated and non-treated lipid extracts of A549 cells. ....	45
Figure 3. 23. The FTIR spectra of the three different doses of atorvastatin treated and non-treated lipid extracts of A549 cells. ....	46
Figure 3. 24. The FTIR spectra of the three different doses of fluvastatin treated and non-treated lipid extracts of A549 cells. ....	46
Figure 3. 25. The FTIR spectra of the three different doses of pravastatin treated and non-treated lipid extracts of A549 cells. ....	47
Figure 3. 26. The FTIR spectra of the three different doses of rosuvastatin treated and non-treated lipid extracts of A549 cells. ....	47
Figure 3. 27. The FTIR spectra of the three different doses of simvastatin treated and non-treated lipid extracts of A549 cells. ....	48

<u>Figure</u>	<u>Page</u>
Figure 3. 28. The FTIR spectra of the doses of IC5 of statins treated and non-treated lipid extracts of A549 cells. ....	50
Figure 3. 29. The FTIR spectra of the doses of IC10 of statins treated and non-treated lipid extracts of A549 cells. ....	50
Figure 3. 30. The FTIR spectra of the doses of IC50 of statins treated and non-treated lipid extracts of A549 cells. ....	51

# CHAPTER 1

## INTRODUCTION

### 1.1. Cancer

Cancer is a very complicated genetic disease generally characterized by the aberrant mechanisms of cellular differentiation, cell survival, proliferation and death pathways in a specific tissue (Evan & Vousden, 2001). This aberrant cell differentiation appears as consequence of a series of mutations in oncogenes and/or tumor suppressor genes, which can be genetically inherited or gained by replication errors, environmental chemicals, carcinogens.

The exposure to tumor promoters such as oncoviruses, defective deoxyribonucleic acid (DNA) repair mechanism, epigenetic alterations and chromosomal aberrations with time transform the cells into a malignant phenotype (Zamay, et al., 2017; Pavlova & Thompson, 2016; Yu X. , Pan, Ma, & Li, 2013). These factors affect genome instability which cause many alterations including sustaining of proliferation signaling, evasion of growth suppressors, resisting to cell death, replication immortality, induction of angiogenesis, activation of invasion and metastasis, reprogramming of energy metabolism and evasion of immune destruction. These variations are called as hallmarks of cancer initiating malignant transformation (Fig.1.1).

In addition to these hallmarks deregulation of cellular energetics appears to be one of the most important characteristics in cancer development. (Yu X. , Pan, Ma, & Li, 2013; Hanahan & Weinberg, 2011).

### 1.1.1. Metabolic Reprogramming in Cancer Development

Although cancer is a genetic disease, malignant transformations that arise due to genetic level alterations on oncogenes and tumor suppressor genes result in metabolic reprogramming at the cell level.

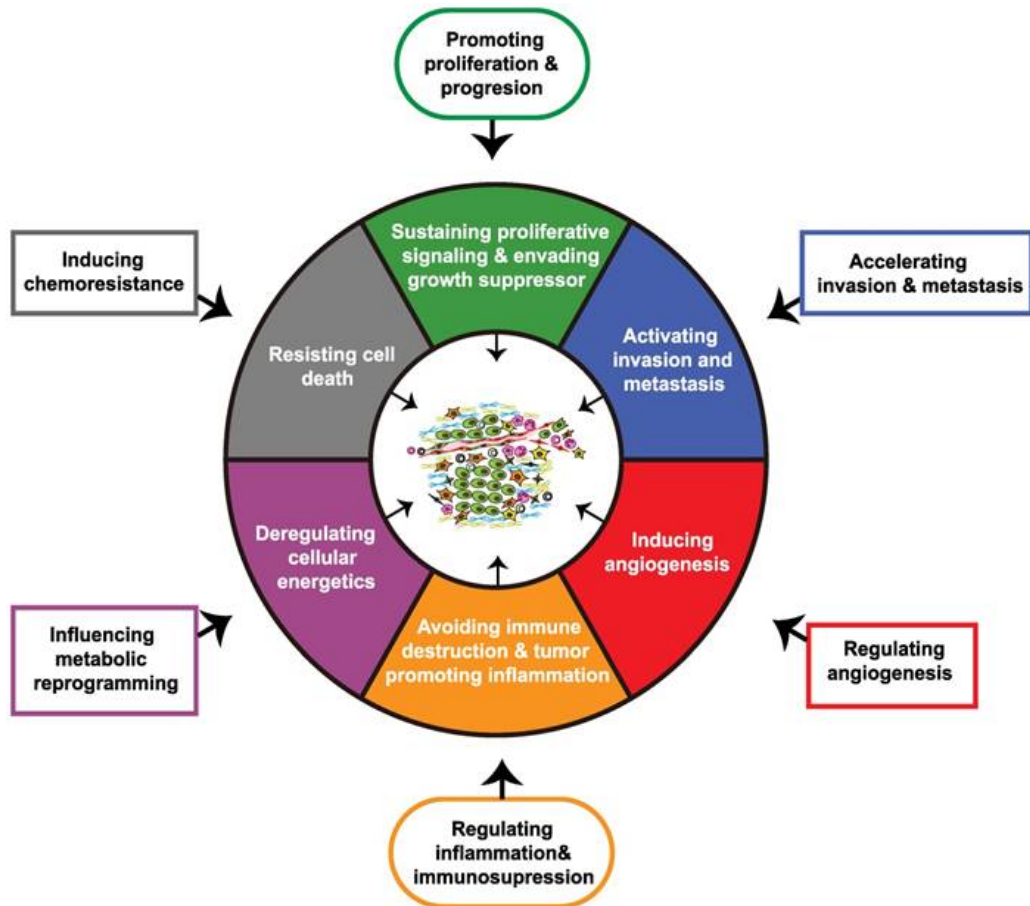


Figure 1. 1. Rearrangement of hallmarks of cancer (Source: Sun, et al., 2018)

These metabolic alterations change cancer cell biosynthetic and bioenergetics requirements. To maintain viability and construction of cell materials, they need to utilize environmental nutrients. Cancer cells overcome this problem by changing their metabolic and energetic status (Pavlova & Thompson, 2016).

The well-known and earliest adaptive metabolic alterations in tumors exacerbate glucose uptake and utilization of glycolysis leading to increased lactate production. These alterations are called by the Warburg effect (Warburg, Wind, & Negelein, 1927).

The other substantial metabolic changes induced by tumor formation include increased glutamine consumption for nitrogen-dependent biosynthesis (Nicklin, et al., 2009). One of the altered metabolic changes in tumor cell biology is the aberrant lipid metabolism and cholesterol-associated pathways (Beloribi-Djefafia, Vasseur, & Guillaumond, 2016).

### **1.1.2. Alteration of Lipid Metabolism in Cancer**

Major role of lipids are sustaining of membrane homeostasis and generation and normal function in cells (Beloribi-Djefafia, Vasseur, & Guillaumond, 2016). Imbalance of lipid metabolism cause abnormal expression of various genes, proteins, dysregulation of cytokines and signaling pathways and endoplasmic reticulum (ER) stress.

Altered lipid metabolism can lead to carcinogenesis and development of cancer as well as many human diseases including metabolic, immune and central nervous system disorders. Membrane lipid saturation reduces membrane fluidity and dynamics. This provides increased chemotherapy resistance. Highly proliferative cancer cells show increased uptake of exogenous (or dietary) lipids, endogenous lipid and cholesterol synthesis. The excessive amount of lipids and cholesterol are stored in lipid droplets (LDs). LDs give rise to resistance to chemotherapy in cancer cells and are now considered as hallmarks of cancer aggressiveness and be used for energy production in nutrient depletion (Zhang & Du, 2012; Baenke, Peck, Miess, & Schulze, 2013).

Changed lipid composition in cell membrane cause altered membrane fluidity and signal transduction. As a phenotype these alterations indicates increased expression of several proteins involved in lipid synthesis such as acetyl-CoA carboxylase (ACC), fatty acid synthase (FASN) and ATP citrate lyase (ACLY) in most tumors that promote cholesterol synthesis (Zhang & Du, 2012; Baenke, Peck, Miess, & Schulze, 2013).

## 1.2. The Lungs and Lung Cancer

The histology of the lungs and lung cancer was explained in section 1.2.1. and 1.2.2.

### 1.2.1. The Lungs

The lungs are composed of right and left lobes, surrounded by a thin membrane called pleura. They are located in the chest, a cone shaped organ as seen in the Figure 1.2.

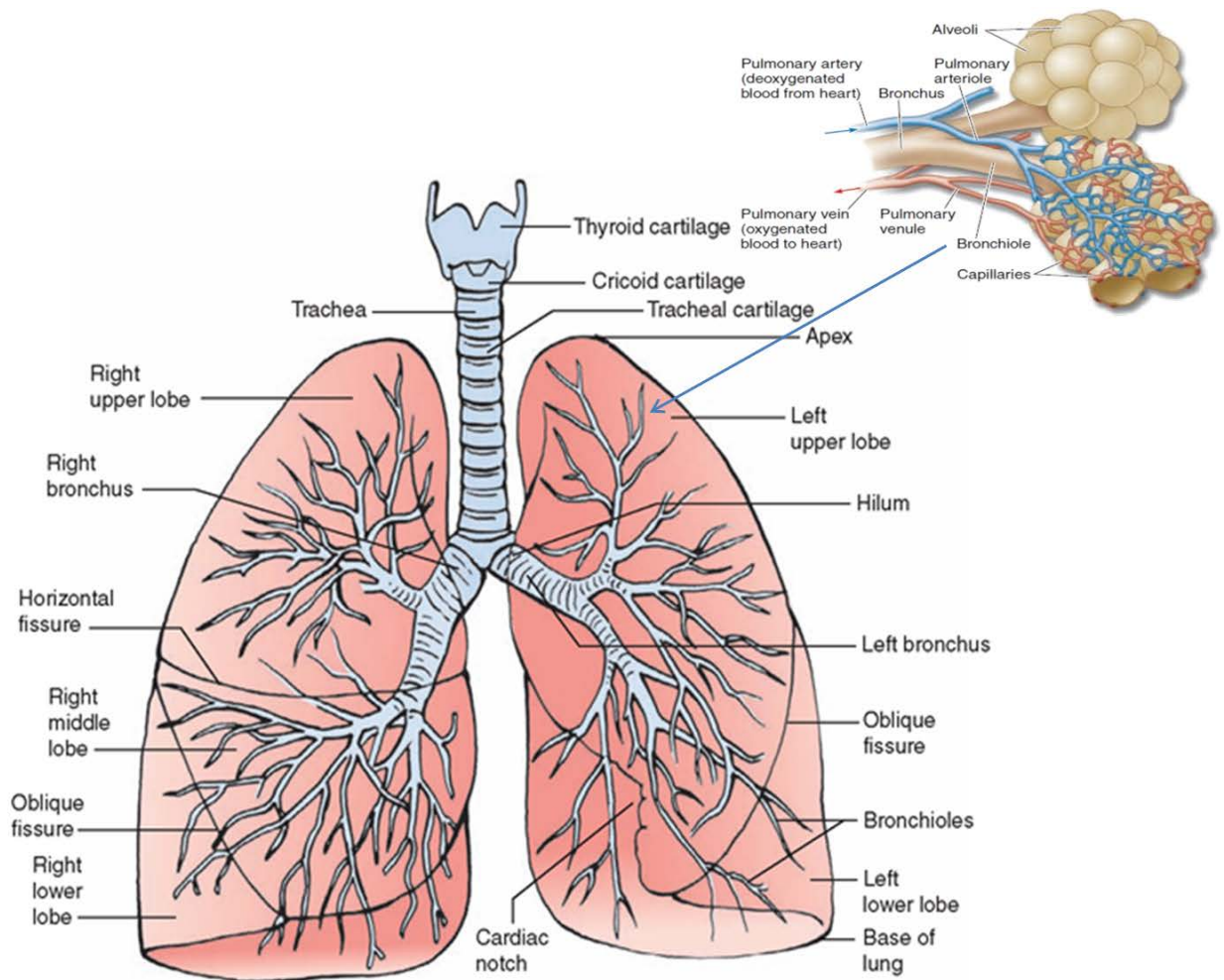


Figure 1. 2. The histology of the lungs (Anonymous).



The lungs have two main interdependent functions. Respiration is the primary function of the lungs. Delivering oxygen to the body and removing carbon dioxide that is produced by the body during inhalation. Another function of the lungs is host defense against airborne pathogens, chemicals and particles (Albertine, 2016). The cells of the human lungs are characterized with the three principal tissue compartments of the septum which are endothelium, epithelium, and interstitium. These compartments are respectively composed of squamous cells, type 1 and 2 epithelial cells and fibroblasts (Gehr, Bachofen, & Weibel, 1978).

### **1.2.2. Lung Cancer**

Lung cancer has the most incidence rate in all types of cancers and one of the most frequently causing to death in the worldwide, in Turkey as well (Yılmaz, et al., 2010; Yu X. , Pan, Ma, & Li, 2013). According to data of 2008, 1.6 million new cases of lung cancer occurred in worldwide that number equals to 13% of all cancer cases and also lung cancer responsible for 1.4 million people death (Özsu & Özlü, 2013). Main reason for lung cancer is smoking as well as radon, asbestos and arsenic exposure, air pollution and also reliant on occupationally and environmentally exposures, genetic factors and personal diet (TDD, 2010). Lung cancers are separated into two main groups according to view of under the microscope. Approximately 85% of lung cancers are called as non-small-cell lung cancers which are divided into three histological types namely, squamous cell carcinoma, adenocarcinoma, and large cell carcinomas shown in Figure 1.3. The second main type is called as small cell lung cancers which consist about 10% - 15% of lung cancers with invasive character. The other type responsible for 5% of lung cancer cases is lung carcinoid tumors also called as lung neuroendocrine tumors (Merino, et al., 2017). A549 cells have been initiated as a model of human alveolar cell carcinoma within the adenocarcinoma subgroup (Lieber, Simith, Szakal, Nelson-Rees, & Todaro, 1976). Early diagnosis can be crucial to treat and overcome the cancer therefore tissue or cell analysis is the key point for diagnosis in oncology. Traditionally, computed tomography (CT) and positron emission tomography (PET) imaging, histological examination of tumor biopsies, bronchoscopy, molecular marker

analysis in blood epidermal growth factor receptor (EGFR) and anaplastic lymphoma kinase (ALK), which are the driver mutations that have been identified, are used in lung cancer diagnosis (Mason, Murray, Nadel, & Gotway, 2015; Wang, Shen, Sheng, Chen, & Liu, 2014; Shim, et al., 2017).

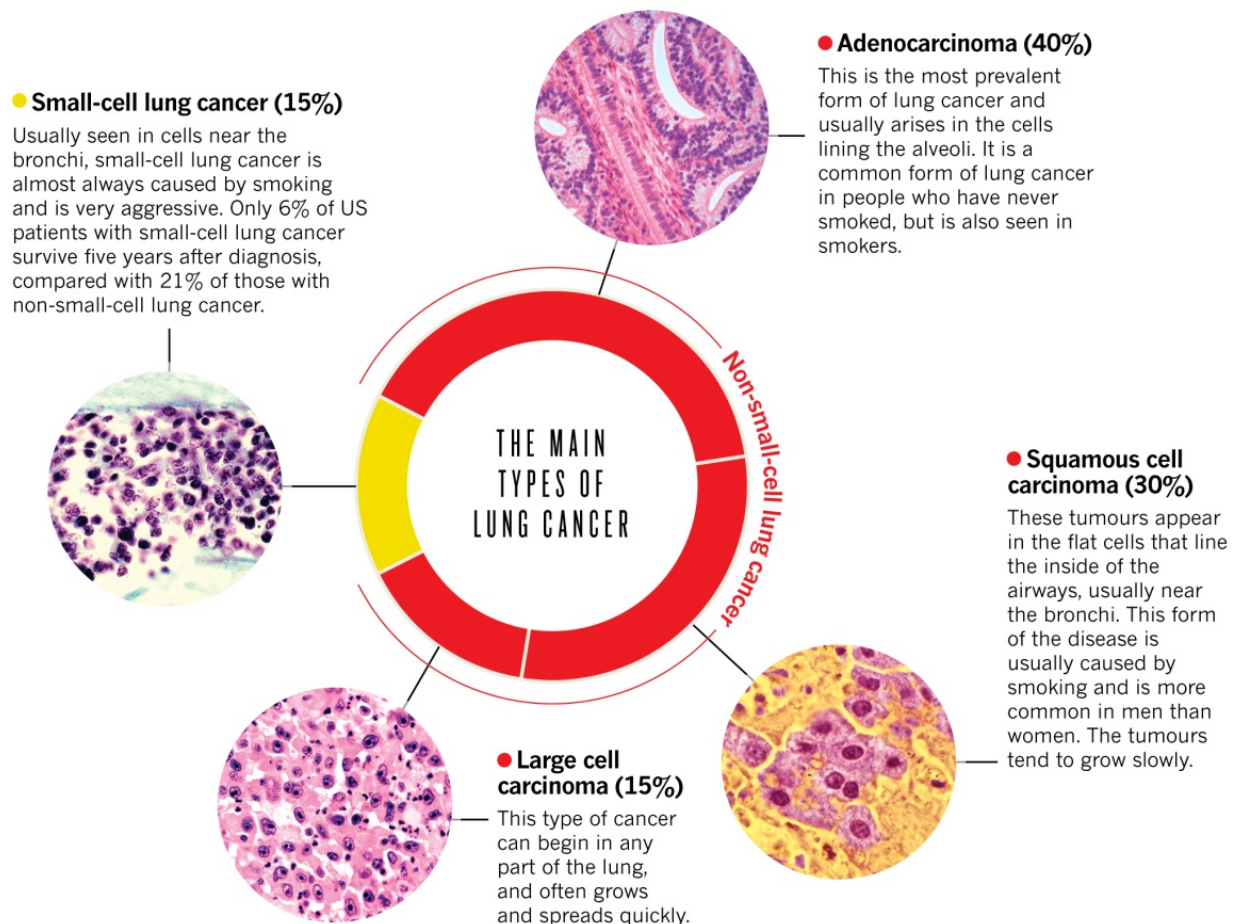


Figure 1. 3. The types of lung cancer (Source: Howlader, et al., 2017)

### 1.2.3. Lung cancer and lipid metabolism

The accumulation of lipid synthesis in cancerous tissues might be due to its contribution to cancer cell energy metabolism and cell structure component production. According to clinical studies tumorous lung tissues show significant accumulation of total cholesterol and esterified cholesterol stored in cells. Cholesterol is possibly needed

for its structural role in new membrane synthesis. Cancer cells have increased rates of membrane synthesis to support high proliferation rates. These ideas are supported by elevated acyl-cholesterol acyltransferase (ACAT) expression levels and other lipogenic enzymes in hyperplastic and neoplastic growth as well (Dessi, et al., 1992). Since lipid molecules and their intermediates actively take roles in essential cell metabolism, signaling, modulation of inflammation and vascular regulation, cell proliferation, adhesion and migration. Changes of lipid metabolism in cell affect both cardiovascular diseases and tumor development, invasion and metastasis (de Cedrón & de Molina, 2016).

### **1.3. The Mevalonate Pathway and Cholesterol Synthesis**

Cholesterol is an essential molecule for whole cells. It is needed in new membrane synthesis since it is one of the major constituent of cell membranes. It also is responsible for signal transduction via lipid rafts within plasma membrane microdomains. In addition to these functions, cholesterol is precursors of steroid hormones, bile acids, and some vitamins. Cholesterol is synthesized at the end of the mevalonate pathway. Firstly 3-hydroxy-3-methylglutaryl-CoA (HMG-CoA) is formed from acetyl coenzyme A and acetoacetyl-CoA catalyzed by HMG-CoA synthase. Then, HMG-CoA is converted to mevalonate by rate-limiting enzyme 3-hydroxy-3-methylglutaryl-CoA reductase (HMG-CoAR). Subsequently mevalonate is converted farnesyl pyrophosphate (FPP), squalene and cholesterol in several steps, respectively. Overview the mevalonate pathway is presented in Figure 1.4. Cholesterol homeostasis is controlled by *de novo* cholesterol synthesis, cellular influx, and cellular efflux (Goldstein JL, 1990).

### **1.4. Statins**

Statins are one class of anti-cholesterolemic drugs which are called 3-hydroxy-3-methyl-glutaryl-Coenzyme A (HMG-CoA) reductase inhibitors as well. HMG-CoA reductase catalyses mevalonate formation by removing CoA from HMG-CoA. In this

rate-limiting step, a four-electron oxido-reduction occurs responsible for cholesterol and other isoprenoids synthesized (Friesen & Rodwell, 2004).

Statins have similar structure with HMG-CoA to bind and occupy the active site of the enzyme. Statins are competitive inhibitors for this enzyme and their mechanism aims to reduce cholesterol in plasma and cellular levels (Tobert, 2003). The chemical structure of statins are shown in Figure 1.5.

All statins have the common dyslipidemic mechanism of action, they have distinct chemical structures, pharmacokinetic profiles and their efficacies. These chemical differences create different water solubility behavior that affects absorption, distribution, metabolism and excretion for each statin. Lovastatin, pravastatin and simvastatin are derived from fungal metabolites with elimination half-lives of 1 to 3 hours. Atorvastatin, fluvastatin and rosuvastatin are synthetic compounds their elimination takes 1 and 19 hours in clinic respectively.

Although atorvastatin, simvastatin, fluvastatin and lovastatin have relatively lipophilic characters as a consequence of polar hydroxyl group and metabolize with cytochrome P450 enzymes, pravastatin and rosuvastatin have hydrophilic characters due to methane sulfonamide group and their metabolized with cytochrome P450 enzymes are more difficult (Schachter, 2005; Gaw, Packard, & Shepherd, 2003). Rosuvastatin showed the most effective reducing properties against low-density lipoprotein cholesterol (LDL-C) in clinical studies but, it has not been studied in terms of its antiproliferative effects on A549 cells.

Several (pre) clinical studies have been done to investigate the potential beneficial effects of statins in A549. This study showed that statins can be given to cancer cells in relatively high dosages. In addition, although some of the statins have been studied in terms of their antiproliferative effects on various cell cultures including A549 cells the results reported have been contradictory (Schachter, 2005). Statins along with reducing of LDL-cholesterol, responsible for increasing high-density lipoprotein cholesterol (HDL-C) and diminishing triglyceride concentration. This class of drugs regarded as a safe and well-tolerated for hypercholesterolemia treatment (Furberg & Pitt, 2001). Statins bind to active site of the enzyme sterically then undergoes a rearrangement. Statin-enzyme binding effectiveness differs for six statins because of their binding modes.

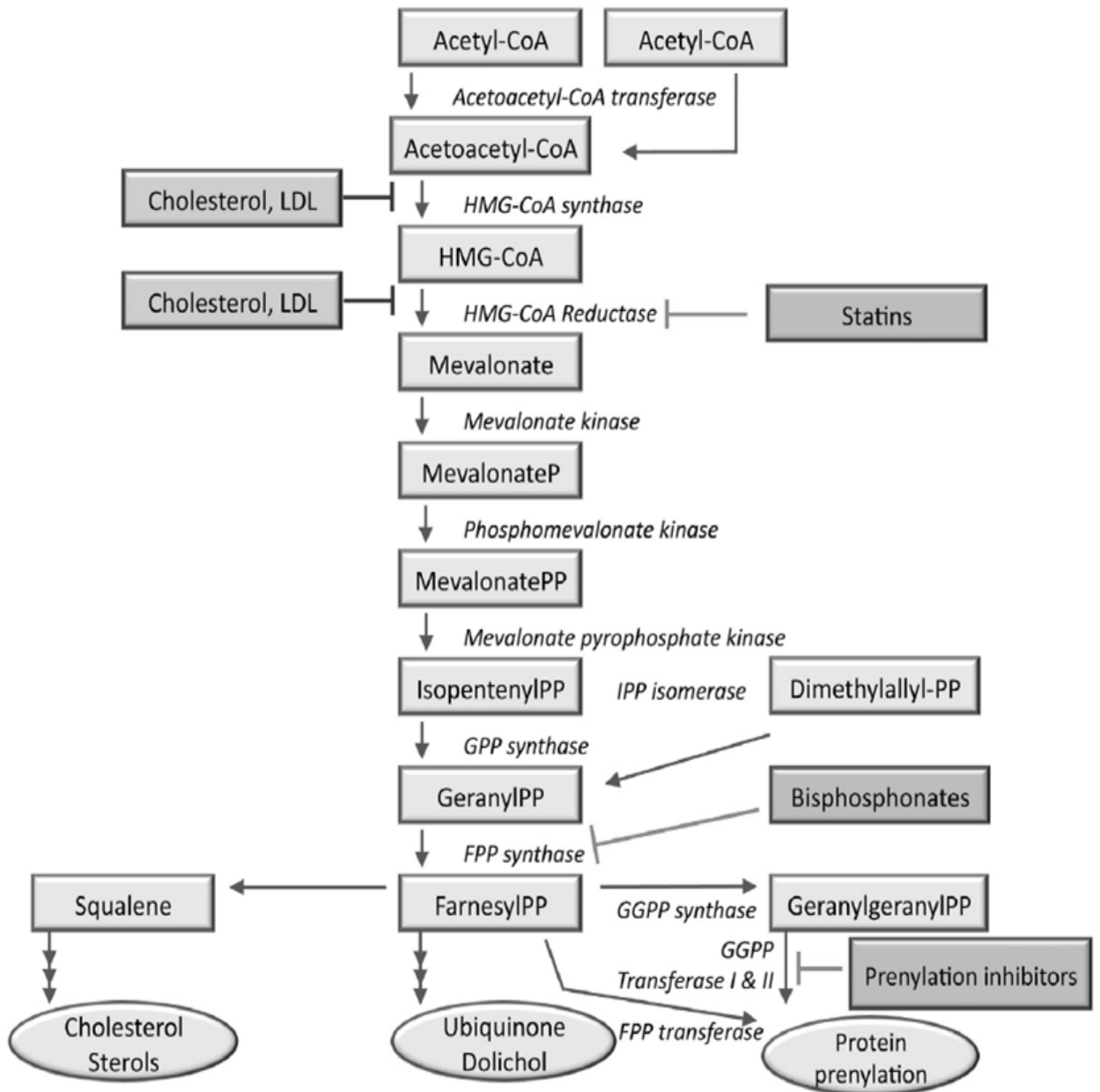


Figure 1. 4. Overview of the mevalonate pathway and its blockage by statins  
 (Source: Likus, et al., 2016)

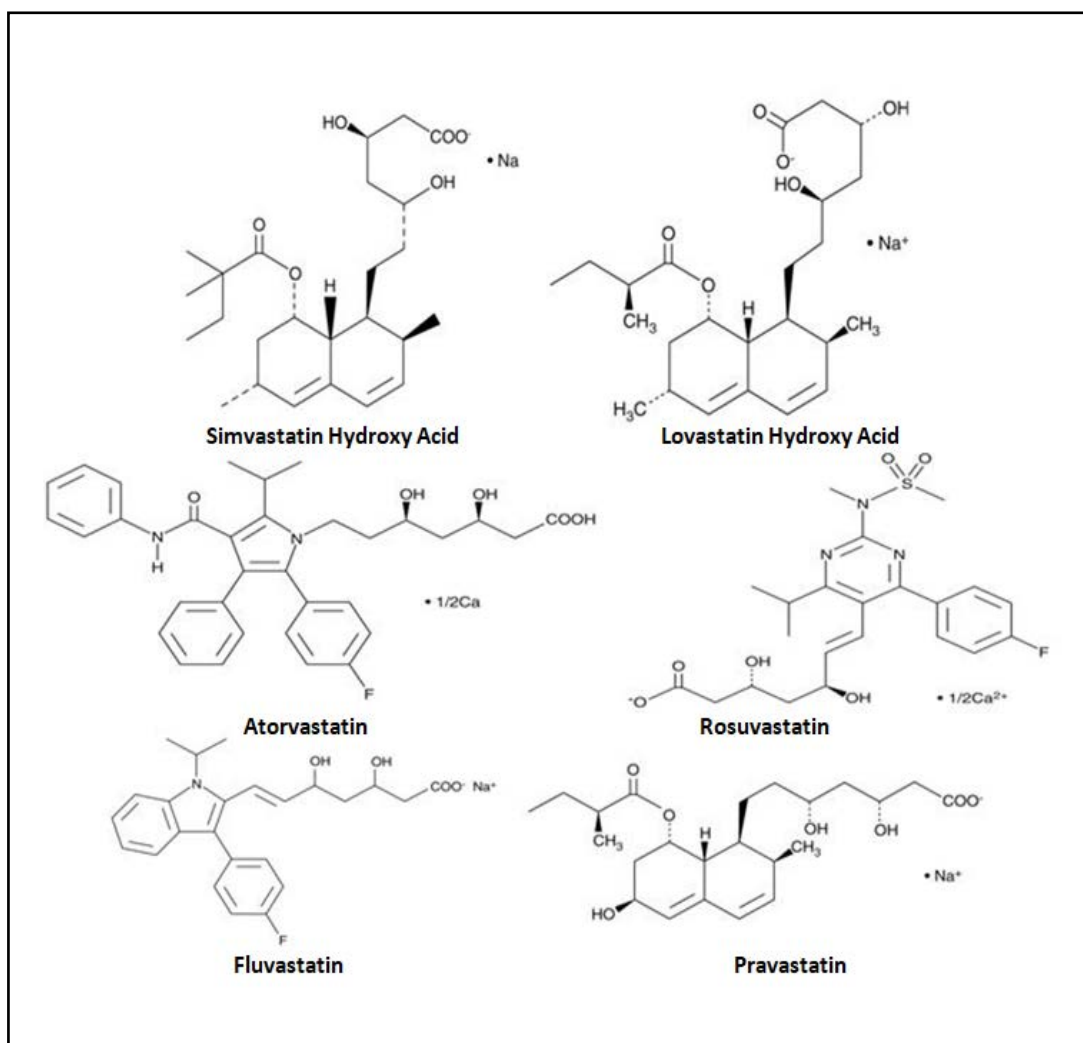


Figure 1.5. Molecular structures of the statins.

## 1.5. Fourier Transform Infrared (FTIR) Spectroscopy

Fourier Transform Infrared (FTIR) spectroscopy is a rapid, sensitive and non-destructive vibrational spectroscopic method that monitors the global chemical composition of the sample (Wu, et al., 2015). The technique is widely used in many research areas such as biochemistry, biomedicine, biophysics and biomaterials to investigate structural components of biosamples (Lin, Li, & Cheng, 2007; Farhadi, Kobarfard, & Shirazi, 2016). It is used in the analysis of biological systems in any physical state providing molecular fingerprints of tissues and cells (Yandim, Ceylan, Elmas, & Baran, 2016). It is a valuable analytical technique for detection of metabolic

changes in cells such as proteins, carbohydrates and nucleic acids at the level of functional groups due to the fact that materials have different infrared absorptions and show different vibrations according to their chemical bonds at the suitable wavelength (Yandim, Ceylan, Elmas, & Baran, 2016; Ceylan, Camgoz, & Baran, 2012). In addition to the characterization of the chemical nature of cellular molecules, it also accounts for conformational changes to various molecular-functional groups (Derenne, Gasper, & Goormaghtigh, 2011). IR spectra as well allow to determine changes between normal and cancerous cells used as a diagnostic tool in medicine. It is used for bacteria classification and identification of new species (Helm, Labischinski, Schallehn, & Naumann, 1991; Naumann, Helm, & Labischinski, 1991; Cohenford & Rigas, 1998). The technique qualitatively and quantitatively investigates shifts in peak positions, changes in bandwidths and band intensities acquiring structural and functional information which offers the opportunity to examine rapid treatment induced during metabolic modifications. This technique can be also used to determine mode of actions of drugs which presents a unique fingerprint of characteristic effects of agents on molecules (Derenne, Gasper, & Goormaghtigh, 2011). Frequencies in a continuous range stand for electromagnetic spectrum which is shown in Figure 1.6. The lowest energy photons associated with the longest wavelength,  $\lambda$ , and with the lowest frequency,  $\nu$ . The area of radio waves is characterized by nuclear magnetic resonance (NMR). Should photons have the highest energy related with the shortest wavelength,  $\lambda$ , and with the highest frequency,  $\nu$ , they are characterized by X-rays and Gamma-rays (Bellisola & Sorio, 2012).

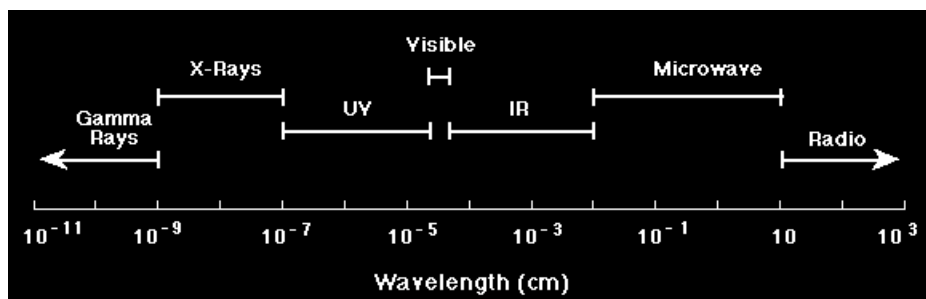


Figure 1.6. A representation of the electromagnetic spectrum.

IR spectroscopy measures the vibrational energies of molecules dependent on the absorption of electromagnetic radiation (waves). When sample is radiated by IR light in the IR spectroscopy, electrical dipole moments of induced vibrations are detected (Fig.1.7). Related to the molecular structure of samples, absorption of IR radiation shows different vibrations such as stretching, bending, deformation or their combined vibrations (Lin, Li, & Cheng, 2007).

The infrared region of the spectrum is divided into three infrared radiation regions which are far infrared (in the wavenumber range  $400\text{-}100\text{ cm}^{-1}$ ), mid infrared (in the wavenumber range  $4000\text{-}400\text{ cm}^{-1}$ ), and the near infrared (in the wavenumber range  $14285\text{-}4000\text{ cm}^{-1}$ ), in which wavenumber represent  $1/\lambda$  (cm) (Salman, 2003). Spectral biodiagnosis of biosamples is mostly based on the mid-IR range of spectrum within  $4000\text{-}600\text{ cm}^{-1}$  (Lin, Li, & Cheng, 2007).

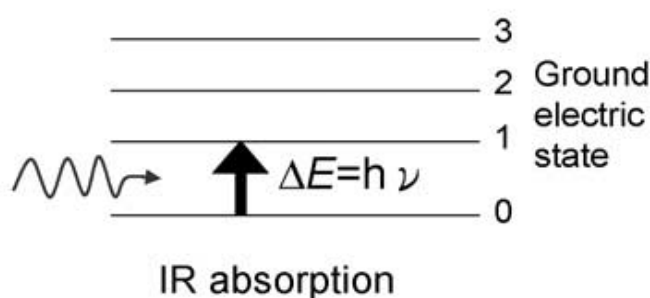


Figure 1.7. Virtual energy levels for IR spectroscopy (Source: Lin, Li, & Cheng, 2007)

IR absorption happens during the molecules dipole moment changing on their covalent bonds. Vibration separates into two primary modes *stretching* and *bending*. There are two types of bond stretching and four types of bond bending. Named as symmetric and asymmetric stretch and in-plane rocking, in-plane scissoring, out-of-plane wagging and out-of-plane twisting respectively (Fig.1.8.).



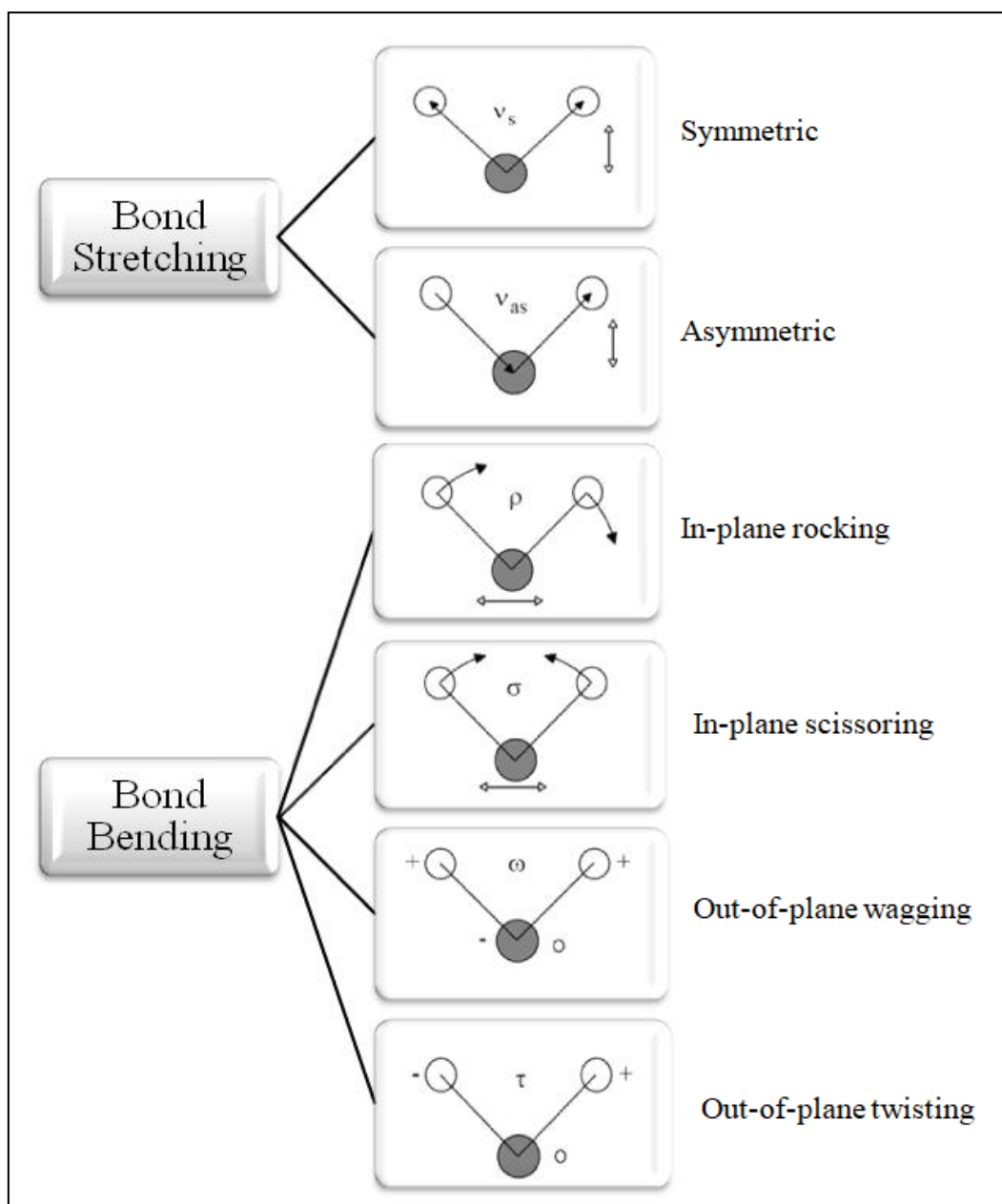


Figure 1. 8. The types of molecular vibrations.

## 1.6. Hypothesis

Since statins have different chemical structures and physicochemical properties, their anti-proliferative, structural, metabolic and dyslipidemic effects on cancer cells should be different. Therefore, it is necessary to carry out a research study for a comparison of the aforementioned properties. We suggest

that there be dose-dependent and statin-dependent changes in the lipidation status of A549 cells upon statin treatment. The lipidation status of the cells is approached by FTIR spectroscopic peak ratios and changes and band shifts and widths. The anti-proliferative effects of statins are examined by MTT assay. The changes in the lipids are examined by FTIR spectroscopy of the lipid extracts of A549 cells. The other structural-metabolic changes are also examined by FTIR spectroscopy as well.

## CHAPTER 2

### MATERIALS AND METHODS

#### 2.1. Chemicals

Statins (Lovastatin Hydroxy Acid (sodium salt), Simvastatin (sodium salt), Atorvastatin (calcium salt), Rosuvastatin (calcium salt), Fluvastatin (sodium salt), Pravastatin (sodium salt)) was purchased from Cayman chemicals. The stock solutions of each statins was prepared in dimethyl sulfoxide (DMSO) at concentrations of 20 mM, stored at -20 °C and diluted in cell culture medium. Penicillin-streptomycin, DMEM-high glucose with L-glutamine, fetal bovine serum (FBS) and phosphate buffered saline (PBS), trypan blue solution, DMSO, thiazolyl blue tetrazolium bromide 98% and potassium bromide (KBr) were obtained from Sigma-Aldrich (USA). Methanol and chloroform were obtained from Merck.

#### 2.2. Cell Culture

A549 cells were obtained from İBG-Dokuz Eylül University. Cells were cultured in high glucose DMEM supplemented with L-glutamine and 10% fetal bovine serum and 1% penicillin-streptomycin in an atmosphere of 5% CO<sub>2</sub> at 37 °C. When the cell confluence reached at 80%, a new cell passage was carried out.

##### 2.2.1. Cell Passaging

Cell medium on the flask surface was removed and flask was washed with 5 mL medium to remove any residual. Then preheated to 37 °C 1 ml of trypsin (0.25%) was added to flask and incubated at 37 °C in 5% CO<sub>2</sub> incubator for 5 minutes. After the incubation period, cell suspension was transferred into a sterile falcon tube with 4 mL

complete media and was centrifuged 5 minutes at 800 rpm. The supernatant was removed and the pellet was re-suspended in growth medium. Next, the cells were counted on Thoma cell counting chamber with trypan blue solution. Finally, the cells were seeded on new flask with fresh medium and separated for test incubated at 37 °C in 5% CO<sub>2</sub> incubator.

### **2.2.2. Cell counting**

To count cells for analysis, the trypsinized cells were subjected to typrhan blue staining (90 µl for each 10 µl sample) then 10 µL stained sample was examined in Thoma cell counting chamber under an inverted cell culture microscope (Leica DM IL LED).

### **2.2.3. Freezing Cells**

Cells were detached from cell culture flasks as described above and centrifuged at 500 rpm for 4 minutes. After removing the supernatant, the pellet was dissolved in growth medium including 10% DMSO and later aliquoted in 1 mL cryotubes, then stored at -80 °C.

### **2.2.4. Thawing Cells**

Vials of frozen A549 cells were taken from -80 °C and transferred to 37 °C water bath for thawing in 2-3 minutes. After the cells were transferred to falcon tube and centrifuged at 500 rpm for 4 minutes. Then the supernatant was removed and pellet was dissolved with new media, it was supplemented with fresh DMEM with 10% fetal bovine serum and 1% penicillin-streptomycin. These cells were added to T25 cell culture flasks and incubated in incubator at 37 °C with 5% CO<sub>2</sub>.

### **2.2.5. Measurement of Cell Viability by MTT Assay**

Anti-proliferative effects of statins on A549 cells were determined by MTT cell proliferation assay. MTT (3-[4,5-dimethylthiazol-2-yl]-2,5-diphenyltetrazolium bromide) is a yellow auxiliary agent that reduced purple formazan crystals in living cells by their active mitochondria. 5000 cells were seeded on each well of 96 well-plate with growth medium and incubated at 37 °C and in 5% CO<sub>2</sub> for 24h-48h until gained normal morphology. Then they were treated with different concentrations of each statins. 5 µL of each concentration was added to wells for triplicate assay. The last concentration was completed to 100 µL. Following this, they stayed for 48 hours at 37 °C in a 5 % CO<sub>2</sub> supplemented incubator. 10 µL of MTT solution (5 mg/mL in PBS) was added to each well and incubated at 37 °C for 4 hours in the carbondioxide incubator. Then, the plate was centrifuged at 1800 rpm for 10 minutes and supernatant was removed. 150 µL DMSO was added into each well to dissolve the formazan crystals and kept on shaker at 130 rpm for 10 minutes. Finally, the absorbance values were measured at 570 nm by a spectrophotometer (Thermo Electron Corporation Multiskan Spectrum, Finland). The number of statin treated living cells and control groups was directly proportional to the intensity of the purple product.

### **2.3. Preparation of Statins**

Firstly, 1, 5, 10, 25, 50, 100, 150, 200, 300 and 400 µM concentration of atorvastatin, fluvastatin, lovastatin, rosuvastatin, simvastatin and pravastatin were prepared in DMSO as the stock solution for each statin with a concentration of 20 mM. The serial dilutions of each statin were prepared based on this stock solution in DMEM. Later, they were incubated for 48 hours at 37 °C an incubator with 5 % CO<sub>2</sub> concentration.

## **2.4. Sample Preparation for FTIR Spectroscopy**

Samples were prepared two steps with freeze drying and lipid extraction.

### **2.4.1. Samples Preparation for Freeze Drying**

In order to prepare the cells for FTIR spectroscopy,  $3 \times 10^4$  cells supplemented with 600  $\mu\text{L}$  of growth medium were seeded into 24 well-plates each well incubated and incubated for 48 hours, and the cells were treated with 3 consecutive concentrations determined before via cell viability test (MTT) at  $\text{IC}_{50}$ , the fifth of  $\text{IC}_{50}$  and the tenth of  $\text{IC}_{50}$  values of each statins. After the incubation period, the cells were washed with 500  $\mu\text{L}$  PBS were treated with 100  $\mu\text{L}$  trypsin and incubated for 5 minutes at  $37^\circ\text{C}$  in the carbon dioxide incubator. Later, the cells collected in eppendorf tubes by centrifugation at  $130 \times g$  for 5 minutes. The supernatants were discarded and, the pellets were washed with 500  $\mu\text{L}$  PBS for twice. To remove the water in the cells they were freeze-dried overnight by Labconco FreeZone lyophilizator under 4.0 Pa and at  $-57^\circ\text{C}$ . The cell powder was mixed with dried potassium bromide (KBr) in a mortar (at a ratio of 1:100). The mixture was then pressurized to  $100 \text{ kg/cm}^2$  (1200 psi) for 5 minutes prior to the FTIR experiments.

### **2.4.2. Lipid Extraction**

For lipid extraction from the cells,  $3 \times 10^4$  cells were seeded into 24 well-plates and incubated for 48 hours, and the cells were treated with three concentrations determined before MTT at  $\text{IC}_{50}$ , the fifth of  $\text{IC}_{50}$  and the tenth of  $\text{IC}_{50}$  values of each statins. Following the incubation period, the cells were washed with 500  $\mu\text{L}$  PBS then were treated with 100  $\mu\text{L}$  trypsin and incubated for 5 minutes at  $37^\circ\text{C}$  in 5 %  $\text{CO}_2$ . The cells collected by centrifugation in eppendorf tubes at  $130 \times g$  for 5 minutes. After the supernatants were removed, the pellets were washed with 500  $\mu\text{L}$  PBS for twice. The cell pellets were homogenized with 600  $\mu\text{L}$  of extraction mixture containing chloroform/methanol (2:1, v/v) via vortexing. The mixture was incubated for 20 minutes at the room temperature. Following the incubation period, 180  $\mu\text{L}$  double-distilled water was added into the each of mixture, homogenized with vortexing and

centrifuged at 500 x g for 10 minutes. At the end of the centrifugation, the upper phase was removed by siphoning (includes gangliosides or small organic polar molecules). 20  $\mu$ L lipid extract was put on the ATR-FTIR diamond. After the solvent was evaporated the spectra was recorded.

## 2.5. FTIR Spectrum Data Analyses

For the lyophilized samples, the spectral analysis was performed by using a Perkin-Elmer spectrometer equipped with MIR TGS detector (Spectrum 100 Instrument, Perkin Elmer). The FTIR spectra of the samples were recorded between 4000 and 450  $\text{cm}^{-1}$  region. The interferograms were recorded with 20 scans at 4  $\text{cm}^{-1}$  resolution against the pure potassium bromide was used as a background. Each sample was studied in triplicates.

For the lipid extracts, the spectral analysis was performed by using a Perkin-Elmer Attenuated total reflectance Fourier transform infrared spectrometer equipped with diamond/ZnSe crystal (UATR Two, Perkin Elmer). FTIR spectra of the samples were recorded between 4000 and 450  $\text{cm}^{-1}$  region. The interferograms were recorded with 20 scans at 2  $\text{cm}^{-1}$  resolution against the background. Each sample was studied in triplicates. Spectrum 100 (Perkin-Elmer) software was used for all of the data manipulations. The triplicates with least two different scans were performed which gave identical spectra. These replicates were averaged and the averaged spectra for each sample were then used for further data manipulation and statistical analysis. For the visual inspection, the averaged spectra were interactively baselined from three arbitrarily selected points. Finally, the baselined spectra were normalized in specific regions for visual comparison of the samples for the studied parameters and control samples. Spectral mathematical manipulations (as the baseline corrections, smoothing, and deconvolution) and statistical parameters (such as peak frequency shifts and intensity ratios of various infrared bands) were calculated using Perkin Elmer software 1B version 3.02.

# CHAPTER 3

## RESULTS

### 3.1. Antiproliferative Effects of Statins on A549 Cells

To assess the antiproliferative effects of statins on A549, the cells were treated with increasing concentrations of statins (1, 5, 10, 25, 50, 100, 150, 200, 300 and 400  $\mu\text{M}$ ) for 48 hours and MTT cell proliferation assay was conducted.

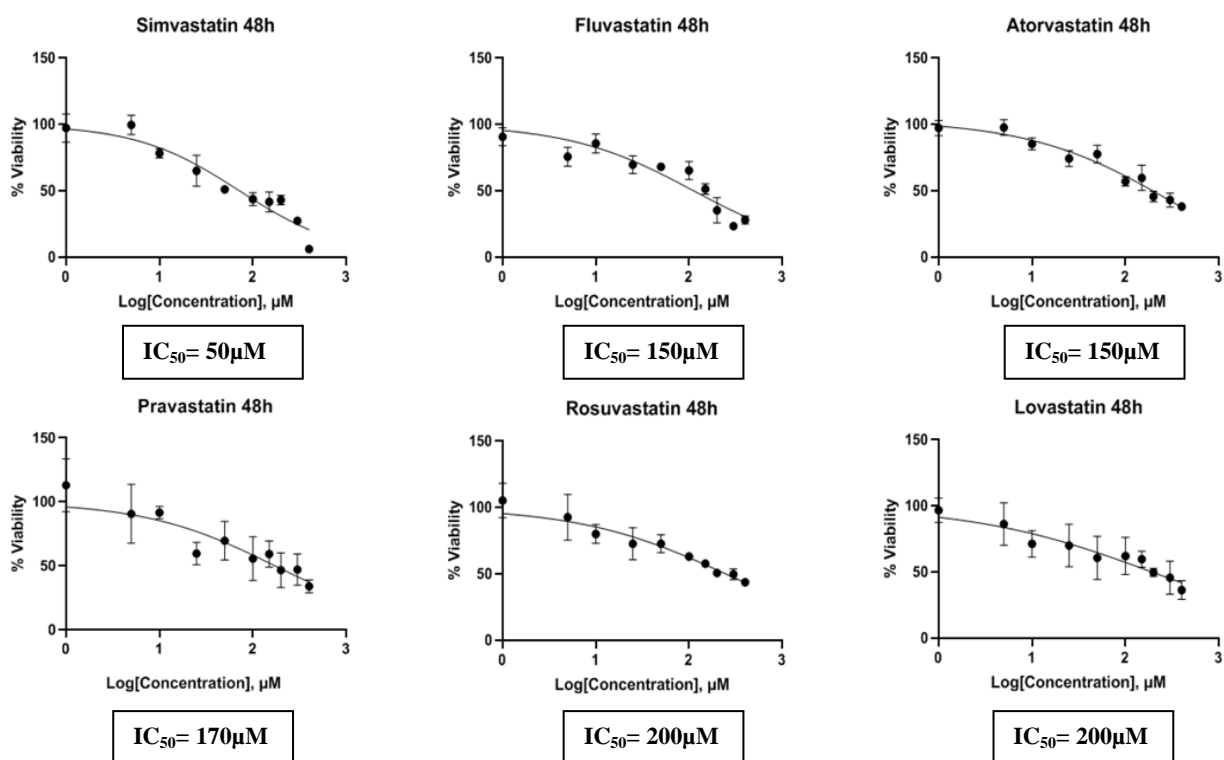


**Figure 3. 1.** The cytotoxicity profiles of statins on A549 cells.



The results indicated that A549 cells showed dose-dependent decreasing cell proliferation response as compared to untreated controls. The  $IC_{50}$  values for each statins were found as shown in Figure 3.1. These values are 150  $\mu$ M for atorvastatin and pravastatin, 200  $\mu$ M for rosuvastatin and lovastatin, 50  $\mu$ M for simvastatin, and 170  $\mu$ M for fluvastatin. The proliferation curves are shown in Figure 3.1.

### 3.2. The Effects of Statins on A549 Cells Studied by FTIR Spectroscopy

The FTIR technique investigates several different biological systems including cancer cells at the molecular and functional group level, it provides useful information about the structure and function of macromolecular structural constituents of the cancer cells such as lipids, nucleic acids, proteins and carbohydrates (Wong, Wong, Caputo, Godwin, & Rigas, 1991).

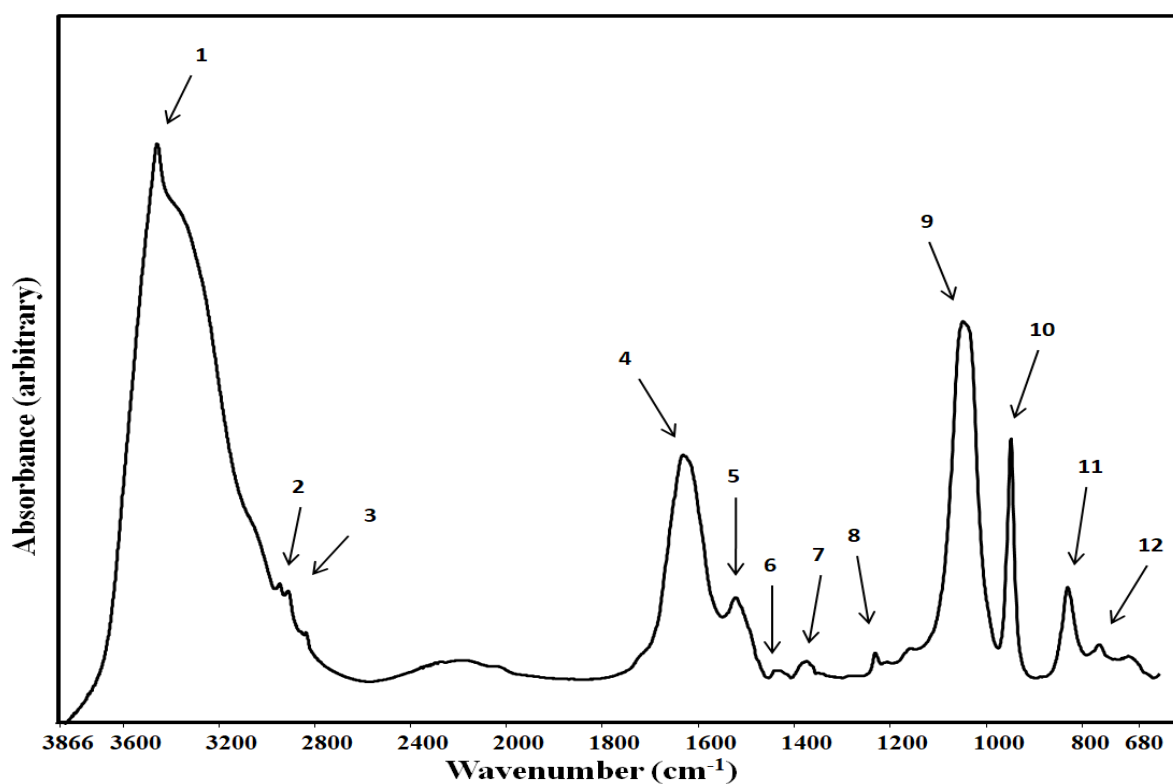


Figure 3. 2. The general FTIR spectrum of A549 cells.

**Table 3. 1.** The general FTIR band assignments of A549 cells.

<b>Band Number</b>	<b>Wavenumber (cm<sup>-1</sup>)</b>	<b>Definitions of The Spectral Assignments</b>	<b>References</b>
1.	3465	Amide A: mostly N-H stretching of proteins, cholesterol and phospholipids, CH <sub>2</sub> stretching vibrations.	(Lieber, Smith, Szakal, Nelson-Rees, & Todaro, 1976)
2.	2963	CH <sub>3</sub> asymmetric stretching vibrations, mostly found in fatty acids of cells and protein component.	(Malek, Wood, & Bambery, 2014)
3.	2929	CH <sub>2</sub> symmetric stretching of saturated lipids and side chains of proteins.	(Farhadi, Kobarfard, & Shirazi, 2016; Malek, Wood, & Bambery, 2014)
4.	1655	Amide I: Stretching of carbonyl group from peptide bond (C = O stretch + NH bend) especially sensitive to the protein secondary structure.	(Wu, et al., 2015; Derenne, Gasper, & Goormaghtigh, 2011)
5.	1547	Amide II (NH bend + C-N): Protein amide N-H bond deformation, (60%) come from amide N-H bending vibrations, (40%) coupled to C-N stretching vibrations.	(Derenne, Gasper, & Goormaghtigh, 2011)
6.	1457	Resulting from many amino acid side chains, fatty acids; CH <sub>2</sub> bending: mostly come from lipids, with the least contributed proteins, asymmetric bending of CH <sub>3</sub> : methyl groups of proteins	(Yandim, Ceylan, Elmas, & Baran, 2016; Wu, et al., 2015)

(cont. on next page) 22

Table 3.1 (cont.).

7.	1401	COO <sup>-</sup> symmetric stretching; derived from many amino acid side chains and fatty acids	(Malek, Wood, & Bambery, 2014)
8.	1260	Characteristic of the asymmetric PO <sup>-2</sup> (phosphodiester) stretching absorptions of nucleic acids, with little contributions from PO <sup>-2</sup> groups of phospholipids	(Liu, Jackson, Sowa, Ju, Dixon, & Mantsch, 1996)
9.	1082	Symmetric PO <sup>-2</sup> stretching absorptions of nucleic acids with minimal contributions from PO <sup>-2</sup> groups of phospholipids, lower wave numbers might indicate a tighter phospholipid structure of the cell membrane	(Liu, Jackson, Sowa, Ju, Dixon, & Mantsch, 1996; Farhadi, Kobarfard, & Shirazi, 2016)
10.	984	Vibrations of PO <sub>4</sub> group absorptions obtain from carbohydrates and phosphates particularly phosphate groups linked with nucleic acids (DNA and RNA)	(Fung, Senterman, Mikhael, Lacelle, & Wong, 1996)
11.	867	A-form of DNA, helix conformation	(Dovbeshko, et al., 2002)
12.	801	C-N-C stretching of ribose- phosphate skeleton, Z formation of DNA	(Malek, Wood, & Bambery, 2014)

Therefore, the technique was used for the analysis of the structural alterations on A549 cells in this study. Figure 3.2. shows the average FTIR spectrum of A549 cells. The assignments of the major bands in Figure 3.2 are given in Table 3.1. The FTIR spectrum of A549 cells consists of several bands indicative of many functional groups of macromolecules and lipids. The spectra can be analysed in separate sections: 3700-2800  $\text{cm}^{-1}$  for the analysis of proteins and lipids, and 1595-1775  $\text{cm}^{-1}$  for the analysis of proteins and lipids, 940-1480  $\text{cm}^{-1}$  for the analysis of the fingerprint region containing bands originating from nucleic acids, lipids, proteins and carbohydrates. All the spectra presented are baselined and then normalized with respect to selected bands for all the control and the treated cells.

### **3.2.1. The Effect of Rosuvastatin on A549 Cells Studied by FTIR Spectroscopy:**

The average FTIR spectra of the A549 cells treated with rosuvastatin the 3768 and 2608  $\text{cm}^{-1}$  region is given in Figure 3.3. Amide A and amide B bands are found in this spectral region. They both have contributions from mainly the N–H stretching of proteins with a small contribution from the O–H stretching of polysaccharides and intermolecular H bonding and contributions from C–N and N–H stretching of proteins, respectively. Rosuvastatin treatment induced remarkable changes in the band width, intensity, and frequency value of the FTIR bands in this region as seen from Fig. 3.3. The C–H stretching vibrations of aliphatic compounds are populated between 2996 and 2840  $\text{cm}^{-1}$  as shown in Fig. 3.3. As seen the same figure the intensities of the aliphatic chains increase upon the rosuvastatin treatment.

The average FTIR spectra of the rosuvastatin-treated A549 cells in the 1777 – 1481  $\text{cm}^{-1}$  spectral region is shown in Figure 3.4. The band/shoulder centered around 1740  $\text{cm}^{-1}$  is assigned to C=O ester stretching vibration of triglycerides and cholesterol esters. The band between 1700 and 1600  $\text{cm}^{-1}$  belongs to proteins (Amide I band) and the band between 1600 and 1500  $\text{cm}^{-1}$  belongs to proteins again (Amide II band) (Derenne, Gasper, & Goormaghtigh, 2011; Wu, et al., 2015). As seen in the figure, the intensity of the band did not show significant changes upon rosuvastatin treatment with dose dependent changes.

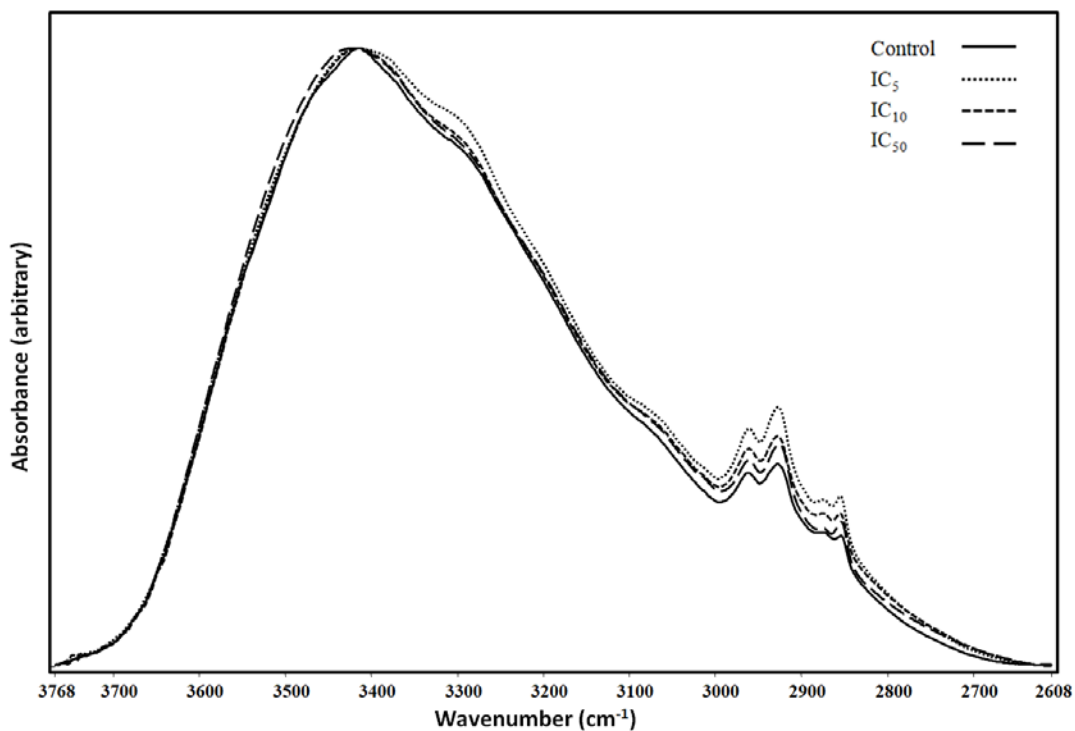


**Figure 3. 3.** The FTIR spectra of the three different doses of rosuvastatin-treated and control A549 cells between 3768 and 2608 cm<sup>-1</sup>.

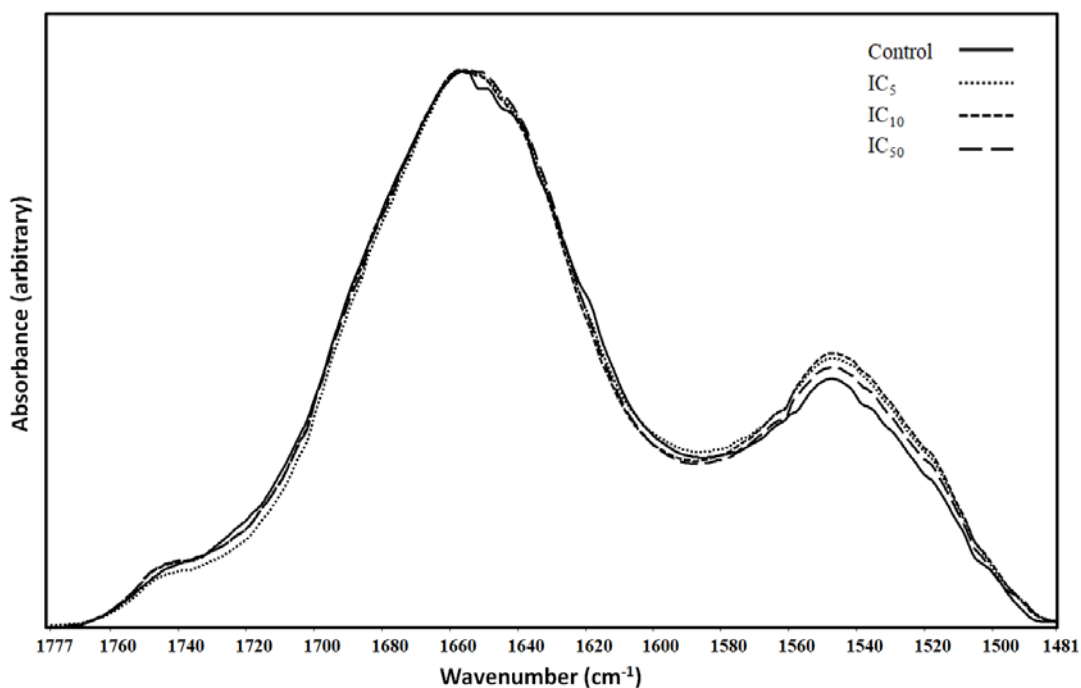


**Figure 3. 4.** The FTIR spectra of the three different doses of rosuvastatin-treated and control A549 cells between 1777 and 1481 cm<sup>-1</sup>.

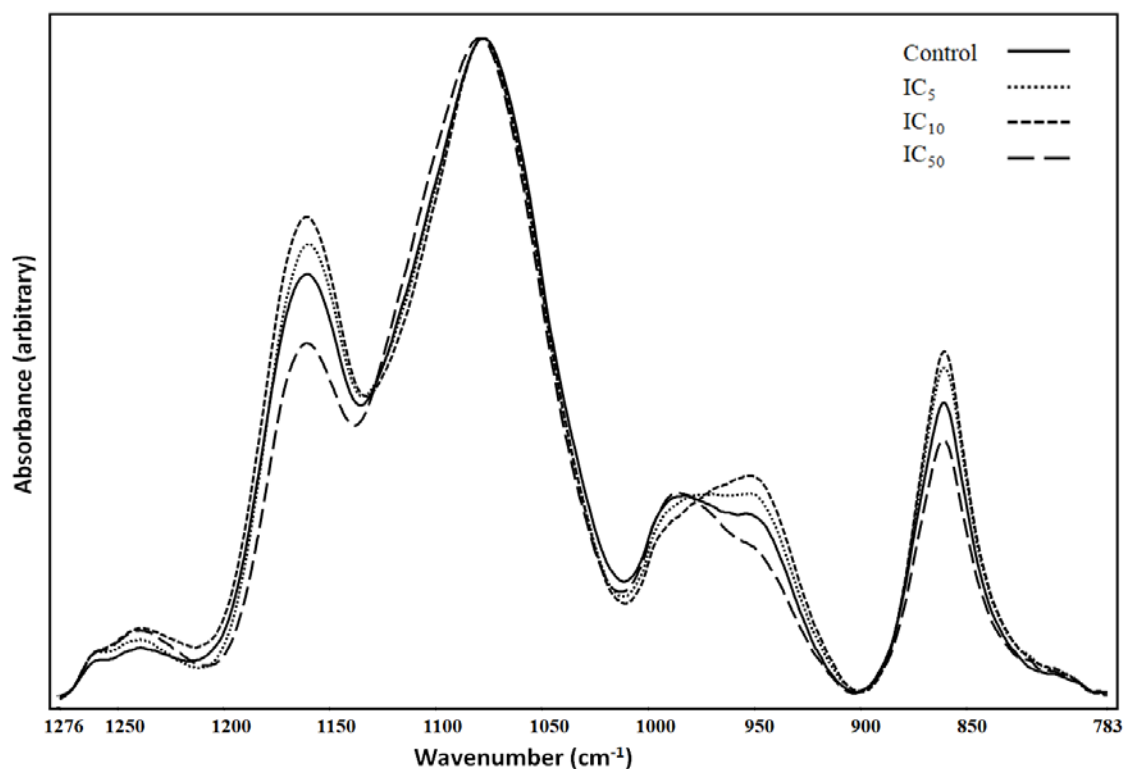


**Figure 3. 5.** The FTIR spectra of the three different doses of rosuvastatin-treated and control A549 cells between 1276 and 783  $\text{cm}^{-1}$ .

The FTIR spectra in the 1276 and 783  $\text{cm}^{-1}$  region is called the fingerprint region. The changes in the bands in this region indicate structural changes upon rosuvastatin administration as Figure 3.5 indicates. The band at 1160  $\text{cm}^{-1}$  indicative of protein side chains shows drug-dose dependent changes. The bands at 1260, 1238, 1082, 984, 867 and 801  $\text{cm}^{-1}$  are related to nucleic acids,  $\text{PO}^{-2}$  absorptions of nucleic acids, conformation changes of DNA and DNA breathing (Al-Jorani, et al., 2018; Malek, Wood, & Bambery, 2014) . Under the rosuvastatin treatment, band intensities showed slight differences at 1260  $\text{cm}^{-1}$ . At 1238  $\text{cm}^{-1}$  intensity values gradually decreased. Changes of band intensity, band shift and changes of band width were observed at 984  $\text{cm}^{-1}$  upon rosuvastatin indicating some changes in the DNA helix conformation. According to the changes in the wavenumber, intensity and the band shape of the DNA bands there seems to be significant changes in the DNA structure and architecture.

### 3.2.2. The Effect of Fluvastatin on A549 Cells Studied by FTIR Spectroscopy:

The average FTIR spectra of the A549 cells treated with fluvastatin the 3710 and 2682  $\text{cm}^{-1}$  region is given in Figure 3.6. Amide A and amide B bands are found in this spectral region. They both have contributions from mainly the N–H stretching of proteins with a small contribution from the O–H stretching of polysaccharides and intermolecular H bonding and contributions from C–N and N–H stretching of proteins, respectively. Fluvastatin treatment induced remarkable changes in the bandwidth, intensity, and frequency value of the FTIR bands in this region as seen from Fig. 3.6. The C–H stretching vibrations of aliphatic compounds are populated between 2996 and 2840  $\text{cm}^{-1}$  as shown in Fig. 3.6. As seen the same figure the intensities of the aliphatic chains increased upon the fluvastatin treatment.

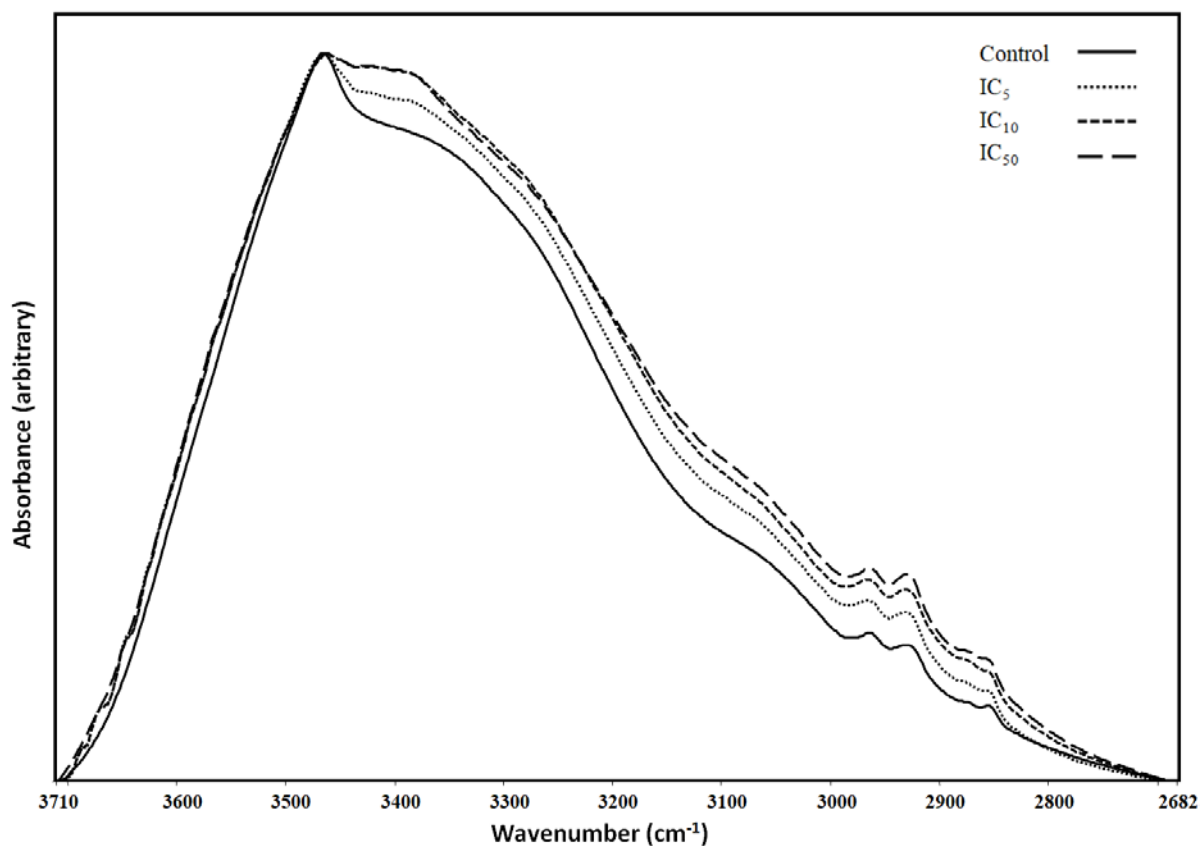


**Figure 3. 6.** The FTIR spectra of the three different doses of fluvastatin-treated and control A549 cells between 3710 and 2682  $\text{cm}^{-1}$ .

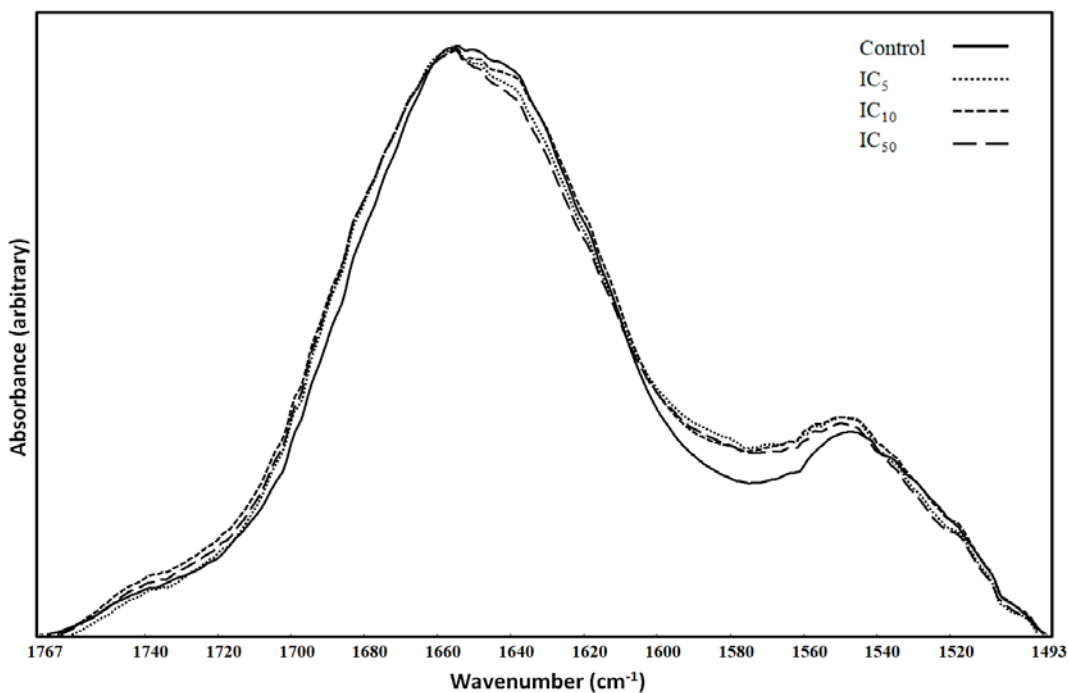


**Figure 3. 7.** The FTIR spectra of the three different doses of fluvastatin-treated and control A549 cells between 1767 and 1493  $\text{cm}^{-1}$ .

The average FTIR spectra of the fluvastatin-treated A549 cells in the 1767 – 1493  $\text{cm}^{-1}$  spectral region is shown in Figure 3.7. The band/shoulder centered around 1740  $\text{cm}^{-1}$  is assigned to C=O ester stretching vibration of triglycerides and cholesterol esters. The band between 1700 and 1600  $\text{cm}^{-1}$  belongs to proteins (Amide I band) and the band between 1600 and 1500  $\text{cm}^{-1}$  belongs to proteins again (Amide II band). As seen in the figure 3.7., the intensity of the band did not show significant changes upon fluvastatin treatment with dose dependent changes.

The FTIR spectra in the 1273 and 786  $\text{cm}^{-1}$  region is called the fingerprint region. The changes in the bands in this region indicate structural changes upon fluvastatin administration as Figure 3.8 indicates. The band at 1160  $\text{cm}^{-1}$  indicative of protein side chains shows drug-dose dependent changes. The bands at 1260, 1238, 1082, 984, 867 and 801  $\text{cm}^{-1}$  are related to nucleic acids,  $\text{PO}^{-2}$  absorptions of nucleic acids, conformation changes of DNA and DNA breathing. The bands at 1261 and 1236  $\text{cm}^{-1}$  showed drug-dose dependent intensity changes. The bands at 984 and 801  $\text{cm}^{-1}$  indicates changes of nucleic acid chains and displayed slight amount of dose-dependent intensity changes.



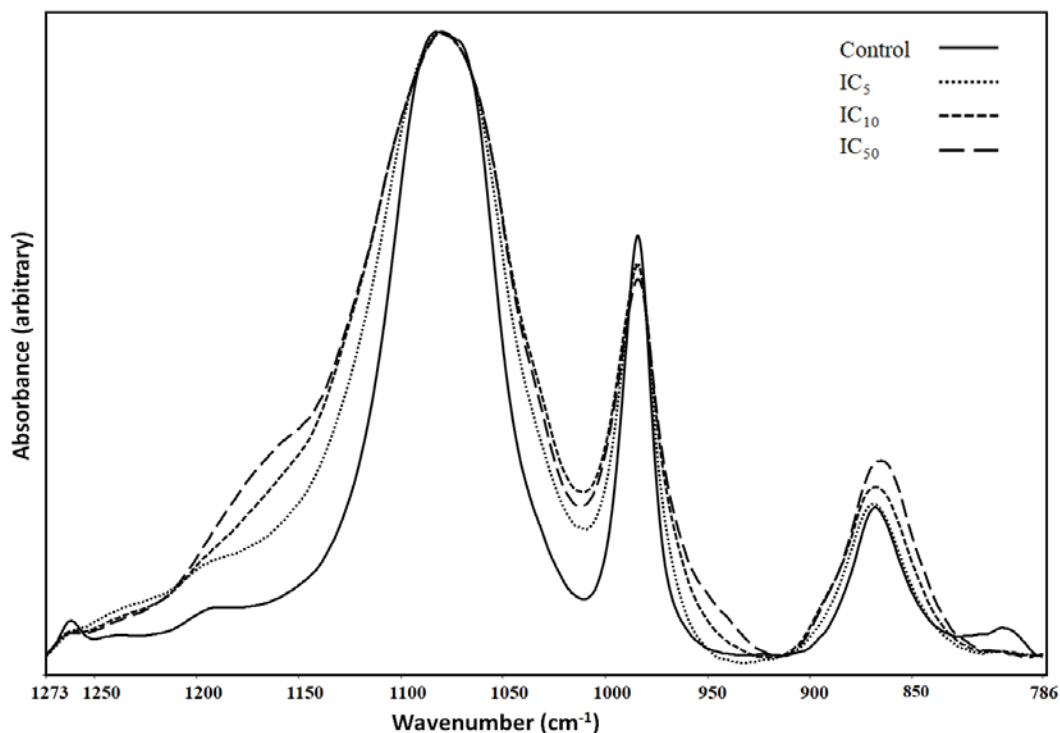


**Figure 3. 8.** The FTIR spectra of the three different doses of fluvastatin-treated and control A549 cells between 1273 and 786  $\text{cm}^{-1}$ .

### 3.2.3. The Effect of Simvastatin on A549 Cells Studied by FTIR Spectroscopy:

The average FTIR spectra of the A549 cells treated with simvastatin in the 3704 and 2784  $\text{cm}^{-1}$  region is given in Figure 3.9. Amide A and amide B bands are found in this spectral region. They both have contributions from mainly the N–H stretching of proteins with a small contribution from the O–H stretching of polysaccharides and intermolecular H bonding and contributions from C–N and N–H stretching of proteins, respectively. Simvastatin treatment induced remarkable changes in the band width, intensity, and frequency value of the FTIR bands in this region as seen from Fig. 3.9. The C–H stretching vibrations of aliphatic compounds are populated between 2996 and 2840  $\text{cm}^{-1}$  as shown in Fig. 3.9. As seen the same figure the intensities of the aliphatic chains increase upon the simvastatin treatment. The average FTIR spectra of the simvastatin-treated A549 cells in the 1769 – 1479  $\text{cm}^{-1}$  spectral region is shown in Figure 3.10.

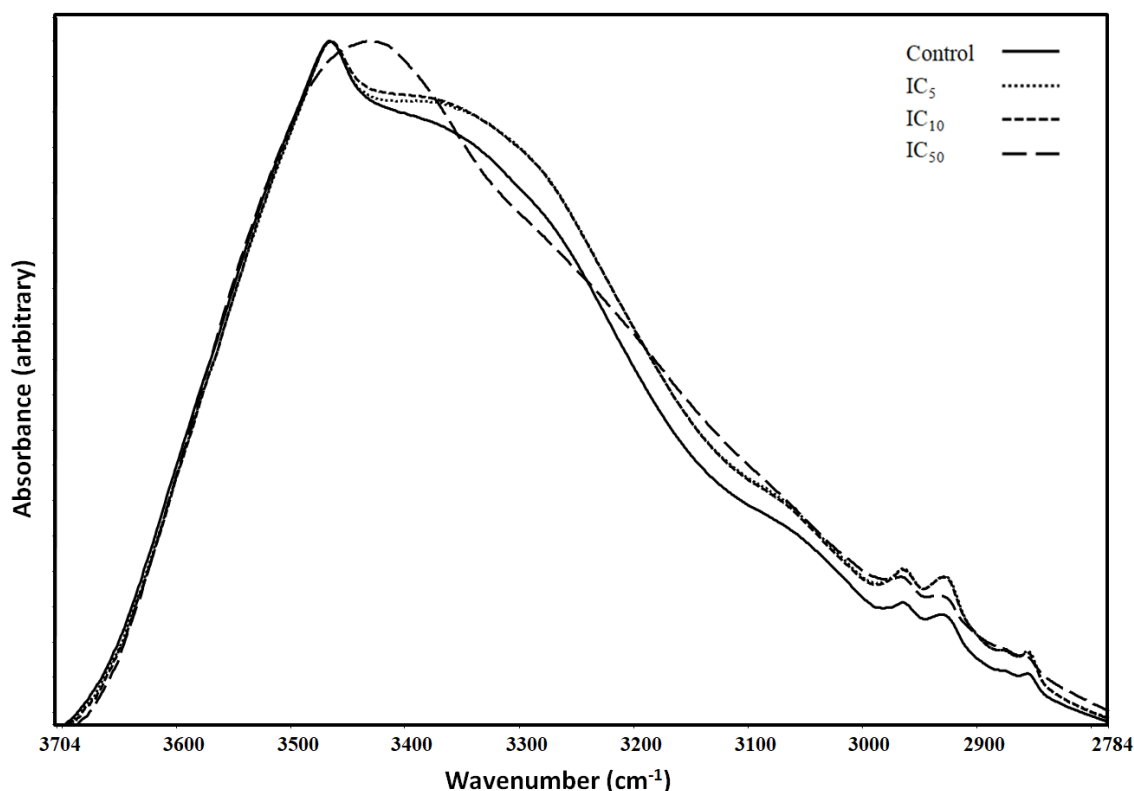


**Figure 3. 9.** The FTIR spectra of the three different doses of simvastatin-treated and control A549 cells between 3704 and 2784  $\text{cm}^{-1}$ .

The band/shoulder centered around  $1740 \text{ cm}^{-1}$  is assigned to  $\text{C}=\text{O}$  ester stretching vibration of triglycerides and cholesterol esters. The band between 1700 and  $1600 \text{ cm}^{-1}$  belongs to proteins (Amide I band) and the band between 1600 and  $1500 \text{ cm}^{-1}$  belongs to proteins again (Amide II band). As seen in the figure, the intensity of the band did not show significant changes upon simvastatin treatment with dose dependent manner but minor intensity changes observed at amide II band.

The FTIR spectra in the  $1274$  and  $785 \text{ cm}^{-1}$  region is called the fingerprint region. The changes in the bands in this region indicate structural changes upon simvastatin administration as Figure 3.8 indicates. The bands at 1260, 1238, 1082, 984, 867 and  $801 \text{ cm}^{-1}$  indicate nucleic acids,  $\text{PO}^{-2}$  absorptions of nucleic acids, conformation changes of DNA and DNA breathing. The bands at 1261, 1236 and  $801 \text{ cm}^{-1}$  intensity values showed slight changes with dose dependency. Around  $1080 \text{ cm}^{-1}$  band shift was observed. The band shifted from 984 to  $988 \text{ cm}^{-1}$  for the  $\text{IC}_{50}$  treatment of simvastatin. Another band shift observed around  $867 \text{ cm}^{-1}$ .

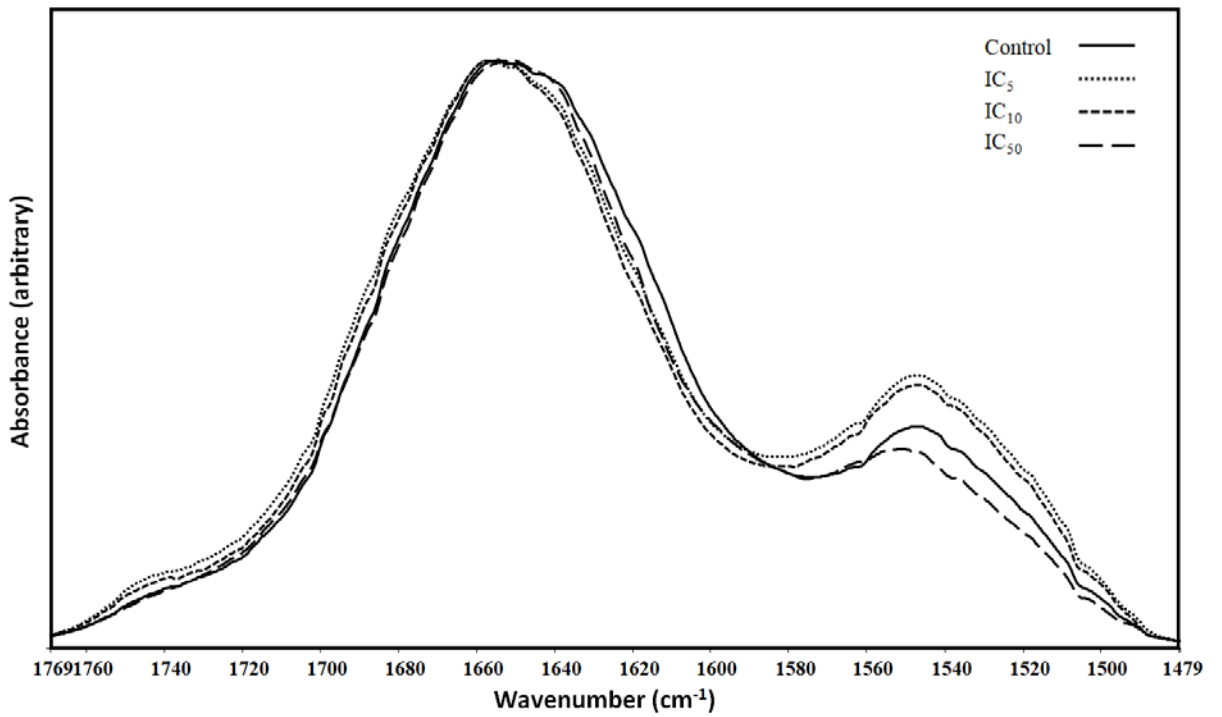


**Figure 3. 10.** The FTIR spectra of the three different doses of simvastatin-treated and control A549 cells between 1769 and 1479  $\text{cm}^{-1}$ .

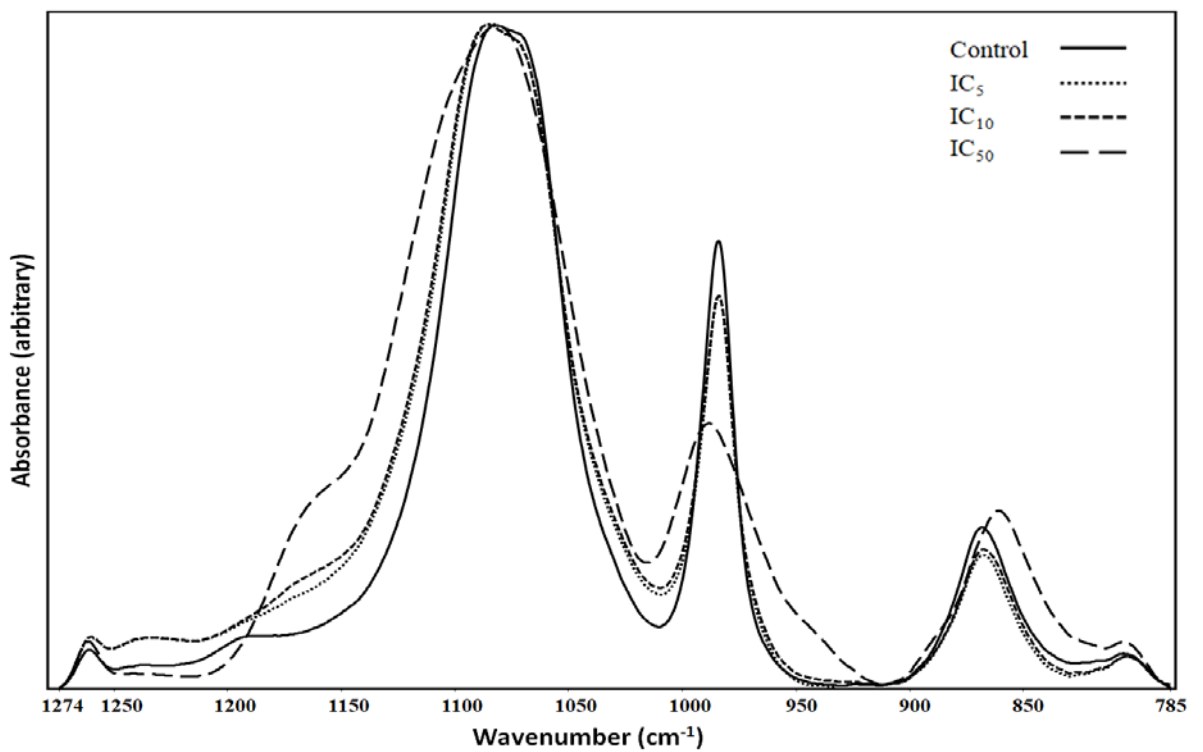


**Figure 3. 11.** The FTIR spectra of the three different doses of simvastatin-treated and control A549 cells between 1274 and 785  $\text{cm}^{-1}$ .

### 3.2.4. The Effect of Atorvastatin on A549 Cells Studied by FTIR Spectroscopy:

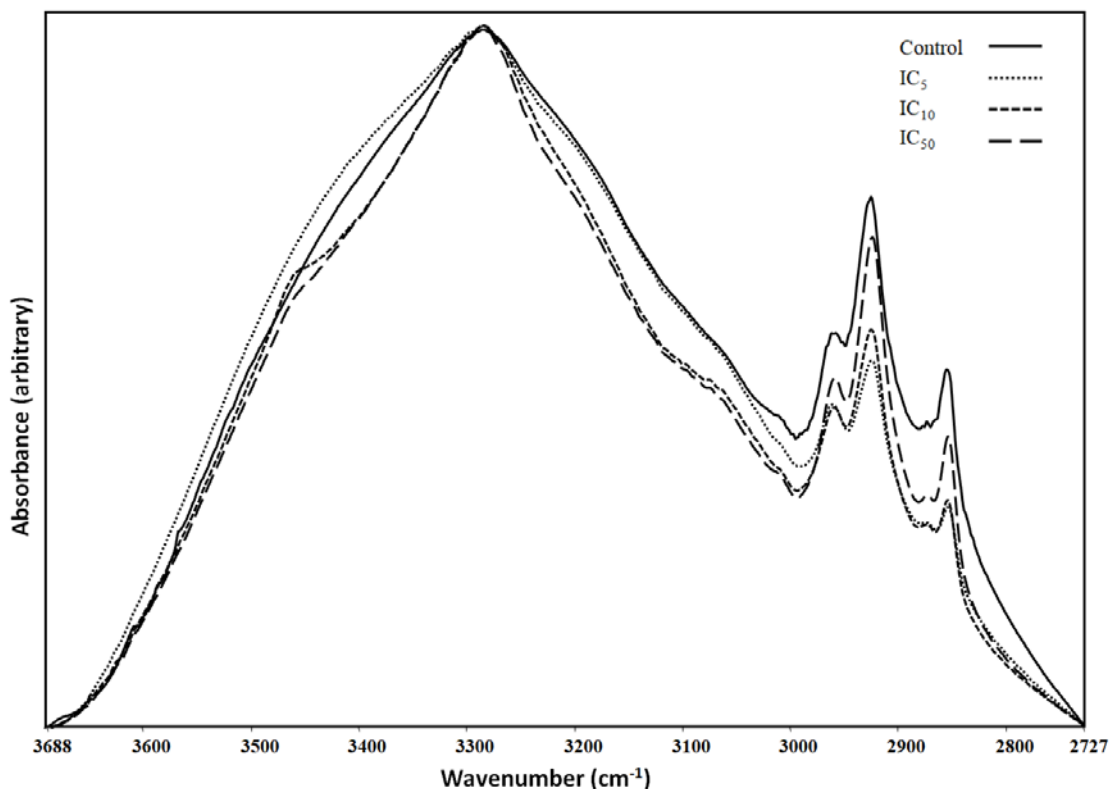


**Figure 3. 12.** The FTIR spectra of the three different doses of atorvastatin-treated and control A549 cells between 3688-2727  $\text{cm}^{-1}$ .

The average FTIR spectra of the A549 cells treated with atorvastatin in the 3688 and 2727  $\text{cm}^{-1}$  region is given in Figure 3.12. Amide A and amide B bands are found in this spectral region. They both have contributions from mainly the N–H stretching of proteins with a small contribution from the O–H stretching of polysaccharides and intermolecular H bonding and contributions from C–N and N–H stretching of proteins, respectively. Atorvastatin treatment induced remarkable changes in the bandwidth, intensity, and frequency value of the FTIR bands in this region as seen from Fig. 3.12. The C–H stretching vibrations of aliphatic compounds are populated between 2996 and 2840  $\text{cm}^{-1}$  as shown in Fig. 3.12. As seen the same figure the intensities of the aliphatic chains decrease upon the atorvastatin treatment.

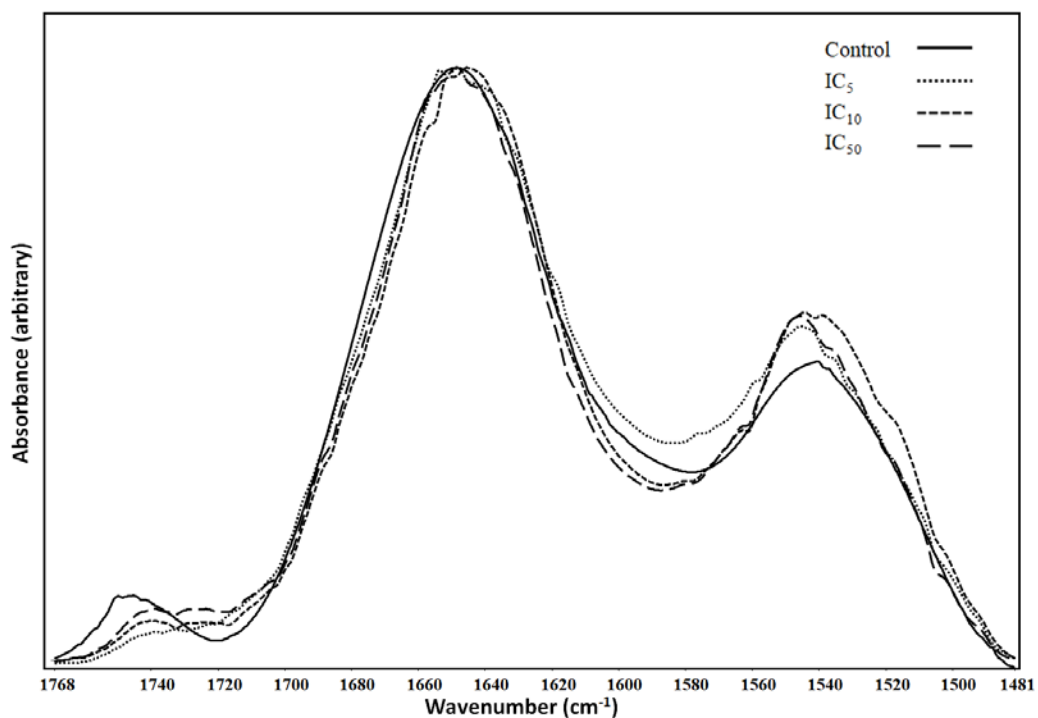


**Figure 3. 13.** The FTIR spectra of the three different doses of atorvastatin-treated and control A549 cells between 1768-1481 cm<sup>-1</sup>.

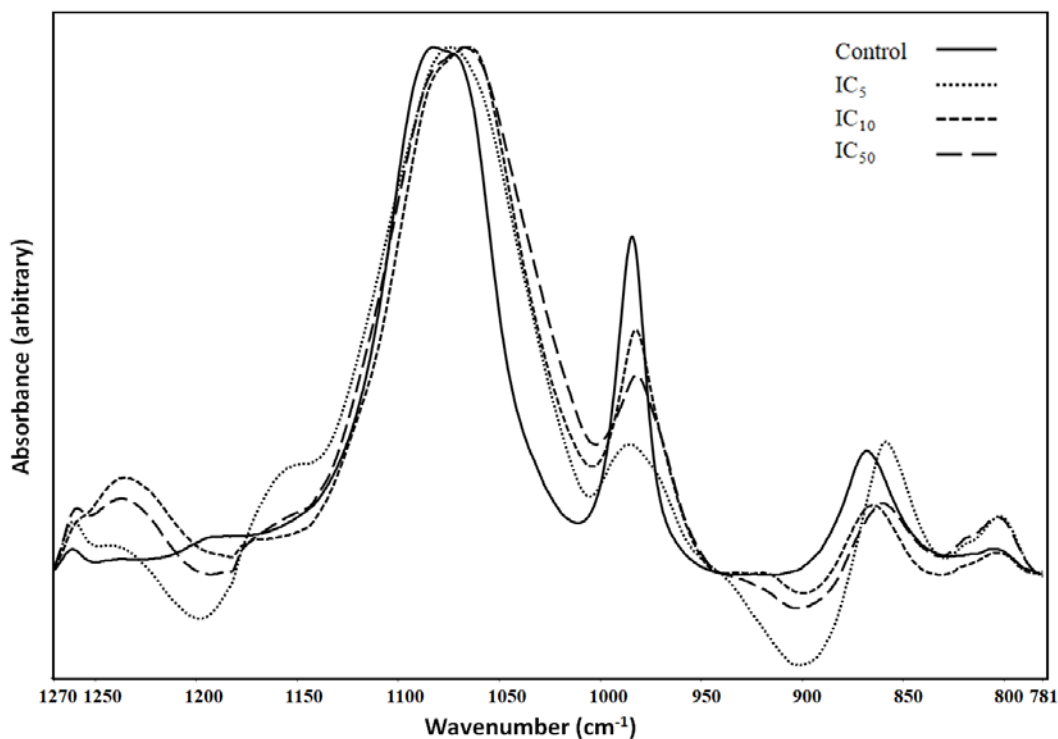


**Figure 3. 14.** The FTIR spectra of the three different doses of atorvastatin-treated and control A549 cells between 1270-781 cm<sup>-1</sup>.

The average FTIR spectra of the atorvastatin-treated A549 cells in the 1768 – 1481  $\text{cm}^{-1}$  spectral region is shown in Figure 3.13. The band/shoulder centered around 1740  $\text{cm}^{-1}$  is assigned to C=O ester stretching vibration of triglycerides and cholesterol esters. The band between 1700 and 1600  $\text{cm}^{-1}$  belongs to proteins (Amide I band) and the band between 1600 and 1500  $\text{cm}^{-1}$  belongs to proteins again (Amide II band). As seen in the figure, the intensity of the band did not show significant changes upon pravastatin treatment with dose dependent changes.

The FTIR spectra in the 1270 and 781  $\text{cm}^{-1}$  region is called the fingerprint region. The changes in the bands in this region indicate structural changes upon atorvastatin administration as Figure 3.14 indicates. The bands around 1260, 1238, 1082, 984, 867 and 801  $\text{cm}^{-1}$  indicate nucleic acids,  $\text{PO}^{-2}$  absorptions of nucleic acids, conformation changes of DNA and DNA breathing. Observable band shifts and intensity increasing were detected around 1261 and 1239  $\text{cm}^{-1}$ . The band around 1080  $\text{cm}^{-1}$  extravagant band shift was observed. Intensities around 984 and 867  $\text{cm}^{-1}$  decreased according to control group. The band at 804  $\text{cm}^{-1}$  showed intensity changing with drug-dose dependency.

### **3.2.5. The Effect of Pravastatin on A549 Cells Studied by FTIR Spectroscopy:**

The average FTIR spectra of the A549 cells treated with pravastatin in the 3685 and 2672  $\text{cm}^{-1}$  region is given in Figure 3.15. Amide A and amide B bands are found in this spectral region. They both have contributions from mainly the N–H stretching of proteins with a small contribution from the O–H stretching of polysaccharides and intermolecular H bonding and contributions from C–N and N–H stretching of proteins, respectively. Pravastatin treatment induced remarkable changes in the bandwidth, intensity, and frequency value of the FTIR bands in this region as seen from Fig. 3.15. The C–H stretching vibrations of aliphatic compounds are populated between 2996 and 2840  $\text{cm}^{-1}$  as shown in Fig. 3.15. As seen the same figure the intensities of the aliphatic chains decrease upon the pravastatin treatment.

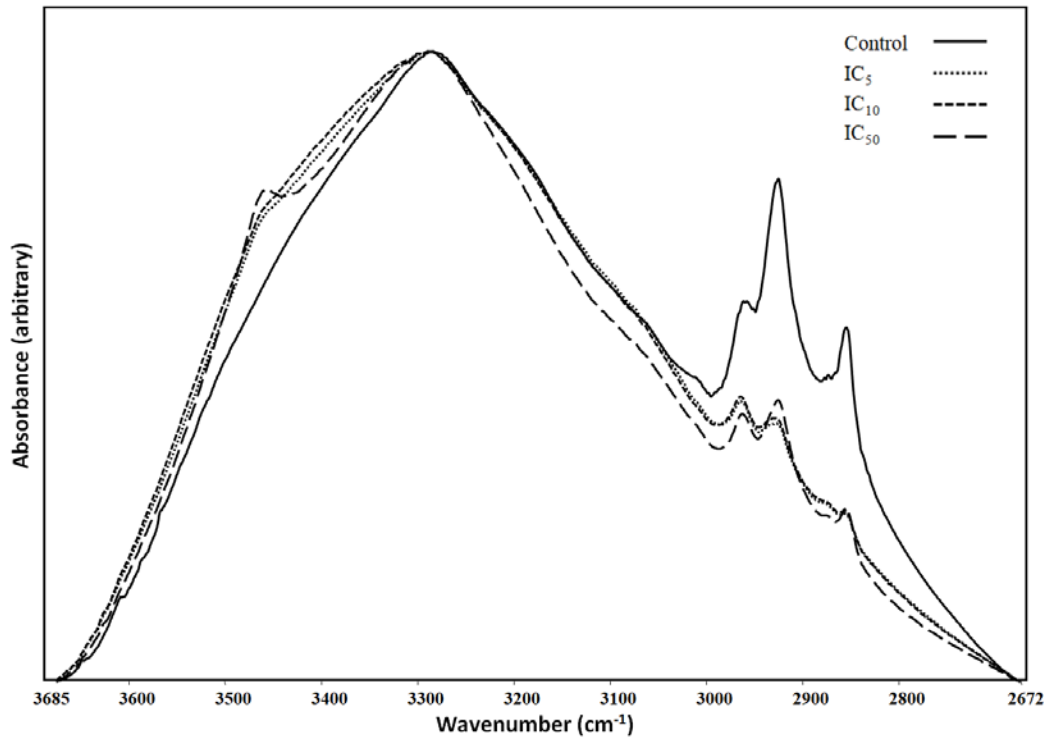


**Figure 3. 15.** The FTIR spectra of the three different doses of pravastatin-treated and control A549 cells between 3685-2672  $\text{cm}^{-1}$ .

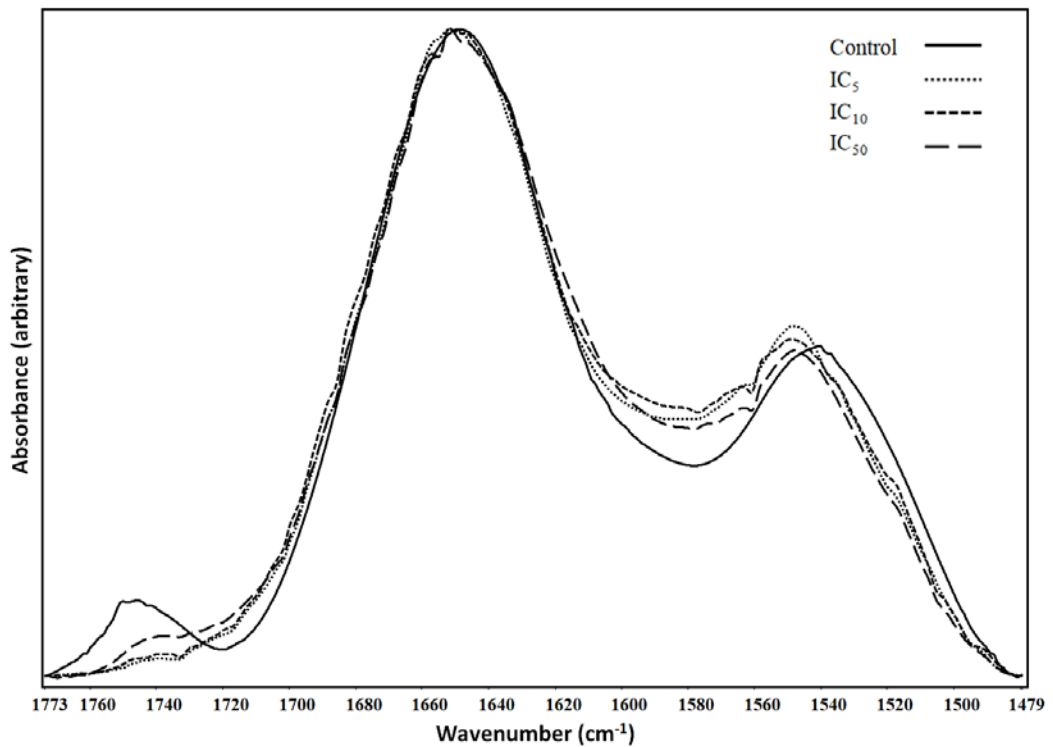


**Figure 3. 16.** The FTIR spectra of the three different doses of pravastatin-treated and control A549 cells between 1773-1479  $\text{cm}^{-1}$ .

The average FTIR spectra of the pravastatin-treated A549 cells in the 1773 – 1479  $\text{cm}^{-1}$  spectral region is shown in Figure 3.16. The band/shoulder centered around 1740  $\text{cm}^{-1}$  is assigned to C=O ester stretching vibration of triglycerides and cholesterol esters. The band between 1700 and 1600  $\text{cm}^{-1}$  belongs to proteins (Amide I band) and the band between 1600 and 1500  $\text{cm}^{-1}$  belongs to proteins again (Amide II band). As seen in the figure, the intensity of the band did not show significant changes upon pravastatin treatment with dose dependent changes.

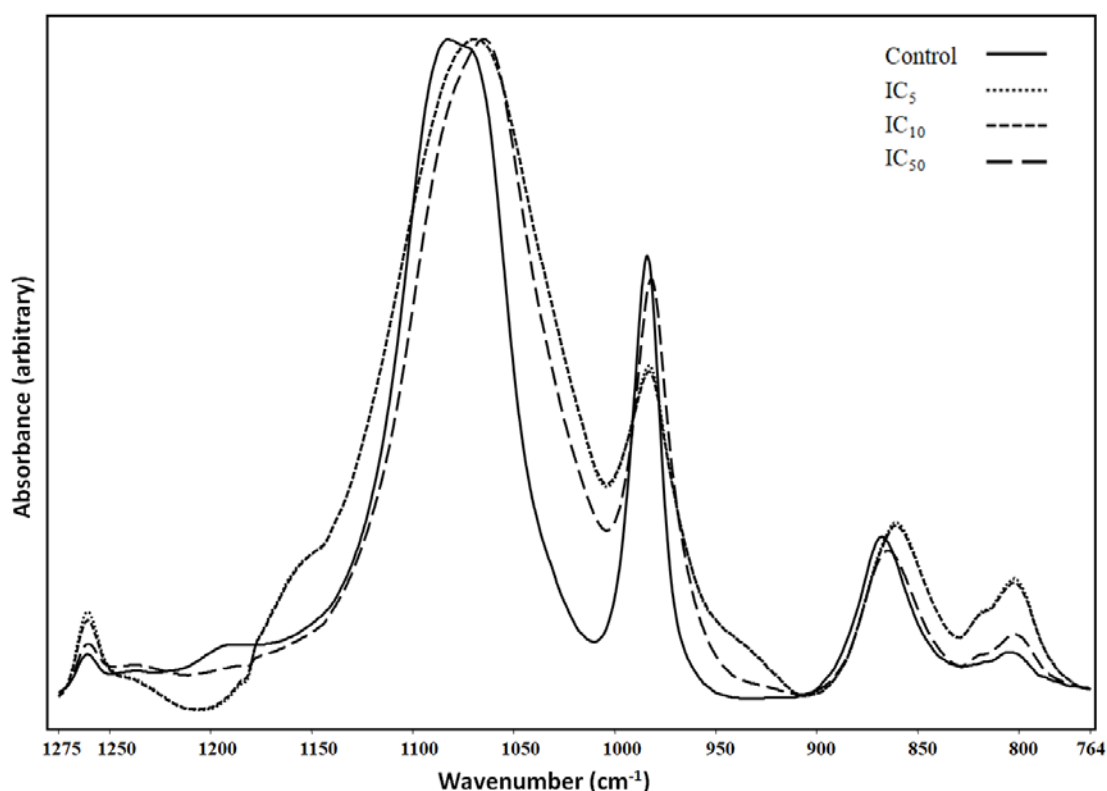


**Figure 3. 17.** The FTIR spectra of the three different doses of pravastatin-treated and control A549 cells between 1275-764  $\text{cm}^{-1}$ .

The FTIR spectra in the 1275 and 764  $\text{cm}^{-1}$  region is called the fingerprint region. The changes in the bands in this region indicate structural changes upon pravastatin administration as Figure 3.17 indicates. The bands around 1260, 1082, 984, 867 and 801  $\text{cm}^{-1}$  indicative of nucleic acid chains showed drug-dose dependent



intensity changes and band shifts. Meaningful band shift was observed around 1082 to 1062 along with pravastatin treatment dose dependent manner.

### **3.2.6. The Effect of Lovastatin on A549 Cells Studied by FTIR**

#### **Spectroscopy:**

The average FTIR spectra of the A549 cells treated with lovastatin in the 3734 and 2837  $\text{cm}^{-1}$  region is given in Figure 3.18. Amide A and amide B bands are found in this spectral region. They both have contributions from mainly the N–H stretching of proteins with a small contribution from the O–H stretching of polysaccharides and intermolecular H bonding and contributions from C–N and N–H stretching of proteins, respectively. Lovastatin treatment induced remarkable changes in the band width, intensity, and frequency value of the FTIR bands in this region as seen from Fig. 3.18. The C–H stretching vibrations of aliphatic compounds are populated between 2996 and 2840  $\text{cm}^{-1}$  as shown in Fig. 3.18. Due to an increase in the Amide B band shoulder it is hard to see the changes in the aliphatic band with respect to Amide A protein band. As seen the same figure the intensities of the aliphatic chains decrease upon the pravastatin treatment.

The average FTIR spectra of the lovastatin-treated A549 cells in the 1774 – 1476  $\text{cm}^{-1}$  spectral region is shown in Figure 3.19. The band/shoulder centered around 1740  $\text{cm}^{-1}$  is assigned to C=O ester stretching vibration of triglycerides and cholesterol esters. The band between 1700 and 1600  $\text{cm}^{-1}$  belongs to proteins (Amide I band) and the band between 1600 and 1500  $\text{cm}^{-1}$  belongs to proteins again (Amide II band). As seen in the figure, the intensity of the band show enormous decreases upon lovastatin treatment with dose dependent changes.

The FTIR spectra in the 1281 and 786  $\text{cm}^{-1}$  region is called the fingerprint region. The changes in the bands in this region indicate structural changes upon lovastatin administration as Figure 3.20 indicates. The bands around 1262, 1239, 1082, 984, 867 and 805  $\text{cm}^{-1}$  indicate nucleic acids,  $\text{PO}^{-2}$  absorptions of nucleic acids, conformation changes of DNA and DNA breathing. Changes of intensities observed at 1262, 1239, 984 and 805  $\text{cm}^{-1}$  bands. The 1082 and 867  $\text{cm}^{-1}$  bands shifted with dose dependent manner.

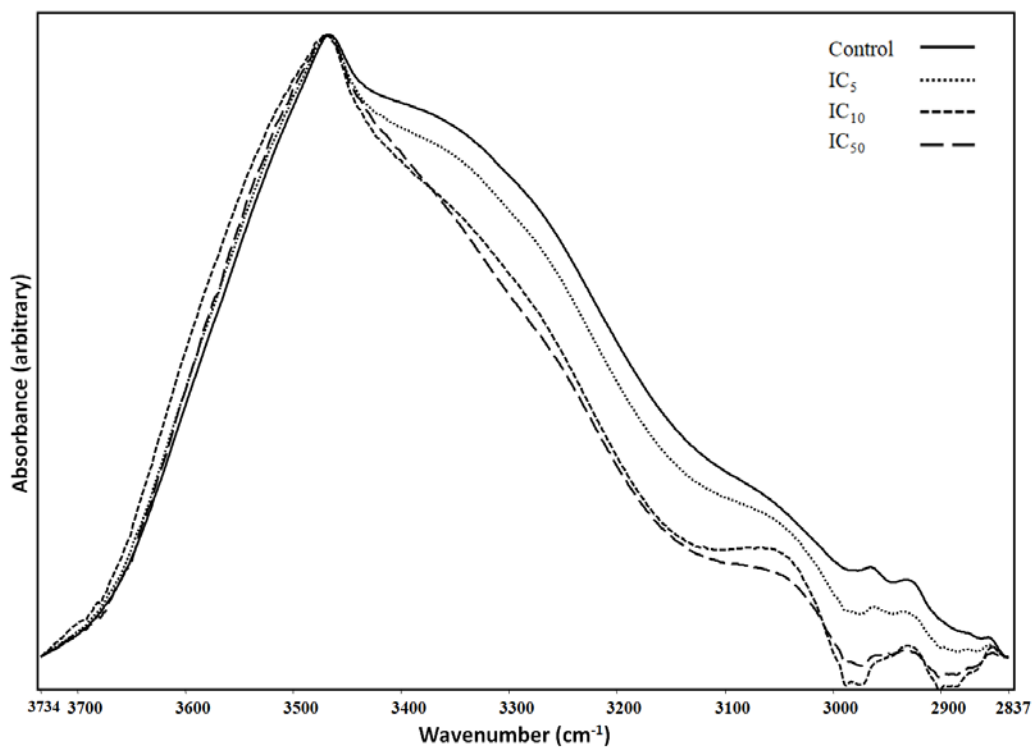


**Figure 3. 18.** The FTIR spectra -of the three different doses of lovastatin-treated and control A549 cells between 3734-2837 cm<sup>-1</sup>.

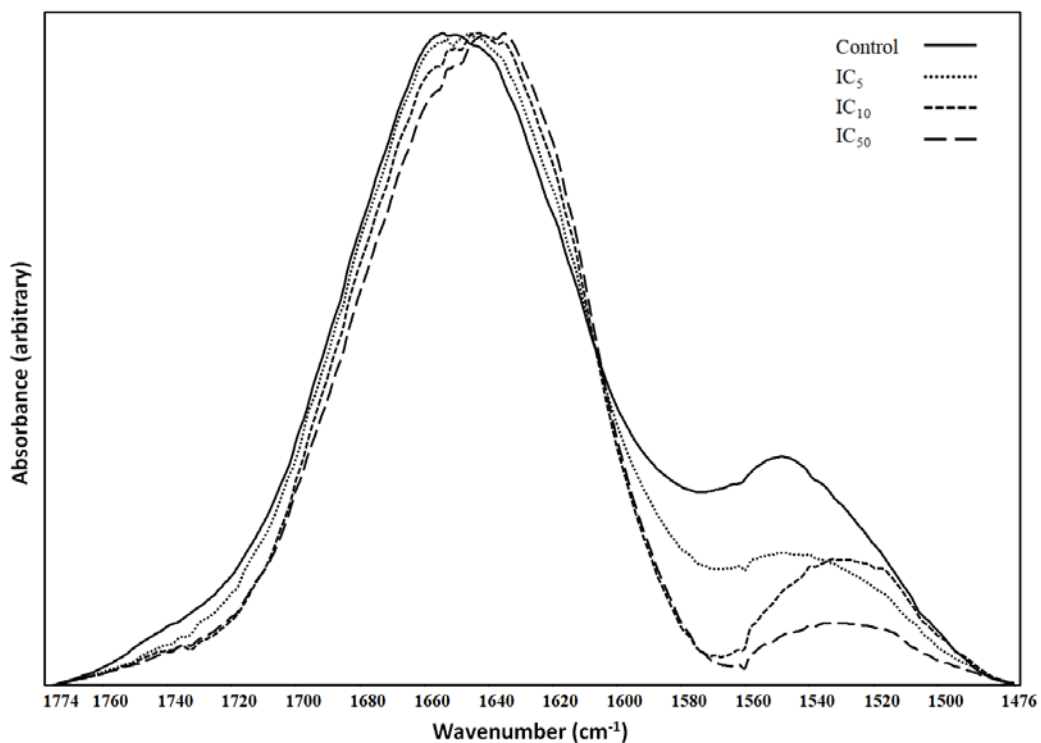


**Figure 3. 19.** The FTIR spectra -of the three different doses of lovastatin-treated and control A549 cells between 1774-1476 cm<sup>-1</sup>.

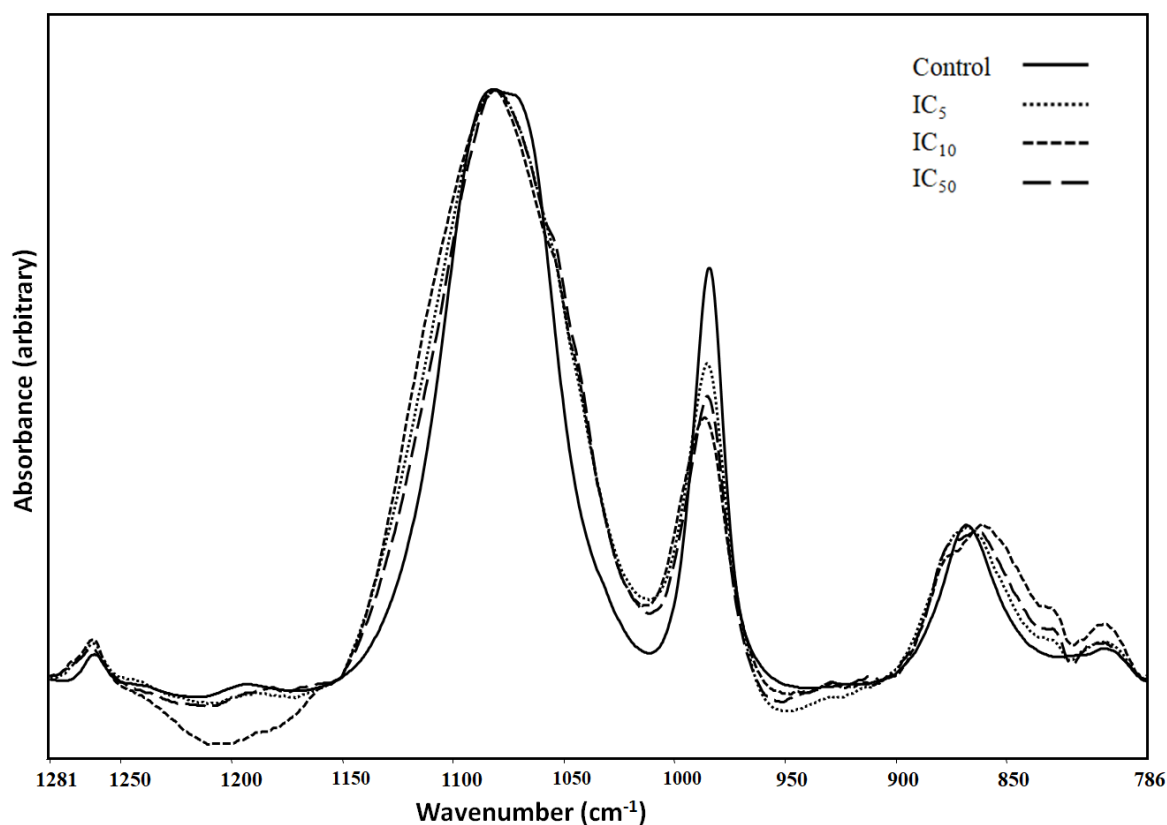


**Figure 3. 20.** The FTIR spectra -of the three different doses of lovastatin-treated and control A549 cells between 1281-786  $\text{cm}^{-1}$ .

### **3.3. The FTIR Band Ratios of The Non-Treated A549 Cells And Three Different Doses Of Statin Treated A549 Cells**

In the Table 3.2. ratios were obtained from lyophilized the non-treated A549 cells and the doses of  $\text{IC}_5$ ,  $\text{IC}_{10}$  and  $\text{IC}_{50}$  of statins treated A549 cells. Ratios were calculated by division of value of control for each ratio.

#### **3.3.1. The Ratio of Amide I/II**

Amide I bands derive from stretching of carbonyl group from peptide bond at  $1655 \text{ cm}^{-1}$  and amide II bands derive from mainly protein amide N-H bond deformation in detail 60% comes from amide N-H bending vibrations and %40 accompanies C-N stretching vibrations at  $1547 \text{ cm}^{-1}$ . The ratio exhibits protein rearrangement, denaturation and compositional changes of proteins in cell. (Ricciardi, Portaccio,

Piccolella, Manti, Pacifico, & Lepore, 2017). Lovastatin treatment in a dose-dependent manner displayed the substantial changes as shown in the Table 3.2. The other treatments illustrated slightly ratio changes according to non-treated ones. In addition, ratio increasing showed in accordance with drug-dose treated manner.

### **3.3.2. The Ratio of 1740/Amide I**

The ratio between the band associated to ester C=O stretching vibration of phospholipids and the amide I band shows the relative content of lipids and proteins in the cell (Fabian, Jackson, Murphy, Watson, Fichtner, & Mantsch, 1995). This ratio refers to lipidation ratio according to lipid to protein amount in the cell. The ratios of lovastatin and pravastatin in a dose dependent manner considerably reduced. Though the ratios of rosuvastatin, simvastatin and fluvastatin showed initially increasing, the ratios depend on the dose increasing, gradually decreased. In contrast to these decreasing, lipidation increased under the atorvastatin treatment in a dose-dependent manner.

### **3.3.3. Ratio of 1740/1080**

Peak located at  $1080\text{ cm}^{-1}$  stands for symmetric stretching of phosphate vibrations from the phosphodiester bond of nucleic acids additionally comes from C-O-P stretching of protein and lipids. This ratio indicates lipid to DNA content in the cell. Under the initial dose applying, the ratios for rosuvastatin, fluvastatin and rosuvastatin treatment increased. Along with amount of drug-dose increasing, in spite of the fact that the ratios gradually decreased, they remained above the control. Lovastatin and pravastatin treatment led to prominent decreasing of lipid to DNA ratio. However, the ratio approximately showed two and a half increase under the atorvastatin treatment.

### **3.3.4. Ratio of Amide I/1080**

This ratio indicates protein to DNA ratio in the cell. The ratios were obtained by division of intensities at  $1655\text{ cm}^{-1}$  to at  $1080\text{ cm}^{-1}$ . Nonetheless, the cells under the atorvastatin treatment indicated increasing higher than two times compare to control

cells, the other type of statins did not cause observable changes on the cells protein levels.

**Table 3. 2.** FTIR band ratios of the non-treated A549 cells and the doses of IC<sub>5</sub>, IC<sub>10</sub> and IC<sub>50</sub> of statins treated A549 cells

	<b>Amide I / Amide II / Control</b>	<b>1740 / Amide I / Control</b>	<b>1740/ 1080 / Control</b>	<b>Amide I / 1080 / Control</b>
The IC <sub>5</sub> of lovastatin treated A549 cells	1,5455	0,7087	0,5918	0,8353
The IC <sub>5</sub> of pravastatin treated A549 cells	0,9379	0,3433	0,4750	1,3839
The IC <sub>5</sub> of rosuvastatin treated A549 cells	0,9134	1,4604	1,5791	1,0816
The IC <sub>5</sub> of atorvastatin treated A549 cells	0,8619	0,6438	1,3444	2,0880
The IC <sub>5</sub> of simvastatin treated A549 cells	0,8112	1,8133	1,8514	1,0213
The IC <sub>5</sub> of fluvastatin treated A549 cells	0,9330	1,9647	1,6827	0,8558
The IC <sub>10</sub> of lovastatin treated A549 cells	1,5548	0,5809	0,6404	1,1041
The IC <sub>10</sub> of pravastatin treated A549 cells	0,9830	0,3935	0,6536	1,6592
The IC <sub>10</sub> of rosuvastatin treated A549 cells	0,9008	1,2546	1,3492	1,0757
The IC <sub>10</sub> of atorvastatin treated A549 cells	0,7981	0,7184	1,6722	2,3267
The IC <sub>10</sub> of simvastatin treated A549 cells	0,8398	1,6432	1,8049	1,0987
The IC <sub>10</sub> of fluvastatin treated A549 cells	0,9398	1,5749	1,5343	0,9741
The IC <sub>50</sub> of lovastatin treated A549 cells	3,1035	0,5696	0,4656	0,8181
The IC <sub>50</sub> of pravastatin treated A549 cells	0,9909	0,6609	0,6416	0,9709
The IC <sub>50</sub> of rosuvastatin treated A549 cells	0,9449	0,8904	1,0095	1,1335
The IC <sub>50</sub> of atorvastatin treated A549 cells	0,8380	0,9933	2,6037	2,6204
The IC <sub>50</sub> of simvastatin treated A549 cells	1,0958	1,0097	1,1108	1,0998
The IC <sub>50</sub> of fluvastatin treated A549 cells	0,9750	1,5184	1,3808	0,9087

### 3.4. The FTIR Spectra of Lipid Extracts of Statin Treated A549 Cells

Assignment of the lipid extracts of three different doses of six different statins treated and non-treated A549 cells investigated in the general scale Fig 3.21. The assignments of the major bands in Figure 3.21. are given in Table 3.3.

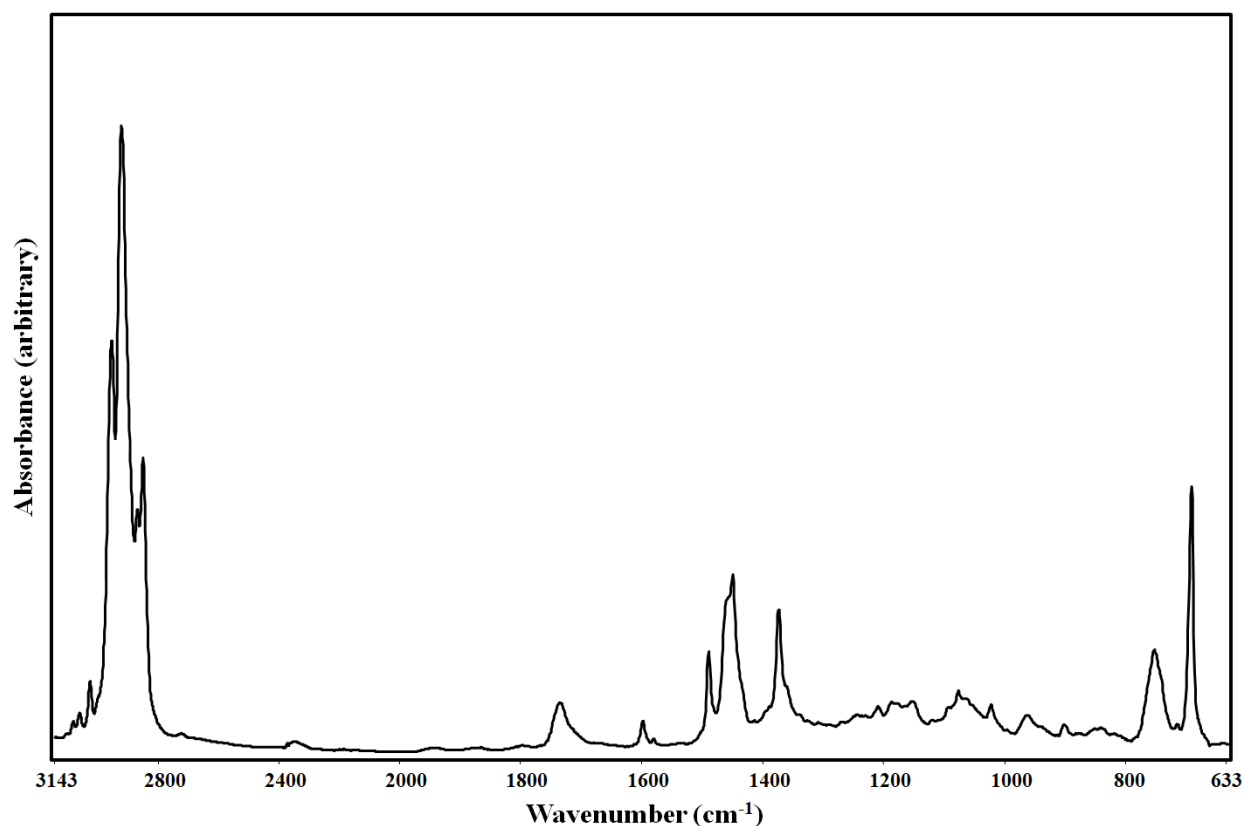


**Figure 3. 21.** The general FTIR spectrum of the lipid extract of A549 cells.

Between 3100-2750  $\text{cm}^{-1}$  bands are originated by the C-H groups stretch vibrations which are dominated by the fatty acids. The region 1800 between 700  $\text{cm}^{-1}$  comprises a fingerprint region for each component, therefore the range is valuable for classification of lipids (Dreissig, Machill, Salzer, & Krafft, 2009). The wavenumber range from 3011 to 3000  $\text{cm}^{-1}$  stands for unsaturated fatty acids and cholesterol esters with the vibration of H-C=C-H (*cis*-alkene) and shows unsaturation ratios in lipids (Shapaval V. , Afseth, Vogt, & Kohler, 2014). The bands at 2954, 2922, 2869 and 2850  $\text{cm}^{-1}$  stand for saturated fatty acids and are assigned to asymmetric stretching vibration of the  $\text{CH}_3$  and  $\text{CH}_2$  group, and symmetric stretching vibration of the  $\text{CH}_3$  and  $\text{CH}_2$  groups respectively (Lamba, Lal, Yappert, Lou, & Borchman, 1991; Oleszko, et al., 2015).

**Table 3. 3.** The FTIR band assignments of lipid extracts of A549 cells.

Wavenumber (cm <sup>-1</sup> )	Assignments	References
3082	C-H ring	(Talari, Martinez, Movasaghi, Rehman, & Rehman, 2017)
3025	Aromatic CH stretching	(Talari, Martinez, Movasaghi, Rehman, & Rehman, 2017)
3001	Olefinic, CH=CH stretching vibration	(Dreissig, Machill, Salzer, & Krafft, 2009; Yandim, Ceylan, Elmas, & Baran, 2016)
2954	Asymmetric stretching vibration of the CH <sub>3</sub> group	(Galeb, Salimon, Eid, Nacer, Saari, & Saadi, 2012)
2922	Asymmetric stretching vibration of the CH <sub>2</sub> group	(Sánchez-Alonso, Carmona, & Careche, 2012)
2869	Symmetric stretching vibration of the CH <sub>3</sub> group	(Hayati, Man, Tan, & Aini, 2005)
2850	Symmetric stretching vibration of the CH <sub>2</sub> group	(Hayati, Man, Tan, & Aini, 2005)
1737	Stretching vibration of the C=O group	(Arrondo & Goni, 1998)
1601	C=C Stretching	(Vidyadharani & Dhandapani, 2013)
1492	Choline derived, asymmetric bending of the N-CH <sub>3</sub> group	(Schwarzott, Lasch, Baurecht, Naumann, & Fringeli, 2004)
1453	Bending vibrations of the CH <sub>2</sub> groups of fatty acids	(Oleszko, et al., 2015)
1377	Bending vibrations of the CH <sub>3</sub> groups of fatty acids	(Dreissig, Machill, Salzer, & Krafft, 2009)
1213	Asymmetric stretching vibration PO <sub>2</sub> <sup>-</sup>	(Yandim, Ceylan, Elmas, & Baran, 2016)
1157	Stretching vibration of the C-O group of lipid ester bond	(Arrondo & Goni, 1998)

(cont. on next page)

Table 3.3 (cont.).

1082	Symmetric stretching vibration of the $\text{PO}_2^-$	(Sánchez-Alonso, Carmona, & Careche, 2012)
970	Asymmetric stretching vibration of the C=C group : conformation <i>trans</i>	(Yoshida, Zhang, Sakuyama, & Matsushima, 2009)
846	Asymmetric stretching vibration of the P-O Stretching vibration of C-C-C	(Dreissig, Machill, Salzer, & Krafft, 2009; Zheng & Tu, 1986)
698	=C-H out-of-plane bending	(Gupta, Singh, Kumar, & Khajuria, 2014)

The C=O group stretching vibrations at  $1737\text{-}1740\text{ cm}^{-1}$  are originated from fatty esters or triglyceride esters with peroxidation of fatty acid chains (Yoshida, Zhang, Sakuyama, & Matsushima, 2009). The band at  $1601\text{ cm}^{-1}$  C=C stretch represents the alkene groups (Vidyadharani & Dhandapani, 2013). A band at  $1492\text{ cm}^{-1}$  is assigned to choline derived asymmetric bending of the N-CH<sub>3</sub> group (Schwarzott, Lasch, Baurecht, Naumann, & Fringeli, 2004). The bands at  $1453$  and  $1377\text{ cm}^{-1}$  are defined for bending vibrations of the CH<sub>2</sub> and CH<sub>3</sub> groups of fatty acids, respectively. The band between  $1213\text{-}18\text{ cm}^{-1}$  is anti-symmetric stretch vibration of  $\text{PO}_2^-$  which includes phosphatidylinositol (PI), phosphatidylethanolamin (PE), phosphatidylcholine (PC) and phosphatidylserine (PS) whereas, the band at  $1082\text{ cm}^{-1}$  is assigned to symmetric stretch vibration of  $\text{PO}_2^-$  (Dreissig, Machill, Salzer, & Krafft, 2009). The range of the  $1157\text{-}1179\text{ cm}^{-1}$  is in charge of asymmetric stretch vibration of the C-O group of lipid ester bonds. Around  $1082\text{ cm}^{-1}$  represents vibration of phospholipids. Vibrations of C-O-P of phospholipids are also observed at  $1028\text{ cm}^{-1}$ . A band near at  $970\text{ cm}^{-1}$  known that asymmetric vibration of HC=CH (*trans*-alkene) in fatty acids represents changes of lipid hydroperoxides with the double bond of *trans* conjugation (Yoshida, Zhang, Sakuyama, & Matsushima, 2009). The band at  $846\text{ cm}^{-1}$  symbolize asymmetric vibrations of P-O group and stretching vibration of C-C-C of cholesterol molecules



(Dreissig, Machill, Salzer, & Krafft, 2009; Zheng & Tu, 1986). Because the lipid extracts were dissolved in chloroform, the band appeared at  $759\text{ cm}^{-1}$  probably as an associated with chloroform contamination (Oleszko, et al., 2015). Around of the band at  $698\text{ cm}^{-1}$  represents the cholesterol (Yandim, Ceylan, Elmas, & Baran, 2016).

The FTIR spectra obtained from the lipid extracts of the statin-treated A549 cells are presented in Figures 3.22., 3.23., 3.24., 3.25., 3.26., and 3.27.

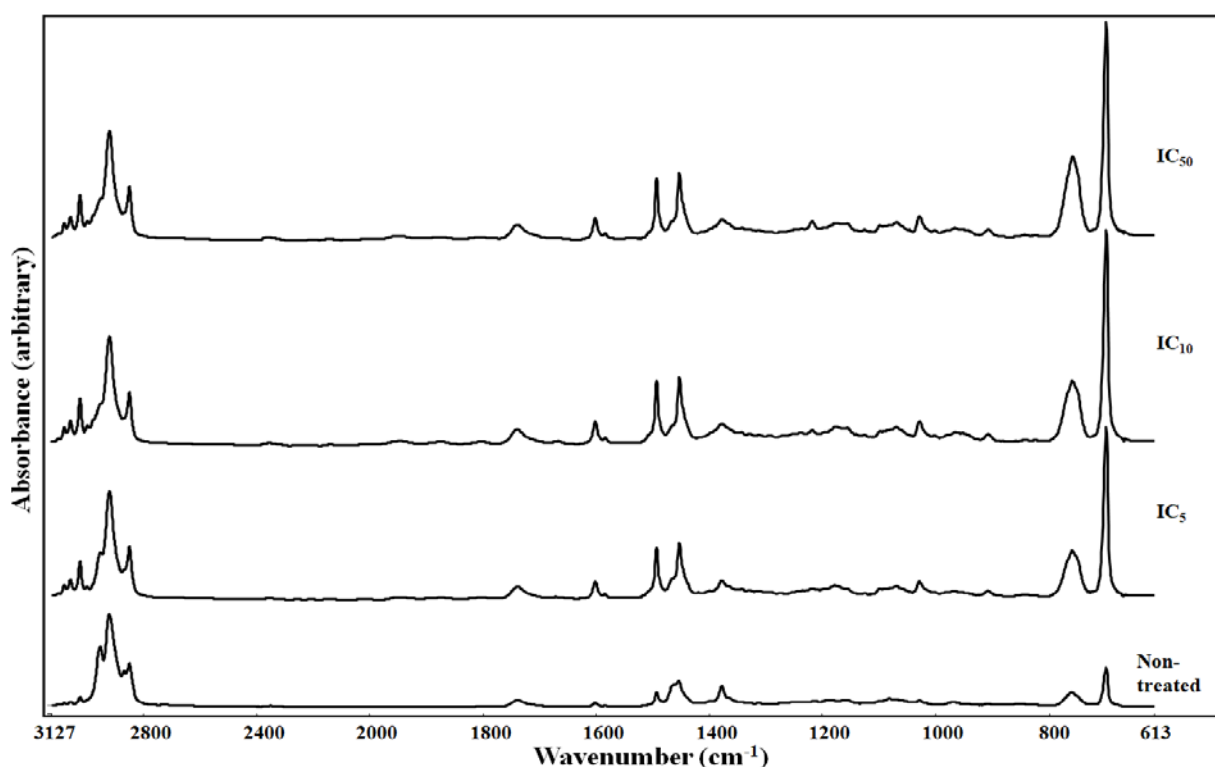


**Figure 3. 22.** The FTIR spectra of the three different doses of lovastatin treated and non-treated lipid extracts of A549 cells.

The bands at  $3082\text{ cm}^{-1}$  did not show any changes of band value but, intensity of the bands increased all the drug treatment except rosuvastatin. Around  $3000\text{ cm}^{-1}$ , olefinic group bands intensities showed minor differences according to statins types and observed minor decreasing except for rosuvastatin treatment. These bands arise from unsaturated hydrophobic chains.

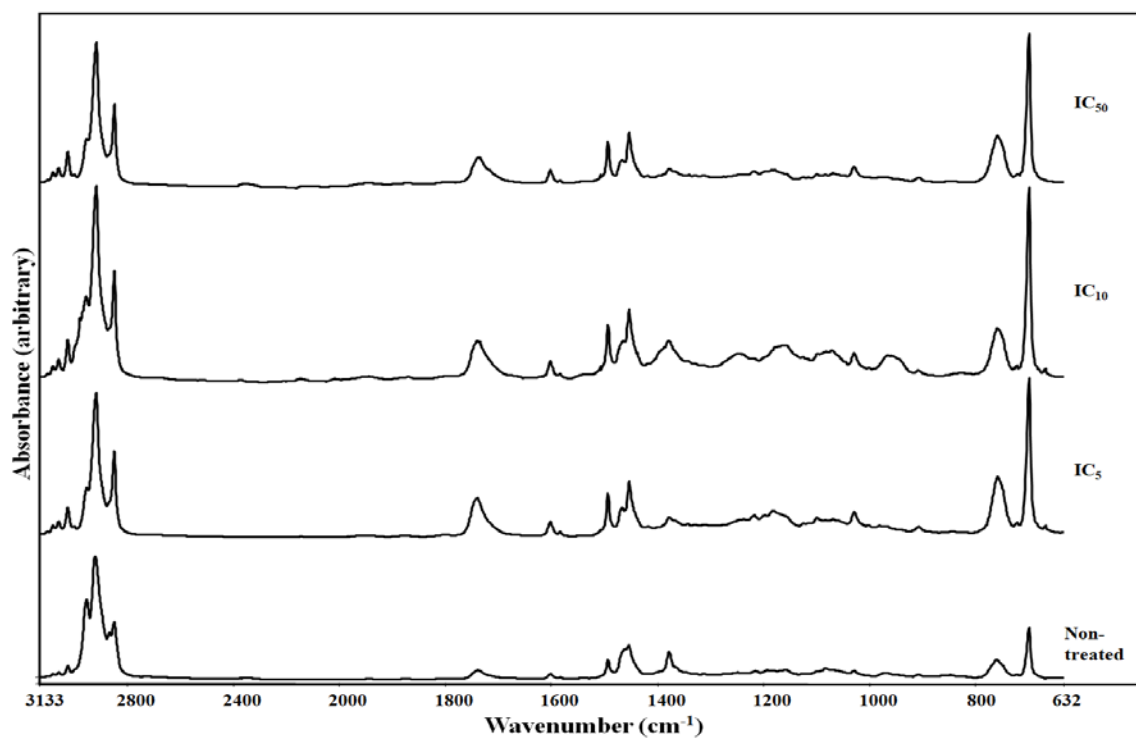


**Figure 3. 23.** The FTIR spectra of the three different doses of atorvastatin treated and non-treated lipid extracts of A549 cells.

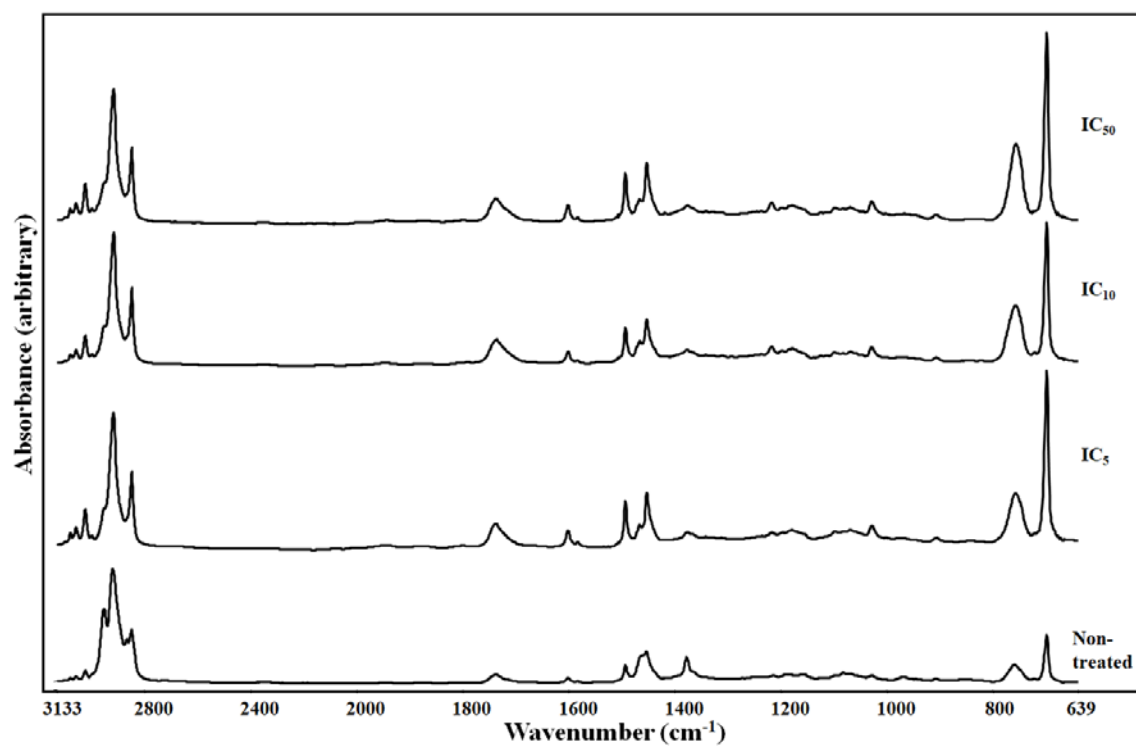


**Figure 3. 24.** The FTIR spectra of the three different doses of fluvastatin treated and non-treated lipid extracts of A549 cells.

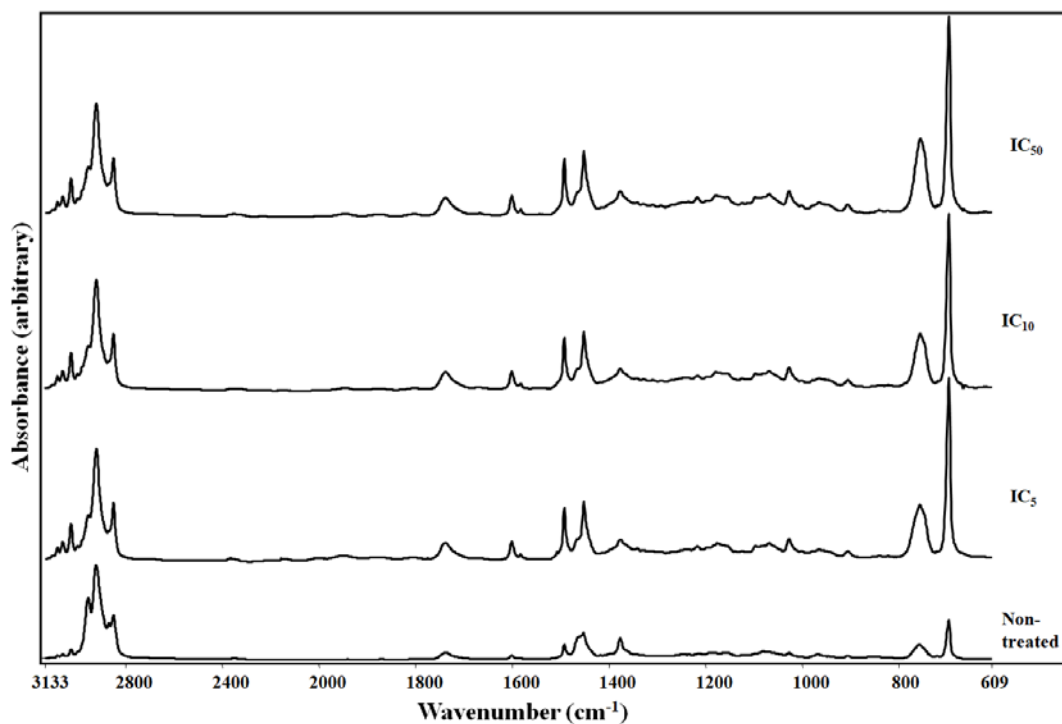


**Figure 3. 25.** The FTIR spectra of the three different doses of pravastatin treated and non-treated lipid extracts of A549 cells.

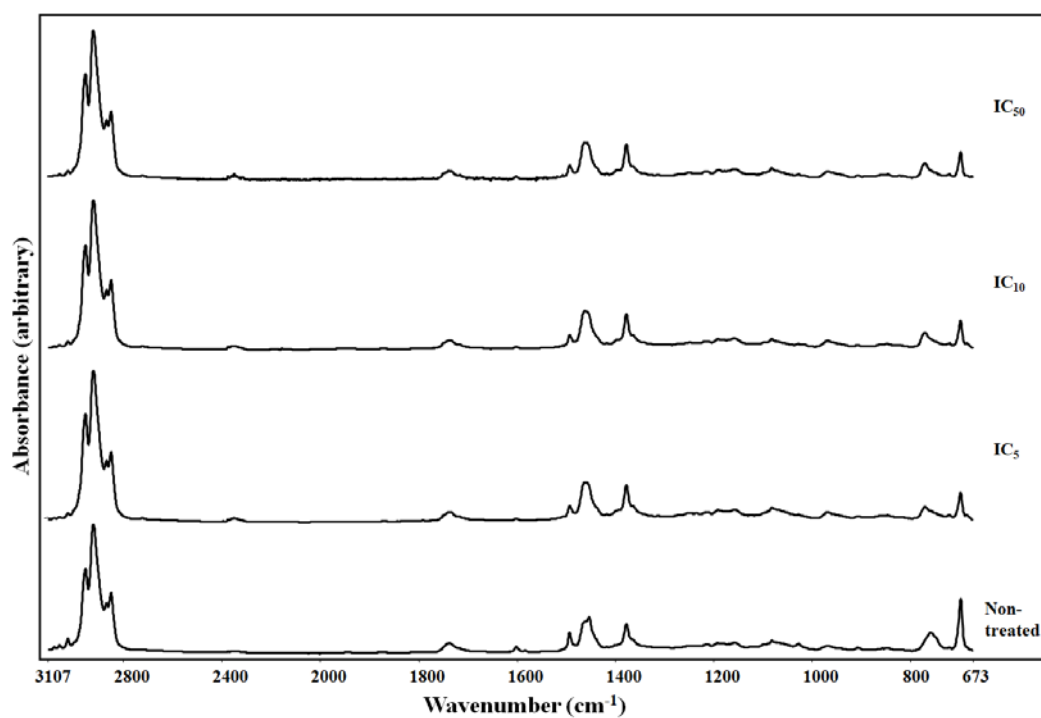


**Figure 3. 26.** The FTIR spectra of the three different doses of rosuvastatin treated and non-treated lipid extracts of A549 cells.

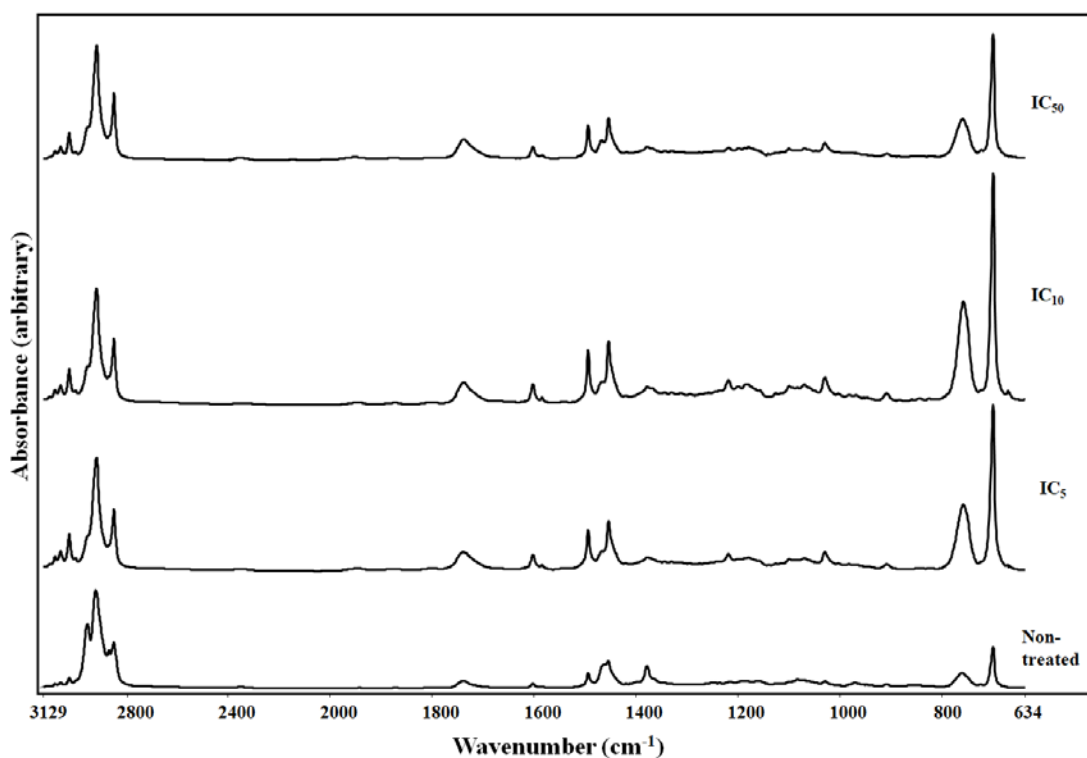


**Figure 3. 27.** The FTIR spectra of the three different doses of simvastatin treated and non-treated lipid extracts of A549 cells.

Despite a decrease of intensity the vibrational asymmetric stretching of  $\text{CH}_3$  band around at  $2950\text{ cm}^{-1}$ , the absorbance value of band remained steady. Additionally, while this band was an exact peak for non-treated cells after statins treatment the peak was observed shoulder at  $2920\text{ cm}^{-1}$  band. Statin treated asymmetric  $\text{CH}_2$  absorbance at  $2922\text{ cm}^{-1}$  decreased except rosuvastatin treatment. It means decreasing of phospholipids. Though, the band at  $2869$  showed as a certain peak in the control spectrum, end of the statins treatment intensity of the band appeared shoulder at  $2850\text{ cm}^{-1}$  band. The symmetric  $\text{CH}_2$  band at  $2850\text{ cm}^{-1}$  stayed nearly same compared to control absorbance (Arrondo & Goni, 1998). Interestingly, while the band at  $1453\text{ cm}^{-1}$  bending vibrations of the  $\text{CH}_2$  remained stable except for rosuvastatin treatment, rosuvastatin treated cells showed the bandshift at  $1462\text{ cm}^{-1}$ . Increasing stretching vibration of the  $\text{C}=\text{O}$  group at  $1737\text{ cm}^{-1}$  derived from lipid oxidation and increased integral absorbance of the band indicates increased lipid oxidation (Oleszko, et al., 2015). The band for the  $\text{IC}_5$  and  $\text{IC}_{10}$  values of lovastatin, atorvastatin, simvastatin treated cells increased according to non-treated group. However, the band absorbance for  $\text{IC}_{50}$  values of atorvastatin and simvastatin treated cells decreased through at  $1734$

$\text{cm}^{-1}$  and  $1735 \text{ cm}^{-1}$  respectively. The absorbance at  $1734 \text{ cm}^{-1}$  for  $\text{IC}_{50}$  value of atorvastatin treated cells stayed same with the non-treated control cells. The choline band at  $1492 \text{ cm}^{-1}$  almost stabled which means statins have restricted effects on choline metabolism. Although the band values at  $1213 \text{ cm}^{-1}$  anti-symmetric stretch vibration of  $\text{PO}_2^-$  rose for five different statins treatment, the band absorbance of the rosuvastatin treated cells remained stable. The drastic bandshift was observed at  $1157 \text{ cm}^{-1}$  through  $1177 \text{ cm}^{-1}$  asymmetric stretch vibration of the C-O group of lipid ester bonds except rosuvastatin which did not show any changes of values. Symmetric stretch vibration of  $\text{PO}_2^-$  of phospholipids band at  $1082 \text{ cm}^{-1}$  showed significantly increased together with statin treatment, yet only rosuvastatin displayed slightly increased. Enhancing this band and the band at  $1213 \text{ cm}^{-1}$  refer to phospholipids increasing. FTIR bands of six different statins treated and respectively their increased concentration showed drastically declining compared to control groups at the  $970 \text{ cm}^{-1}$ . The band known as a lipid hydroperoxidation due to the double bond of *trans* conjugation. The band at  $846 \text{ cm}^{-1}$  had the least intensity in the spectral area. The band as symbolized with asymmetric vibrations of P-O group and also stretching vibration of C-C-C of cholesterol. According to increasing concentration treatment, this band intensity value decreased and showed bandshift in the atorvastatin treatment. The cholesterol associated band intensity at  $698 \text{ cm}^{-1}$  notably increased for all statin treatment and all their doses except rosuvastatin according to non-treated A549 cells.

#### **3.4.1. The comparison of the FTIR spectra of the different statin groups for same concentration**

The comparison of the FTIR spectra obtained from the lipid extracts of the  $\text{IC}_5$ ,  $\text{IC}_{10}$  and  $\text{IC}_{50}$  of the statin-treated A549 cells are presented in Figures 3.28., 3.29. and 3.30.

Take into account figure 3.28., 3.29 and figure 3.30, major differences observed the bands at  $3026$ ,  $1738$ ,  $757$  and  $698 \text{ cm}^{-1}$ . The band at  $3026 \text{ cm}^{-1}$  showed consistently increased atorvastatin, fluvastatin, rosuvastatin and lovastatin treatment. Treating of pravastatin stayed same intensity accordingly initial concentration, yet simvastatin treatment diminished to accordance with dose dependent manner. This peak may indicate O-H vibration of hydroperoxides (Oyman, Ming, & Van der Linde, 2003).

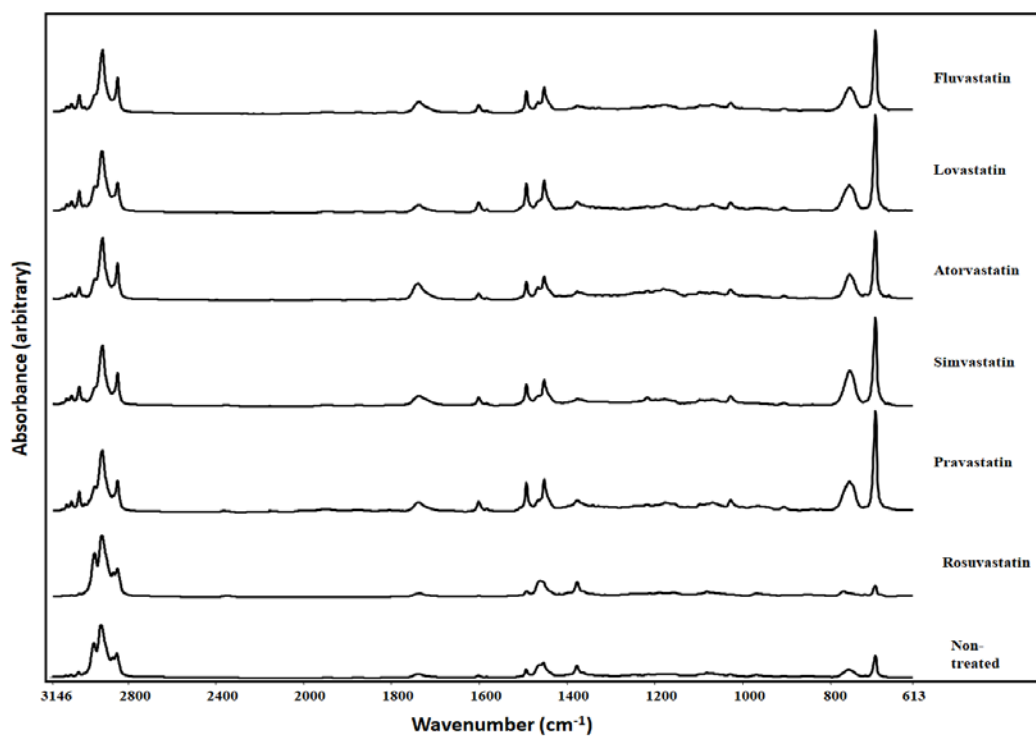


**Figure 3. 28.** The FTIR spectra of the doses of IC<sub>50</sub> of statins treated and non-treated lipid extracts of A549 cells.

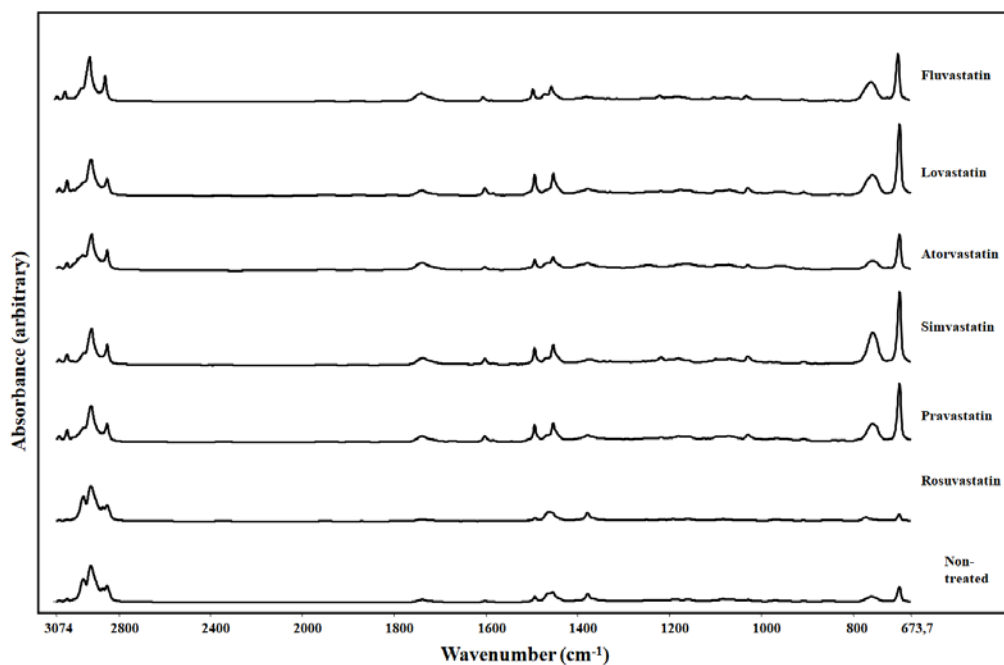


**Figure 3. 29.** The FTIR spectra of the doses of IC<sub>10</sub> of statins treated and non-treated lipid extracts of A549 cells.

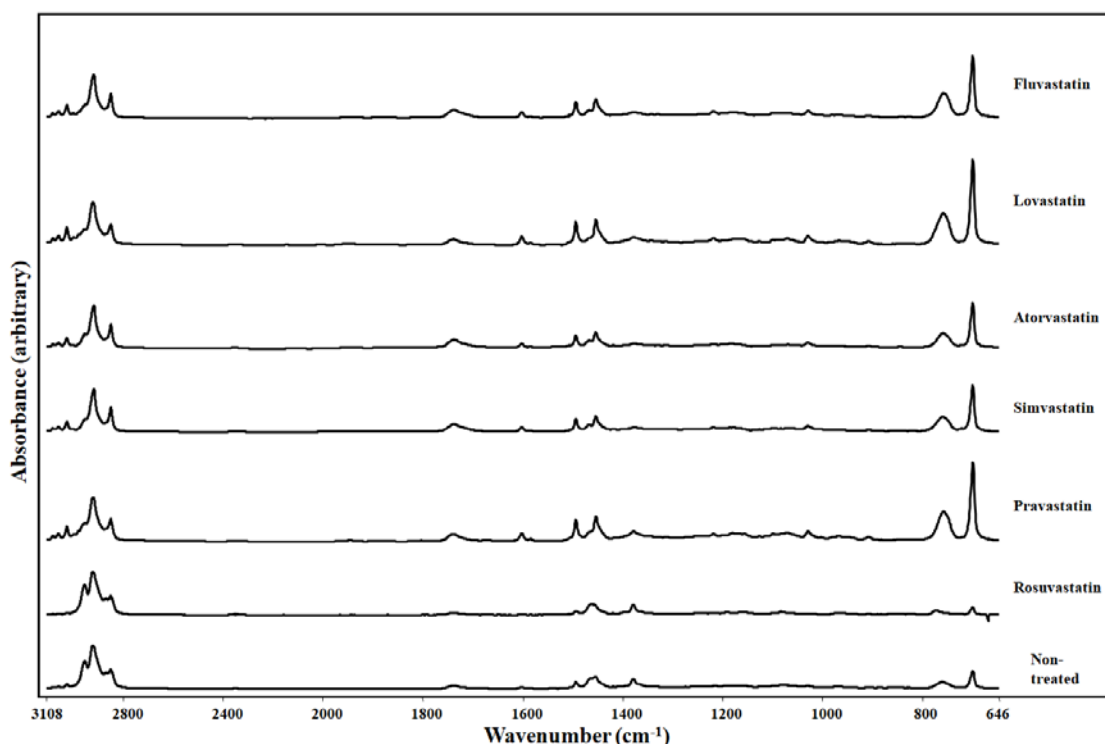


**Figure 3. 30.** The FTIR spectra of the doses of IC<sub>50</sub> of statins treated and non-treated lipid extracts of A549 cells.

The band at 1738 displayed significant raised the treatment of the doses IC<sub>10</sub> of fluvastatin, pravastatin and simvastatin and the dose of IC<sub>50</sub> lovastatin and the dose IC<sub>5</sub> of atorvastatin. The intensity decreased for different rosuvastatin concentration. The increasing trend was observed at 757 cm<sup>-1</sup>. For all treatments except rosuvastatin which showed a decreased of intensity, were detected the considerable increases. The most significant absorbance was recorded for IC<sub>10</sub> simvastatin IC<sub>50</sub> lovastatin. Together with increased drug concentration, the bands intensity at and 698 cm<sup>-1</sup> significantly increased. These bands stand for asymmetric stretching vibration of the CH<sub>2</sub> group for saturated fatty acids and H-C=C-H out-of-plane bending vibrations as mostly characterized aromatic substitution pattern and adjacent hydrogen atom on the ring respectively (Gupta, Singh, Kumar, & Khajuria, 2014). The highest intensity was detected for lovastatin as five times higher as control groups. Nonetheless rosuvastatin treating caused to slightly dropping of the band.

### 3.4.2. The band ratios of the lipid extracts of non-treated A549 cells and three different doses of statins treated A549 cells

After the statin treatment, the band intensities were shown in the Table 3.4.

**Table 3. 4.** FTIR band ratios of the non-treated A549 cells and three different doses of the six different statins treated A549 cells.

	<b>Unsaturation index/ Control</b>	Hydrocarbon chain length/ Control	<b>PO<sub>2</sub>/ CH<sub>2</sub>/ Control</b>	<b>Number of acyl chains/ Control</b>
The IC <sub>5</sub> of lovastatin treated A549 cells	37,9286	2,2958	1,5552	1,4971
The IC <sub>5</sub> of pravastatin treated A549 cells	31,7857	2,9638	1,6090	1,8880
The IC <sub>5</sub> of rosuvastatin treated A549 cells	4,7143	0,9340	0,7313	0,7832
The IC <sub>5</sub> of atorvastatin treated A549 cells	18,2857	2,7835	1,3313	2,9223
The IC <sub>5</sub> of simvastatin treated A549 cells	30,2857	5,0724	2,9731	1,8350
The IC <sub>5</sub> of fluvastatin treated A549 cells	25,2857	5,9652	0,8776	1,9612
The IC <sub>10</sub> of lovastatin treated A549 cells	48	10,1034	2,0896	1,7916
The IC <sub>10</sub> of pravastatin treated A549 cells	30,2857	3,7092	1,6448	1,9003
The IC <sub>10</sub> of rosuvastatin treated A549 cells	3,7143	0,9258	0,6925	0,7469
The IC <sub>10</sub> of atorvastatin treated A549 cells	3,6429	7,9054	0,5403	2,2149
The IC <sub>10</sub> of simvastatin treated A549 cells	26	5,2068	4,5134	1,9294
The IC <sub>10</sub> of fluvastatin treated A549 cells	20,6429	5,4180	2,5254	1,8984
The IC <sub>50</sub> of lovastatin treated A549 cells	41,5714	7,2242	4,4507	1,7340
The IC <sub>50</sub> of pravastatin treated A549 cells	29,0000	3,1159	2,9493	1,8188
The IC <sub>50</sub> of rosuvastatin treated A549 cells	6,0714	0,8708	0,8657	0,7877
The IC <sub>50</sub> of atorvastatin treated A549 cells	14,8571	3,4119	1,0149	2,0440
The IC <sub>50</sub> of simvastatin treated A549 cells	22,7857	4,5165	1,2388	1,7443
The IC <sub>50</sub> of fluvastatin treated A549 cells	33	6,7453	3,8955	1,9508

#### 3.4.2.1. Unsaturation index

This ratio indicates membrane dynamics and flexibility. To examine the ratio of unsaturation in lipids, olefinic (HC =CH vibration) intensity come from 3001 cm<sup>-1</sup>



deriving from unsaturated fatty acids in the cell was divided by CH<sub>2</sub> band intensity observed around 2850 cm<sup>-1</sup> (Shapaval V. , Afseth, Vogt, & Kohler, 2014). Then the ratio was divided by control group intensity. After the all statin treatment unsaturation index showed noticeable increasing compared to non-treated A549 cells. However, rosuvastatin and atorvastatin treatment showed small differences. The highest unsaturation index increasing was observed under the lovastatin treatment.

#### **3.4.2.2. Hydrocarbon chain length**

Hydrocarbon chain length was calculated CH<sub>2</sub> bands at 2850 cm<sup>-1</sup> intensity by division of CH<sub>3</sub> bands intensity around 2868 cm<sup>-1</sup>. This length drastically raised for the five statins treatment. The highest ratio observed for dose of IC<sub>10</sub> of lovastatin as a 10,1034. The little increasing was observed under the rosuvastatin treatment.

#### **3.4.2.3. PO<sub>2</sub>/CH<sub>2</sub>**

To calculate phospholipid containing lipids or fatty acids and triglycerides such as phosphatidic acid, glycerophospholipids, phosphatidyl ethanolamine, phosphatidyl choline, phosphatidyl serine, phosphatidyl inpsitole and glycerophospholipids, PO<sub>2</sub> at 1217 cm<sup>-1</sup> and CH<sub>2</sub> at 2850 cm<sup>-1</sup> were used. In addition, this ratio was divided by control group intensity. When lovastatin, pravastatin, fluvastatin and simvastatin were applied on the cells, the ratio showed observable increasing. The ratio displayed slight decrease for rosuvastatin treatment.

#### **3.4.2.5. Number of acyl chains**

This ratio indicates carbonyl index. Number of acyl chains was calculated with C=O bands at 1740 cm<sup>-1</sup> intensity to CH<sub>2</sub> at 2850 cm<sup>-1</sup>. The ratio was divided by control group intensity as well. Compared to control group, ratios of treated groups raised except for rosuvastatin treatment.

## CHAPTER 4

### DISCUSSION

Lung cancer is one of the most prevalent cancer types in the worldwide (Cheng, Cramb, Baade, Youlden, Nwogu, & Reid, 2016). Abnormal lipid metabolism is a newly recognized area in the cancer research. Therefore, targeting lipid metabolism in cancer can pave the way for rapid diagnosis and recovery of the disease (Beloribi-Djefafli, Vasseur, & Guillaumond, 2016). Statins have been frequently used against cardiovascular diseases for the blockage of cholesterol synthesis (Taylor, et al., 2011). Additionally, statins have been found to have anti-proliferative properties in many cancer types (Jones, et al., 2017; Paškevičiūtė & Petrikaitė, 2017). Particularly, the half maximal concentration (IC<sub>50</sub>) for the most of the statins has been already detected on A549 cells. Considering the scientific literature, the IC<sub>50</sub> values of fluvastatin (12 μM), lovastatin (15 μM), atorvastatin (39 μM) were found to be lower than our findings except for simvastatin (Varbanov, Kuttler, Banfi, Turcatti, & Dyson, 2017; Maksimova, Yie, & Rom, 2008; Ramharack, 2015; Yu X. , Pan, Ma, & Li, 2013). Although there have been considerably lower IC<sub>50</sub> values reported by other researchers, we proceeded to determine our own values. Therefore, the cytotoxicity values of statins were detected regardless of the literature. FTIR spectroscopy examines molecules in specimen by means of mid-IR radiation. The absorbance presents much information about the cell-omics and changes of the cell-omics, because of the fact that this technique can not characterize metabolites in the cell. Similarly individual effects of drugs and their different doses on cells or tissue can be reliably determined (Bellisola & Sorio, 2012). FTIR spectroscopy has been used for cell line or species identification, biodiagnosis and prognosis (Cohenford & Rigas, 1998). In this study by using this technique, structural differences and cell component changes could be determined after the treatment of six different statins and their three different doses. This research especially focused on calculation of metabolite types such as lipid to protein ratio, lipid to DNA and protein to DNA differences, changes of cell protein conformation with the amid I/amid II and lipid

extracts composition changes. According to FTIR spectra, nucleic acid chains are affected by all statin treatment because changes of the band intensity and ranges of the band shift were observed at 1260, 1238, 1082, 988, 867 and 816  $\text{cm}^{-1}$ . Amide I band can qualify the protein secondary structure. This band intensity represents an alpha helix structure in this study (Malek, Wood, & Bambery, 2014). Statins can not cause the any changes of protein secondary structure. Since elevating of amide I/II ratio observed for the lovastatin-treated A549 cells, it can be contributed to cellular proteins cleavaging and also indicates protein denaturation and compositional changes in the cell (Pacifico, Piccolella, Papale, Nocera, Lettieri, & Catauro, 2016). The choline band at 1492  $\text{cm}^{-1}$  almost stabled which means statins have restricted effects on choline metabolism. Choline is used for membrane synthesis and as a neurotransmitter (Sanders & Zeisel, 2007). The band at 3026  $\text{cm}^{-1}$  from the lipid extracts showed consistently increased atorvastatin for most statin types treated cells. Owing to the fact that this band relates to hydroperoxides, peroxidation increased in the cell. (Oyman, Ming, & Van der Linde, 2003) An increasing trend was observed at 757  $\text{cm}^{-1}$  for lipid extracts. Around 757  $\text{cm}^{-1}$  probably stand for linoleic acid (Boyaci, et al., 2015). Statins can cause to convert linoleic acid to polyunsaturated fatty acids. Some of statins inhibit sterol synthesis, others stimulate the conversion of linoleic acid. The reason why, the band can show differences for intensity values (Ris , Ghezzi, & Galli, 2003). The band at 698  $\text{cm}^{-1}$  from the lipid extracts represents saturated fatty acid. The band intensity noticeable increased lovastatin-treated cells. Enhanced saturated fatty acids in the cell membrane phospholipids can decrease unsaturated fatty acids composition of membrane and can cause severe injury in cell membrane and cell growth inhibition (Doi, Doi, Schroeder, Alberts, & Vagelos, 1978). Increased unsaturation index can lead to statins insensitive. Because statins affect not only cholesterol metabolism but also fatty acid metabolism, statins increased lipid droplets which contain neutral lipids. Therefore raised unsaturated fatty acids can be related to statin therapy unresponsiveness (Lettiero, Inasu, Kimbung, & Borgquist, Insensitivity to atorvastatin is associated with increased accumulation of intracellular lipid droplets and fatty acid metabolism in breast cancer cells., 2018). Additionally, in accordance with the literature statin treatment caused increasing of desaturase subsequently caused rising of unsaturation (Lettiero, Inasu, Kimbung, & Borgquist, Insensitivity to atorvastatin is associated with increased

accumulation of intracellular lipid droplets and fatty acid metabolism in breast cancer cells., 2018). This explains enormous unsaturation index increasing. Along with the other cancer types, according to the scientific literature lung cancer cells increased their elongase levels (Tang, Zhou, Hooi, Jiang, & Lu, 2018). This increasing clarifies increased hydrocarbon chain length for the most statin treatment. Increased hydrocarbon chain length can affect membrane permeability and can be added to insensitivity as well (Uchiyama, Oguri, Mojumdar, Gooris, & Bouwstra, 2016). Carbonyl index increased for atorvastatin and simvastatin-treated cells represents increased esterification degree because of the increased oxidation (Shapaval V. , Afseth, Vogt, & Kohler, 2014). FTIR technique results can be combined other sophisticated techniques or methods to obtained results reliability.

## CHAPTER 5

### CONCLUSION

This study was carried out to see any dose and type-dependent changes of statins on A549 cells. The anti-proliferative effects of statins based on the IC<sub>50</sub> values regarding to efficacy were found as simvastatin, atorvastatin, pravastatin, fluvastatin, rosuvastatin and lovastatin. According to the FTIR spectroscopy results, all statins induced remarkable changes in band width, intensity and frequency of FTIR bands between 3700-2800 cm<sup>-1</sup>. Whereas rosuvastatin, fluvastatin and simvastatin caused increasing of aliphatic chains, atorvastatin, pravastatin and lovastatin gave rise to diminish for aliphatic compounds. Except lovastatin, statins did not show significant effects at 1800-1600 cm<sup>-1</sup> bands region. In addition, fingerprint region indicated prominent changes in the DNA structure. Lovastatin and pravastatin displayed more potent lipid lowering properties at the same cytotoxic doses in terms of lipid to protein and lipid to DNA ratios. The other treatments caused lipidation especially atorvastatin led to enormous amount of lipidation. Lovastatin treatment brought about noticeable proteome changes according to amide I/II ratio as well. Under the atorvastatin treatment, cells indicated increasing of protein level according to protein to DNA ratio. The other protein ratios were not affected prominently.

According to FTIR spectroscopy results of lipid extracts of A549 cells; Although the band representing the unsaturated fatty acids and cholesterol esters at 3001 cm<sup>-1</sup> seemed as a clear band on the control cells, the band intensities showed drastic increasing under the statins treatment except rosuvastatin. The intensities of bands at 3082, 3060 and 3026 cm<sup>-1</sup> notably increased compare to control. These bands are associated C-H including lipid groups such as sterols, glycerolipids and sphingomyelin and are also related O-H vibration of hydroperoxides. The band intensity at 698 cm<sup>-1</sup> prominently rose for all statins treatment except rosuvastatin. The hydrocarbon chain length drastically increased under the all statin concentration. The enormous unsaturation index was observed in the lovastatin-treated cells. Nonetheless,

rosuvastatin treatment led to slight increasing compared to other treatment. Along with the increasing of unsaturation index, membrane dynamics increased because of the double bond increasing. Subsequently, this increasing led to rising of membrane flexibility. Phospholipid containing lipid ratios increased for lovastatin, pravastatin, simvastatin and fluvastatin treatment. This rising is based on the increasing of membrane phospholipids and membrane thickening. Only rosuvastatin induced a decreasing in the carbonyl index. The other statin treatments caused to increase carbonyl index and increased carbonyl index responsible for increased esterification and increased oxidation. Increased esterification led to increase esterified lipids such as triglycerides, sphingolipids and glycerophospholipids. Additionally, considering output of lipid extracts, unsaturation index, hydrocarbon chain length, phospholipid containing lipids ranges significantly increased except for rosuvastatin. As a main result, rosuvastatin showed different effects on lipid metabolism for A549 cells compare to other types. This study indicated that statins caused significant structural and compositional changes on A549 cells based on the spectroscopic evaluation.

## REFERENCES

- Albertine, K. H. (2016). Anatomy of the lungs. *Murray and Nadel's textbook of respiratory medicine* , 3-21.
- Al-Jorani, K., R  ther, A., Martin, M., Haputhanthri, R., Deacon, G., Li, H., et al. (2018). The Application of ATR-FTIR Spectroscopy and the Reversible DNA Conformation as a Sensor to Test the Effectiveness of Platinum (II) Anticancer Drugs. *Sensors* , 18 (12), 4297.
- Anonymous. (n.d.). *what-when-how, In Depth Tutorials and Information*. Retrieved from The Respiratory System (Structure and Function) (Nursing) Part 2: <https://what-when-how.com/nursing/the-respiratory-system-structure-and-function-nursing-part-2/>
- Arrondo, J., & Goni, F. M. (1998). Infrared studies of protein-induced perturbation of lipids in lipoproteins and membranes. *Chemistry and physics of lipids* , 96 (1-2), 53-68.
- Baenke, F., Peck, B., Miess, H., & Schulze, A. (2013). Hooked on fat: the role of lipid synthesis in cancer metabolism and tumour development. *Disease models & mechanisms* , 6 (6), 1353-1363.
- Bellisola, G., & Sorio, C. (2012). Infrared spectroscopy and microscopy in cancer research and diagnosis. *American journal of cancer research* , 2 (1), 1.
- Beloribi-Djefafliya, S., Vasseur, S., & Guillaumond, F. (2016). Lipid metabolic reprogramming in cancer cells. *Oncogenesis* , 5 (1), e189.
- Boyaci, I., Temiz, H., Geniř, H., Soykut, E., Yazgan, N., G  ven, B., et al. (2015). Dispersive and FT-Raman spectroscopic methods in food analysis. *Rsc Advances* , 5 (70), 56606-56624.
- Ceylan, C., Camgoz, A., & Baran, Y. (2012). Macromolecular changes in nilotinib resistant K562 cells; an in vitro study by Fourier transform infrared spectroscopy. *Technology in cancer research & treatment* , 11 (4), 333-344.
- Cheng, T., Cramb, S., Baade, P., Youlden, D., Nwogu, C., & Reid, M. (2016). The international epidemiology of lung cancer: latest trends, disparities, and tumor characteristics. *Journal of Thoracic Oncology* , 11 (10), 1653-1671.
- Cohenford, M. A., & Rigas, B. (1998). Cytologically normal cells from neoplastic cervical samples display extensive structural abnormalities on IR spectroscopy:

implications for tumor biology. *Proceedings of the National Academy of Sciences* , 95 (26), 15327-15332.

- de Cedrón, G., & de Molina, R. (2016). Microtargeting cancer metabolism: opening new therapeutic windows based on lipid metabolism. *Journal of lipid research* , 52 (2), 193-206.
- Derenne, A., Gasper, R., & Goormaghtigh, E. (2011). The FTIR spectrum of prostate cancer cells allows the classification of anticancer drugs according to their mode of action. *Analyst* , 136 (3), 1134-1141.
- Dessi, S., Batetta, B., Pulisci, D., Spano, O., Cherchi, R., Lanfrango, G., et al. (1992). Altered pattern of lipid metabolism in patients with lung cancer. *Oncology* , 49 (6), 436-441.
- Doi, O., Doi, F., Schroeder, F., Alberts, A., & Vagelos, P. (1978). Manipulation of fatty acid composition of membrane phospholipid and its effects on cell growth in mouse LM cells. *Biochimica et Biophysica Acta (BBA)-Biomembranes* , 509 (2).
- Dovbeshko, G., Chegel, V., Gridina, N., Repnytska, O., Shirshov, Y., Tryndiak, V., et al. (2002). Surface enhanced IR absorption of nucleic acids from tumor cells: FTIR reflectance study. *Biopolymer (Biospectroscopy)* , 67, 470-486.
- Dreissig, I., Machill, S., Salzer, R., & Krafft, C. (2009). Quantification of brain lipids by FTIR spectroscopy and partial least squares regression. *Spectrochimica Acta Part A: Molecular and Biomolecular Spectroscopy* , 71 (5), 2069-2075.
- Evan, G. I., & Vousden, K. H. (2001). Proliferation, cell cycle and apoptosis in cancer. *nature* , 342.
- Fabian, H., Jackson, M., Murphy, L., Watson, P., Fichtner, I., & Mantsch, H. (1995). A comparative infrared spectroscopic study of human breast tumors and breast tumor cell xenografts. *Biospectroscopy* , 1 (1), 37-45.
- Farhadi, E., Kobarfard, F., & Shirazi, F. H. (2016). FTIR Biospectroscopy Investigation on Cisplatin Cytotoxicity in Three Pairs of Sensitive and Resistant Cell Line. *Iranian journal of pharmaceutical research: IJPR* , 15 (1), 213-220.
- Friesen, J. A., & Rodwell, V. W. (2004). The 3-hydroxy-3-methylglutaryl coenzyme-A (HMG-CoA) reductases. *Genome biology* , 5 (11), 248.
- Fung, M., Senterman, M., Mikhael, N., Lacelle, S., & Wong, P. (1996). Pressure-tuning fourier transform infrared spectroscopic study of carcinogenesis. *Biospectroscopy* , 2 (3), 155-165.
- Furberg, C. D., & Pitt, B. (2001). Withdrawal of cerivastatin from the world market. *Trials* , 2 (5), 205.



- Galeb, H., Salimon, J., Eid, E., Nacer, N., Saari, N., & Saadi, S. (2012). The impact of single and double hydrogen bonds on crystallization and melting regimes of Ajwa and Barni lipids. *Food research international* , 48 (2), 657-666.
- Gault, N., Rigaud, O., Poncy, J., & Lefaix, J. (2005). Infrared microspectroscopy study of  $\gamma$ -irradiated and H<sub>2</sub>O<sub>2</sub>-treated human cells. *International journal of radiation biology* , 81 (10), 767-779.
- Gaw, A., Packard, C. J., & Shepherd, J. (2003). Statins: the HMG CoA reductase inhibitors in perspective. *CRC Press*.
- Gehr, P., Bachofen, M., & Weibel, E. (1978). The normal human lung: ultrastructure and morphometric estimation of diffusion capacity. *Respiration physiology* , 32 (2), 121-140.
- Goldstein JL, B. M. (1990). Regulation of the mevalonate pathway. *Nature* , 343: 425-430.
- Gupta, U., Singh, V., Kumar, V., & Khajuria, Y. (2014). Spectroscopic studies of cholesterol: fourier transform infra-red and vibrational frequency analysis. *Materials Focus* , 3 (3), 211-217.
- Hanahan, D., & Weinberg, R. A. (2011). Hallmarks of cancer: the next generation. *Cell* , 144 (5), 646-674.
- Hayati, I., Man, Y., Tan, C., & Aini, I. (2005). Monitoring peroxide value in oxidized emulsions by Fourier transform infrared spectroscopy. *European Journal of Lipid Science and Technology* , 107 (12), 886-895.
- Helm, D., Labischinski, H., Schallehn, G., & Naumann, D. (1991). Classification and identification of bacteria by Fourier-transform infrared spectroscopy. *Microbiology* , 137 (1), 69-79.
- Howlader, N. N., Noone, A., Krapcho, M., Miller, D., Bishop, K., Kosary, C., et al. (2017). SEER cancer statistics review, 1975–2014. *Bethesda, MD: National Cancer Institute, 2018*.
- Jones, H., Fang, Z., Sun, W., Clark, L., Stine, J., Tran, A., et al. (2017). Atorvastatin exhibits anti-tumorigenic and anti-metastatic effects in ovarian cancer in vitro. *American journal of cancer research* , 7 (12), 2478.
- Kim, J., Lee, H., & Lee, K. (2018). Effect of statins on fasting glucose in non-diabetic individuals: nationwide population-based health examination in Korea. *Cardiovascular diabetology* , 17 (1), 155.
- Lamba, O. P., Lal, S., Yappert, M. C., Lou, M. F., & Borchman, D. (1991). Spectroscopic detection of lipid peroxidation products and structural changes in a sphingomyelin model system. *Biochimica et Biophysica Acta (BBA)-Lipids and Lipid Metabolism* , 1081 (2), 181-187.
- Lettiero, B., Inasu, M., Kimbung, S., & Borgquist, S. (2018). Insensitivity to atorvastatin is associated with increased accumulation of intracellular lipid

- droplets and fatty acid metabolism in breast cancer cells. *Scientific reports* , 8 (1), 5462.
- Li, Y., Fu, J., Yuan, X., & Hu, C. (2014). Simvastatin inhibits the proliferation of A549 lung cancer cells through oxidative stress and up-regulation of SOD2. *Die Pharmazie - An International Journal of Pharmaceutical Sciences* , 69 (8), 610-614.
- Lieber, M., Smith, B., Szakal, A., Nelson-Rees, W., & Todaro, G. (1976). A continuous tumor-cell line from a human lung carcinoma with properties of type II alveolar epithelial cells. *International journal of cancer* , 17 (1), 62-70.
- Likus, W., Siemianowicz, K., Bieńk, K., Pakuła, M., Pathak, H., Dutta, C., et al. (2016). Could drugs inhibiting the mevalonate pathway also target cancer stem cells?. *Drug resistance updates* , 25, 13-25.
- Lin, S. Y., Li, M. J., & Cheng, W. T. (2007). FT-IR and Raman vibrational microspectroscopies used for spectral biodiagnosis of human tissues. *Journal of Spectroscopy* , 21 (1), 1-30.
- Liu, K., Jackson, M., Sowa, M., Ju, H., Dixon, I., & Mantsch, H. (1996). Modification of the extracellular matrix following myocardial infarction monitored by FTIR spectroscopy. *Biochimica et Biophysica Acta (BBA)-Molecular Basis of Disease* , 1315 (2), 73-77.
- Maksimova, E., Yie, T., & Rom, W. (2008). In vitro mechanisms of lovastatin on lung cancer cell lines as a potential chemopreventive agent. *Lung* , 186 (1), 45-54.
- Malek, K., Wood, B., & Bambery, K. (2014). FTIR imaging of tissues: techniques and methods of analysis. . *In Optical spectroscopy and computational methods in biology and medicine* , 419-473.
- Masmoudi, H., Le Dréau, Y., Piccerelle, P., & Kister, J. (2005). The evaluation of cosmetic and pharmaceutical emulsions aging process using classical techniques and a new method: FTIR. *International journal of pharmaceutics* , 289 (1-2), 117-131.
- Mason, R. C., Murray, F. J., Nadel, J. A., & Gotway, M. (2015). Murray & Nadel's Textbook of Respiratory Medicine E-Book. *Elsevier Health Sciences* .
- Merino, S. M., de Cedrón Gómez, M., Moreno, R. J., Falagán, M. S., Sánchez, M. R., Casado, E., et al. (2017). Lipid metabolism and lung cancer. *Critical reviews in oncology/hematology* , 31-40.
- Naumann, D., Helm, D., & Labischinski, H. (1991). Microbiological characterizations by FT-IR spectroscopy. *Nature*, 351(6321), 81-82. , 351 (6321), 81-82.
- Nicklin, P., Bergman, P., Zhang, B., Triantafellow, E., Wang, H., Nyfeler, B., et al. (2009). Bidirectional transport of amino acids regulates mTOR and autophagy. *Cell* , 136 (3), 521-534.

- Oleszko, A., Olsztyńska-Janus, S., Walski, T., Grzeszczuk-Kuć, K., Bujok, J., Gałęcka, K., et al. (2015). Application of FTIR-ATR spectroscopy to determine the extent of lipid peroxidation in plasma during haemodialysis. *BioMed research international*, 2015 .
- Oyman, Z., Ming, W., & Van der Linde, R. (2003). Oxidation of model compound emulsions for alkyd paints under the influence of cobalt drier. *Progress in organic coatings* , 48 (1), 80-91.
- Özsu, S., & Özlü, T. (2013). Epidemiology of Lung Cancer in Turkey. *Güncel Göğüs Hastalıkları Serisi* , 7-11.
- Pacifico, S., Piccolella, S., Papale, F., Nocera, P., Lettieri, A., & Catauro, M. (2016). A polyphenol complex from *Thymus vulgaris* L. plants cultivated in the Campania Region (Italy): New perspectives against neuroblastoma. *Journal of functional foods* , 20, 253-266.
- Paškevičiūtė, M., & Petrikaitė, V. (2017). Differences of statin activity in 2D and 3D pancreatic cancer cell cultures. *Drug design, development and therapy* , 11, 3273.
- Pavlova, N. N., & Thompson, C. B. (2016). The emerging hallmarks of cancer metabolism. *Cell metabolism* , 23 (1), 27-47.
- Ramharack, P. (2015). HMG-CoA Reductase Inhibitor, Atorvastatin, Induces Apoptosis in Human Lung Adenocarcinoma Cells (A549). Durban: University of KwaZulu-Natal .
- Ricciardi, V., Portaccio, M., Piccolella, S., Manti, L., Pacifico, S., & Lepore, M. (2017). Study of SH-SY5Y cancer cell response to treatment with polyphenol extracts using FT-IR spectroscopy. *Biosensors* , 7 (4), 57.
- Risé, P., Ghezzi, S., & Galli, C. (2003). Relative potencies of statins in reducing cholesterol synthesis and enhancing linoleic acid metabolism. *European journal of pharmacology* , 467 ((1-3)), 73-75.
- Salman, A. S. (2003). Characterization of normal and malignant cells in culture and human colonic tissues using ftir microspectroscopy, and advanced computational methods. *Doctor of philosophy's thesis* . Ben-Gurion University of the Negev.
- Sánchez-Alonso, I., Carmona, P., & Careche, M. (2012). Vibrational spectroscopic analysis of hake (*Merluccius merluccius* L.) lipids during frozen storage. *Food Chemistry* , 132 (1), 160-167.
- Sanders, L., & Zeisel, S. (2007). Choline: dietary requirements and role in brain development. *Nutrition today* , 42 (4), 181.
- Schachter, M. (2005). Chemical, pharmacokinetic and pharmacodynamic properties of statins: an update. *Fundamental & clinical pharmacology* , 19 (1), 117-125.

- Schwarzott, M., Lasch, P., Baurecht, D., Naumann, D., & Fringeli, U. (2004). Electric field-induced changes in lipids investigated by modulated excitation FTIR spectroscopy. *Biophysical journal* , 86 (1), 285-295.
- Shapaval, V., Afseth, N. K., Vogt, G., & Kohler, A. (2014). Fourier transform infrared spectroscopy for the prediction of fatty acid profiles in *Mucor* fungi grown in media with different carbon sources. *Microbial cell factories* , 13 (1), 86.
- Shim, H. S., Choi, Y., Kim, L., Chang, S., Kim, W., Roh, M. S., et al. (2017). Molecular testing of lung cancers. *Journal of pathology and translational medicine* , 51 (3), 242.
- Singh, J., Dasgupta, A., Adayev, T., Shahmehdi, S., Hammond, D., & Banerjee, P. (1996). Apoptosis is associated with an increase in saturated fatty acid containing phospholipids in the neuronal cell line, HN2-5. *Biochimica et Biophysica Acta (BBA)-Lipids and Lipid Metabolism* , 1304 (3), 171-178.
- Sun, Q., Zhang, B., Hu, Q., Qin, Y., Xu, W., Liu, W., et al. (2018). The impact of cancer-associated fibroblasts on major hallmarks of pancreatic cancer. *Theranostics* , 8 (18), 5072.
- Talari, A., Martinez, M., Movasaghi, Z., Rehman, S., & Rehman, I. (2017). Advances in Fourier transform infrared (FTIR) spectroscopy of biological tissues. *Applied Spectroscopy Reviews* , 52 (5), 456-506.
- Tang, Y., Zhou, J., Hooi, S., Jiang, Y., & Lu, G. (2018). Fatty acid activation in carcinogenesis and cancer development: Essential roles of long-chain acyl-CoA synthetases. *Oncology letters* , 16 (2), 1390-1396.
- Taylor, F., Ward, K., Moore, T., Burke, M., Smith, G., Casas, J., et al. (2011). Statins for the primary prevention of cardiovascular disease. *Cochrane database of systematic reviews* , 1.
- TDD. (2010). Türkiye’de Temel Akciğer Sağlığı Sorunları ve Çözüm Önerileri. In *Türk Toraks Derneği Beyaz Kitap* (pp. 89-93). Ankara: Sentez Matbaacılık ve Yayıncılık.
- Tobert, J. A. (2003). Lovastatin and beyond: the history of the HMG-CoA reductase inhibitors. *Nature reviews Drug discovery* , 2 (7), 517-526.
- Uchiyama, M., Oguri, M., Mojumdar, E., Gooris, G., & Bouwstra, J. (2016). Free fatty acids chain length distribution affects the permeability of skin lipid model membranes. *Biochimica et Biophysica Acta (BBA)-Biomembranes* , 1858 (9), 2050-2059.
- Varbanov, H., Kuttler, F., Banfi, D., Turcatti, G., & Dyson, P. (2017). Repositioning approved drugs for the treatment of problematic cancers using a screening approach. *PloS one* , 12 (2), e0171052.
- Vidyadharani, G., & Dhandapani, R. (2013). Fourier transform infrared (FTIR) spectroscopy for the analysis of lipid from *Chlorella vulgaris*. *Elixir Appl. Biology* 61 , 16753-16756.

- Wang, X., Shen, X., Sheng, D., Chen, X., & Liu, X. (2014). FTIR spectroscopic comparison of serum from lung cancer patients and healthy persons. *Spectrochimica Acta Part A: Molecular and Biomolecular Spectroscopy* (122), 193-197.
- Warburg, O., Wind, F., & Negelein, E. (1927). The metabolism of tumors in the body. *The Journal of general physiology* , 8 (6), 519.
- Wong, P., Wong, R., Caputo, T., Godwin, T., & Rigas, B. (1991). Infrared spectroscopy of exfoliated human cervical cells: evidence of extensive structural changes during carcinogenesis. *Proceedings of the National Academy of Sciences* , 88 (24), 10988-10992.
- Wu, B. B., Gong, Y. P., Wu, X. H., Chen, Y. Y., Chen, F. F., Jin, L. T., et al. (2015). Fourier transform infrared spectroscopy for the distinction of MCF-7 cells treated with different concentrations of 5-fluorouracil. *Journal of translational medicine* , 13 (1), 108.
- Yandim, M. K., Ceylan, C., Elmas, E., & Baran, Y. (2016). A molecular and biophysical comparison of macromolecular changes in imatinib-sensitive and imatinib-resistant K562 cells exposed to ponatinib. *Tumor Biology* , 37 (2), 2365-2378.
- Yılmaz, H. H., Yazıhan, N., Tunca, D., Sevinç, A., Olcayto, E. Ö., Özgül, N., et al. (2010). Cancer trends and incidence and mortality patterns in Turkey. *Japanese journal of clinical oncology* , 41 (1), 10-16.
- Yoshida, S., Zhang, Q., Sakuyama, S., & Matsushima, S. (2009). Metabolism of fatty acids and lipid hydroperoxides in human body monitoring with Fourier transform Infrared Spectroscopy. *Lipids in health and disease* , 8 (1), 28.
- Yu, X., Pan, Y., Ma, H., & Li, W. (2013). Simvastatin inhibits proliferation and induces apoptosis in human lung cancer cells. *Oncology Research Featuring Preclinical and Clinical Cancer Therapeutics* , 20 (8), 351-7.
- Zamay, T. N., Zamay, G. S., Kolovskaya, O. S., Zukov, R. A., Petrova, M. M., Gargaun, A., et al. (2017). Current and prospective protein biomarkers of lung cancer. *Cancers* , 9 (11), 155.
- Zhang, F., & Du, G. (2012). Dysregulated lipid metabolism in cancer. *World journal of biological chemistry* , 3 (8), 167.
- Zheng, S., & Tu, A. (1986). Raman spectroscopic identification of bilirubin-type gallstone. *Applied spectroscopy* , 40 (8), 1099-1103.